IACMI/R009-2021/5.7

Tailored Fiber Placement for Complex Preforms

Author: Daniel Rapking
and Gyaneshwar Tandon
Date: 03/30/2021

Final Technical Report
PA16-0349-5.7-01

Approved for Public Release.
Distribution is Unlimited.

DOCUMENT AVAILABILITY

Reports produced after January 1, 1996, are generally available free via US Department of Energy (DOE) SciTech Connect.

Website http://www.osti.gov/scitech/

Reports produced before January 1, 1996, may be purchased by members of the public from the following source:

National Technical Information Service
5285 Port Royal Road
Springfield, VA 22161
Telephone 703-605-6000 (1-800-553-6847)
TDD 703-487-4639
Fax 703-605-6900
E-mail info@ntis.gov
Website http://www.ntis.gov/help/ordermethods.aspx

Reports are available to DOE employees, DOE contractors, Energy Technology Data Exchange representatives, and International Nuclear Information System representatives from the following source:

Office of Scientific and Technical Information
PO Box 62
Oak Ridge, TN 37831
Telephone 865-576-8401
Fax 865-576-5728
E-mail reports@osti.gov
Website http://www.osti.gov/contact.html

The information, data, or work presented herein was funded in part by the Office of Energy Efficiency and Renewable Energy (EERE), U.S. Department of Energy, under Award DE- EE0006926

The authors would like to acknowledge the financial support by IACMI, JobsOhio, Airbus Americas Inc., Lockheed Martin Corporation and ZSK to conduct this study, and to Michigan State University for their technical help with this project.

Tailored Fiber Placement for Complex Preforms

Principal Investigator: G.P Tandon

Organization: University of Dayton Research Institute

Address: 300 College Park, Dayton, OH 45469-7641

Phone: 937-229-4511

Email: gyaneshwar.tandon@udri.udayton.edu

Co-authors: Daniel Rapking, Michael Braginsky, Eric Zhou, Scott Huelskamp, Matthew Cameron, Caleb Tanner, Olivia Bowman, Christian J. Pfledderer, Jayson Lotz, Ron Trejo, Haythem Marawi, Bradley R Hripko, Ryan Seifert, Brian Rice, Erik Stitt*, Mahmood Haq*

*Michigan State University

Date Published:

Prepared by:
Institute for Advanced Composites Manufacturing Innovation
Knoxville, TN 37932
Managed by Collaborative Composite Solutions, Inc.
For the
U.S. DEPARTMENT OF ENERGY
Under contract DE- EE0006926

Project Period:
(06/2019 – 02/2021)

Approved For Public Release

TABLE OF CONTENTS

1. LISTS

1.1 LIST OF ACRONYMS

TFP: Tailored Fiber Placement
UDRI: University of Dayton Research Institute
BSAM: A finite element tool (formerly stood for B-Spline Analysis Method)
VTMS: Virtual Textile Morphology Suite
ZSK: ZSK Machines
ASTM: American Society for Testing and Materials
ILT: Interlaminar Tensile (strength)
RXFEM- Regularized eXtended Finite Element Method
DDM: Discrete Damage Methodology
GUI: Graphical User Interface
IM7: Intermediate Modulus Fiber #7
AS4: Standard Modulus Fiber 4
RTM: Resin Transfer Molding
MTS: Material Testing System (MTS Corporation)
NGSA: Non-dominated Genetic Sorting Algorithm
CT: Computed Tomography

1.2 List of Figures

1.3 List of Tables

1.4 List of Appendices

2. EXECUTIVE SUMMARY

Tailored Fiber Placement (TFP) offers a novel approach to optimize fiber architecture for the fabrication of complex, structural parts not traditionally suitable for advanced composites. This technology not only offers new routes for weight reduction via metal substitution, it also offers cost reduction through minimization of material scrap and reduced labor. This reduction in component weight leads to increased fuel efficiency, and reduced production energy consumption, thereby, helping to achieve the stated IACMI technical goals. This technology leverages centuries of manufacturing development in support of the textile and embroidery industry. One major drawback to this technology is the lack of commercial or non-proprietary structural performance data and robust analytical tools used to optimize fiber architecture and predict performance. This project was structured to utilize common sub-element features to validate analytical performance tools, generate performance data, and gather cost and performance data on components of interest. This project was designed to give industry sponsors the confidence and ability to take full advantage of TFP to fabricate primary, highly loaded structure and integrate features such as metallic fasteners. The project focused principally on the use of high strength carbon fiber, such as T700, and the use of aerospace epoxy resin matrix to primarily support development of new composite applications in vehicle, aerospace, and industrial markets.

This project applied previously developed analytical tools to predict the performance of TFP produced parts. This work focused on developing the pipeline to characterize material in order to accurately predict component performance when modifying the TFP print paths and stitch density. This focused on experimental characterization via standardized ASTM testing, alongside experimental testing of more representative service components by testing curved beam strength, beam shear performance, a large scale TFP lug, and ultimately designing a fully TFP clip bracket that reduced weight and cost compared to a traditional metallic component.

The new knowledge gained from this program included: 1) development and demonstration of novel analytical tools applied to analysis of TFP preforms; 2) development and demonstration of a building block approach using coupons and sub-elements to optimize the design of a more complex component; 3) demonstration that optimized fiber orientation using TFP can exceed performance of conventional textile composite materials and can open new applications currently limited to metallic components; 4) Demonstration of performance and cost benefits of the TFP process as compared to metallic and conventional textile composites. Recommendations for follow-on work include development of design allowables to assess the impact of high temperature/moisture exposure or saturation during loading, tracking the impact of stitching needle wear on the performance of parts and ability to stitch thicker preforms, using TFP preforms as local reinforcement at areas of bearing or complex loading, and topology optimization of components by tow steering.

The expertise developed during the course of this project can be leveraged to provide commercial engineering design and fabrication services using TFP. UDRI is in the process of formalizing their partnership with Spintech, who will serve as the commercialization partner for this technology and provide molding services and deliver finished components to the end user. UDRI will continue to produce the preforms until the economics allow Spintech to procure its own TFP equipment or lease UDRI equipment, at which point UDRI will step away from manufacture and serve as the engineering and design lead on product development.

3. INTRODUCTION

Tailored fiber placement (TFP) is a manufacturing technique that automatically lays down fiber bundles (of various sizes) at specified locations, with the ability to provide out-of-plane reinforcement via localized stitching. This process offers a novel approach to optimize fiber architecture for the fabrication of complex structural parts not traditionally suitable for advanced composites. This process promises to improve mechanical performance and reduce component weight by laying down fiber reinforcements in a strategic and geometrically optimized manner. This not only offers routes for component weight reduction by substituting for traditionally metallic components, but it also offers cost reductions through the minimization of material scrap and reduced manual labor. This reduction in component weight leads to increased fuel efficiency, and reduced production energy consumption.

The TFP technology provides methods for producing near net-shape preforms for composite structures that receive increased out-of-plane strength via local stitching reinforcements. This leverages centuries of manufacturing development in support of the textile and embroidery industry [1]. The current limitation is the lack of commercial or non-proprietary structural performance data and robust analytical tools required to optimize component architecture and performance. This task applied previously developed analytical tools to support the design of composite parts made with TFP preforms. Two specialized software packages co-developed by UDRI and the United States Air Force were employed for this effort. Virtual Textile Morphology Suite (VTMS) software was used to predict the effects of draping and consolidation on the tow alignment and shape. BSAM, a specialized finite element software, was used to predict mechanical performance of the final structure. A key objective of this task was to determine the design methodology needed to best utilize these tools regarding TFP.

This project was structured to utilize common aerospace sub-element features to validate the analytical performance of the developed toolset, while simultaneously generating performance and cost data. This effort was focused on utilizing high strength carbon fiber and aerospace grade epoxy resins. The first sub-element was a 90-degree angle bracket subjected to 4-point bending. Local stitching reinforcement was added to the angle bracket at the bend radius, guided by the finite element simulations, to assess the effect of stitch density on improving the mechanical performance of the angle bracket, as well as exploring the ability to prevent damage growth critical to the complex part. Both unstitched and stitched laminates were fabricated and tested to assess performance improvements.

The second sub-element chosen was a bolted joint, with the bearing surface reinforced by the addition of steered TFP fiber tows around the bearing surface. . The goal was to show that bearing performance could be improved at a lower cost than traditional prepreg or fabric construction. Bolted connections are commonly used in preference to other joining techniques because they allow greater freedom in assembly and repair. Carbon fiber reinforced composite structures generally outperform metallic ones, but this is not the case when the structure is loaded in bearing. A more efficient solution to reinforcing holes can be provided by selective fiber placement [2]. In principle, directed fiber placement can be added to an existing laminate at an orientation that matches the local load-carrying requirements exactly; ensuring that the part achieves the minimum possible weight, highest stiffness, and improved bearing strength. A lug geometry that could be utilized in a bolted joint configuration was selected in consultation with industry and University partner engineers. Lugs were fabricated with 1) a traditional fabric, 2) TFP preform with no integrated hardpoints, and 3) TFP preform with integrated hardpoints. In addition, project partner Lockheed Martin expressed an interest in using TFP to increase the bearing strength of bolted joints in conventional prepreg structures. During this program, the project team investigated the use of dry doilies made using TFP that can be added into the ply stack of a prepreg layup. The doilies used a preferred fiber orientation not possible with woven or uni- directional reinforcement. The cured laminates were tested in bearing.

Finally, a complex part of interest that showcased the benefits of engineered TFP preforms with or without integration of hard points and load bearing conditions for evaluation was identified in coordination with industry partner Airbus. The complex part component was determined to be a clip bracket. BSAM/VTMS were used to model the formation of the TFP parts and predict its performance. The analytical models were used to predict the location of initial failure and the failure strength. The analytical predictions were correlated with the experimental observations and measurements. Additionally, Airbus had interest in comparing traditional cost and weight estimates and performance for these parts to those of TFP fabricated parts, and the realized benefits and deficiencies of this approach when compared to metallic and conventional composites.

Overall, the work accomplished in this program was designed to give industry sponsors the confidence to take advantage of TFP's ability to fabricate primary, highly loaded structures; whilst integrating locating/bearing features like fasteners. The project developed and demonstrated analytical tools to predict TFP performance alongside a building block approach using coupons/sub-elements in order to optimize the design process, and in demonstrating that TFP can be used to exceed the performance of traditional textile composite materials, and open areas currently limited to metallic components.

The development of this technology could lead to widespread adoption of TFP processes in both the automotive and aerospace fields where increasing fuel costs and requirements to improve fuel efficiency requires the development of new approaches for designing and cost effectively building structures. This program has developed expertise in optimizing fiber architecture for various load configurations while demonstrating the robust predictive performance of the analytical tools. This expertise could be leveraged to provide commercial engineering design and fabrication services using TFP. UDRI is in the process of formalizing their partnership with Spintech, who will serve as the commercialization partner for this technology.

4. BACKGROUND

One of the main design limiting aspects of composite materials is low through thickness strength. Aerospace manufacturers have explored different techniques to improve through thickness properties: through stitches, z-stitching, tailored interfaces, etc. These techniques have demonstrated improvements in out-of-plane performance, but generally at the cost of reductions in in-plane mechanical properties or an increase in associated fabrication costs. The use of conventional methods of improving out-of-plane performance has been extensively researched [1, 3-4] and has shown many potential benefits and drawbacks of various methods. The aerospace industry in particular has explored this approach to improve fracture toughness and impact damage tolerance. The general agreement in literature shows that the inclusion of z-stitching will increase interlaminar properties (toughness/strength) at the cost of reducing in-plane properties (modulus/strength). This, coupled with the increase in cost compared with simply stitching traditional composite structures, has ultimately limited the widespread adoption of z-stitching.

Tailored fiber placement (TFP) is a process akin to embroidery that can be used to produce near net-shape composite preforms, which are inherently z-stitched as a product of the manufacturing technique [5-6]. The TFP process uses tow steering in order to produce a composite structure by layering tows upon each other, with all layers being attached to a carrier cloth. This composite can be constructed of multiple layers of preforms consisting of various curvilinear tow paths. Due to the ability to explicitly steer each individual tow path, it is possible to optimize [6] the tow paths to maximize part performance. A simplified schematic shows how carbon fiber tows can be laid down along specific paths using the TFP process in Figure 1. This shows how the carbon tow is held in place using a polyester holding thread that has various stitch lengths and widths. This image also shows a close up of the stitching head on the ZSK machine.

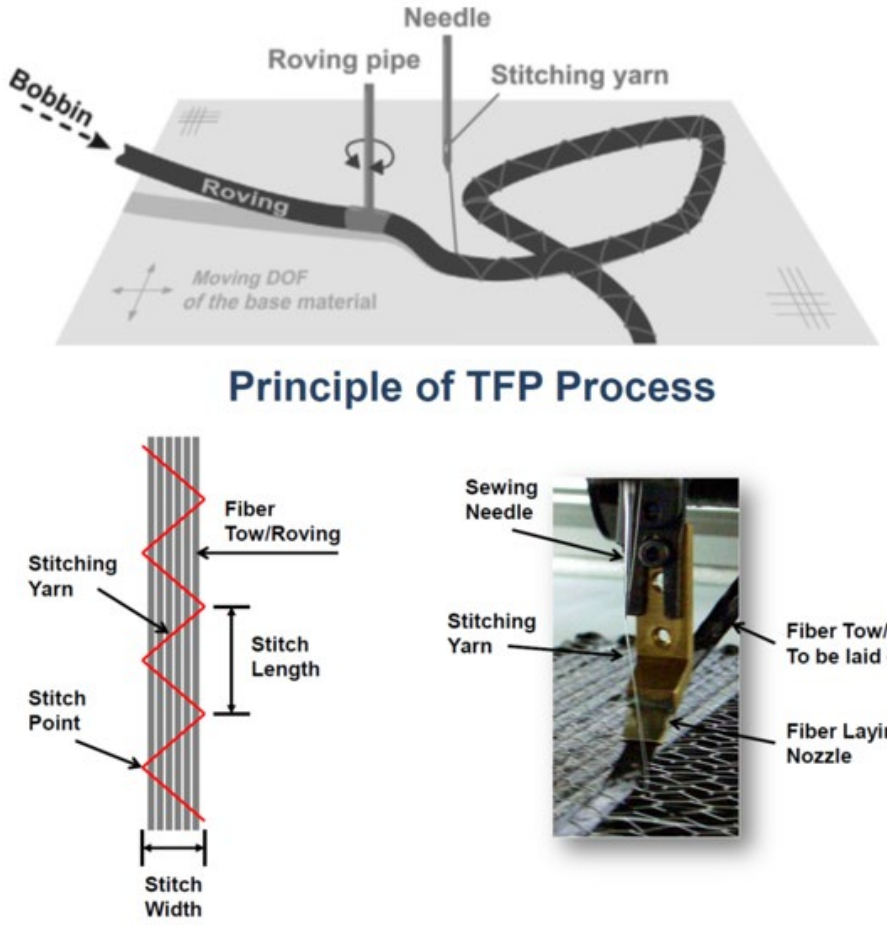

Previous work has shown that the TFP forming process is compatible with a wide array of tow materials, and sizes including 50k heavy tow (Koricho, Khomenko, Fristedt, & Haq, 2015). Heavy tow carbon, sometimes referred to as commercial-grade carbon, has lower properties compared to aerospace-grade carbon, but it is significantly cheaper to manufacture (Fiber reinforcement forms, 2014). It also allows much faster laminate build-up rates, further reducing the cost of part fabrication. By pairing heavy tow carbon with the automated TFP process that inherently adds z-stitching, there is potential to build very cost-effective preforms that exhibit superior toughness and impact damage tolerance. This could be very attractive to industries such as the automotive industry that have been slow to adopt composite materials for cost and/or performance reasons.

In order to apply TFP most effectively, there needs to be a roadmap which helps predict performance for a given fiber architecture, or perhaps more practically, identify the necessary fiber architecture which would yield the desired performance. Unfortunately, a straightforward and accurate roadmap is not yet available. Instead, the design process has mainly relied on iterative experimentation, which is both costly and time-consuming. Although computational methods have explored ways of optimizing and simulating various textile geometries, composite materials often have competing damage mechanisms that lead to ultimate failure, including matrix cracking and fiber failure.

The present work seeks to establish the described roadmap for simulating the distortion of fiber due to stitching, as well as the increase in strength associated with it, while working to minimize the need for experimentation. This is being done by employing finite element tool BSAM in conjunction with Virtual Textile Morphology Suite (VTMS) which allows a user to simulate textile processing, including compaction effects, to produce detailed tow morphologies. BSAM is a finite element toolbox that uses discrete damage modeling (DDM) to capture the progressive damage evolution of composite materials during loading [6-8]. The DDM methods employed by BSAM allow for the representation of matrix cracks, delaminations, and fiber failure. Matrix cracks are based on the mesh independent crack (MIC) technique termed the regularized extended finite element method (RXFEM) [9]. Plies are coupled together using a cohesive interface governed by a traction separation law described in the work by Turon et al [10]. Fiber failure is modeled utilizing a traditional continuum damage mechanics (CDM) approach [11-12]. The DDM approach utilized by BSAM simulates progressive failure by explicitly modeling individual damage events allowing multiple failure/damage mechanisms to interact. VTMS consists of five modules: textile pattern design module, relaxation module, tow modification module, mesh generator module, and BSAM export module. Each individual module is a standalone software code with graphic user interface (GUI), which can handle a specific task. Depending on the situation, not all modules need to be employed to produce an FEA model. It can serve as a preprocessor and visualization tool for a stress and damage analysis software. The development of these software packages by UDRI over two decades was funded by the Air Force and is remarkably suitable to predict the effects of microstructural variations on material properties and macrostructural performance in polymer matrix composites. These packages can be used separately or in tandem.

In the present work, BSAM is used to study a component's strength and toughness as a function of layup pattern and density of Kevlar stitches. This task applies previously developed analytical tools to support the design of composite parts made with TFP preforms and determine the design methodology needed to best utilize these tools for such parts.

5. RESULTS AND DISCUSSION

5.1 Experimental Work

The primary goal of this project was to develop a computational model capable of simulating the change in mechanical performance as a function of various reinforcement stitch densities and TFP paths. The development and verification of this computational approaches requires material characterization and experimental validation. The first step involved the characterization of the material of interest as an input to the finite element package BSAM. This characterization required extensive testing following ASTM standards to develop a fully characterized material data set. The material characterization matrix can be seen in Table 1. This test matrix was largely informed by the previous work by Huelskamp et al [13]. This test matrix allowed for the characterization of the impact on modulus, strength, and toughness as a function of several different stitch densities. This testing allowed UDRI to characterize how various stitch densities impacts the mechanical performance of the composite perform.

Table 1. Material Characterization Test Matrix

			Stitch spacing/Density			
Material Property	Property Description	Test Method	0/cm^2	8/cm^2	16/cm^2	30/cm^2
E_1^T (GPa)	Modulus in fiber direction in tension	ASTM D 3039	Unstitched laminate as baseline for each data set.	3	3	3
X^T (MPa)	Max stress in fiber direction in tension			3	3	3
E_2^T (GPa)	Modulus in 90 degree direction in tension	ASTM D 3039		3	3	3
Y^T (MPa)	Max stress in 90 degree direction in tension			3	3	3
E_1^C (GPa)	Modulus in fiber direction in compression	ASTM D 6641 (CLC)		3	3	3
X^C (MPa)	Max stress in 0 degree direction in compression			3	3	3
E_2^C (GPa)	Modulus in 90 degree fiber direction in compression	ASTM D 6641 (CLC)		3	3	3
Y^C (MPa)	Max stress in 90 degree direction in compression			3	3	3
G_{12} (GPa)	Shear modulus	ASTM D 7078 (V-notch rail shear)		3	3	3
S_{12} (MPa)	In Plane Shear Strength			3	3	3
$G_{IC\text{-}SS}$ (J/m^2)	Critical energy release rate for Mode I crack steady state	ASTM D 5528 (DCB)		3	3	3
$G_{IIC\text{-}PC}$ (J/m^2)	Critical energy release rate for Mode II precracked initiation	ASTM D 7905 (ENF)		3	3	3
F^{tu} (MPa)	Max stress in thickness direction in tension	ASTM D7291 (ILT)		3	3	3
Modulus, Strength	1-3 and 2-3 Shear Properties	ASTM D 7078 (ILS)		3	3	3
Modulus, Strength	Stitching Fiber	ASTM D3379-75		5-7 specimens		

Panels for each test were constructed using a ZSK SGVA 0109 TFP machine. This model of the ZSK TFP machine can steer tows of various sizes ranging from 52 Tex up to 50,000 Tex while stitching at speeds up to 850 stitches per minute across a construction area of 1.3 by 1.4 meters. An example of how the various stitch

densities were constructed can be seen in *Figure* 4. This figure shows an increasing stitch density across part preforms prior to resin infusion. Preforms were constructed of Toray T700S 12k carbon fiber tows and with Hexcel RTM6 epoxy resin. Samples were cured in an autoclave according to the manufacturer recommended cure cycle at 350°F. An example of a standard stacking sequence utilized during the cure cycle can be seen in Figure 5. Samples for material characterization were fabricated as large-scale panels with sections of various levels of stitch densities, in other words one panel was fabricated for ASTM D3039 specimens with 4 different subsections of 0, 8, 16, and 30 stitches/cm^2. Panels were fabricated with an upper thread tension of 1.5 N and lower tension of 0.45 N for polyester holding thread, which provides no mechanical benefit, and serves only to secure the carbon tow, in place, while the Kevlar thread used to provide through thickness reinforcement had an upper thread tension of 4.0 N and lower tension of 0.65 N. Figure 1 shows the style ZSK machine utilized for this effort, with the polyester holding and Kevlar thread bobbin locations highlighted with blue ellipses. The tension setting is adjusted to modify the tension on the thread as it passes through the material. The stitch spacing parameters used to hold the fiber in place (the polyester holding thread spacing information) is shown in Figure 3.

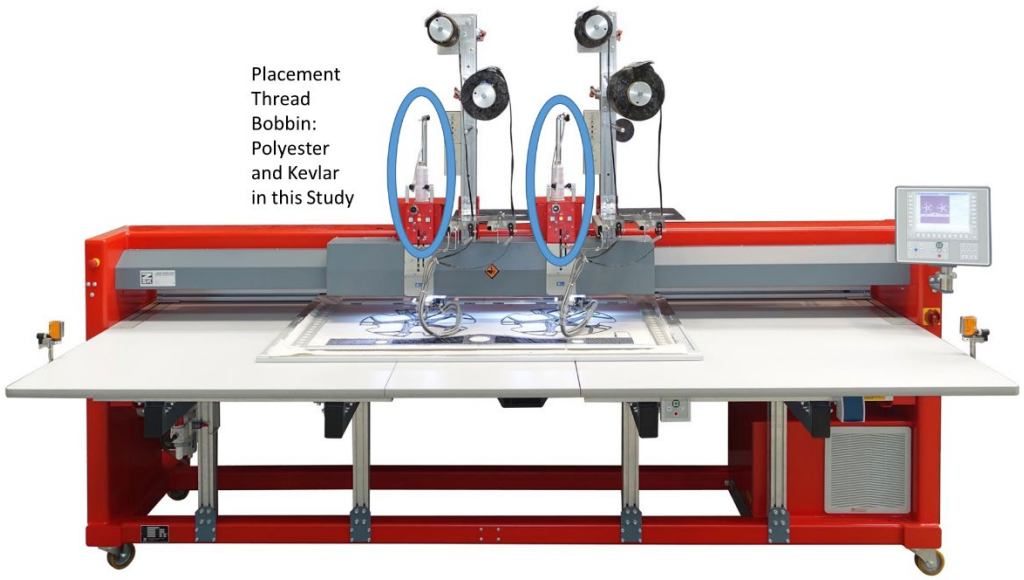

Figure 2. ZSK TFP Machine Showing Bobbin Location and Tension Mechanism (Image Curtesy of ZSK)

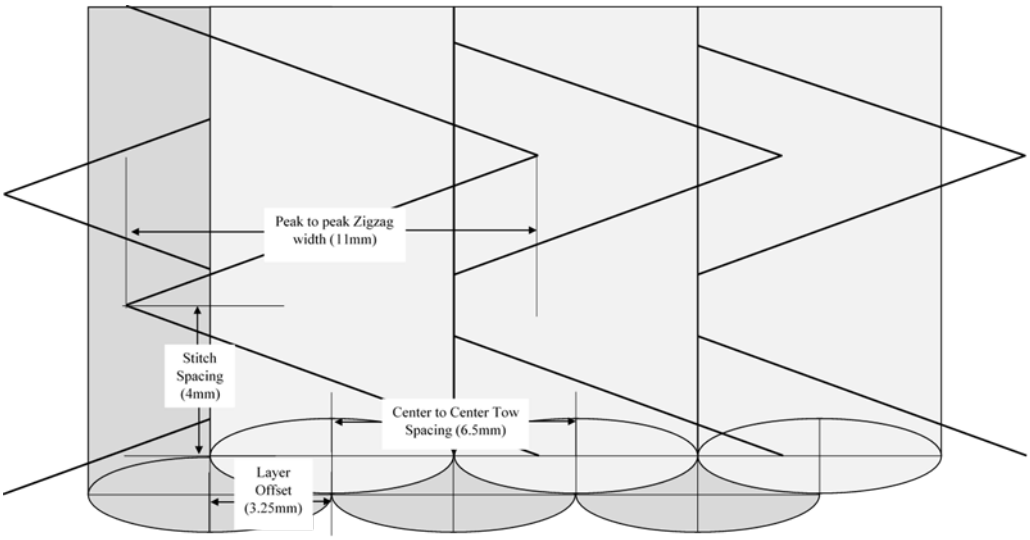

Figure 3. TFP Spacing Parameter Diagram for Polyester Holding Thread

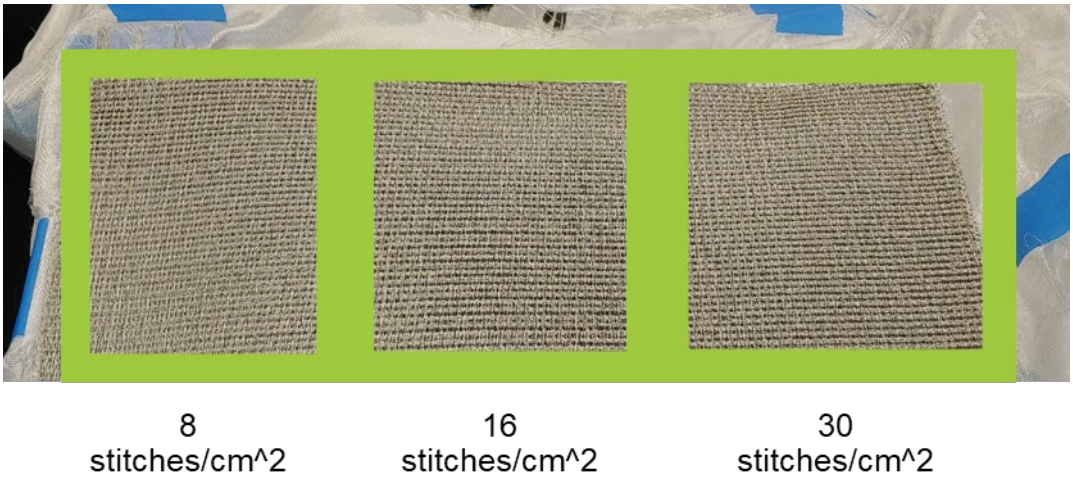

Figure 4. ASTM Standard Test Coupon Preform Fabrication with Various Stitch Densities

Panels were cured according to the primary cure cycle provided by the manufacturer on the material safety data sheet. This cure cycle required a two hour hold at 350°F. The cure cycle ramped from room temperature to 350°F at a rate of 2°F/minute, and vacuum/pressure was applied according to Figure 6. After removal from the autoclave samples were cut into specimens according to the test matrix listed in Table 1. All samples were cut using a diamond wet saw and were machined to a tolerance of ±0.01 mm. Samples for mode I and II fracture toughness testing were pre-cracked according to the ASTM standards. Once the material test characterization test panels were cured and infused, samples were prepped for testing according to the relevant ASTM standards.

Interlaminar Tension

The first round of testing involved the testing of interlaminar tensile strength (ILT). Initial testing was conducted at Cincinnati Test Labs (CTL). Samples were cut to the nominal 1" diameter and adhered to steel test pucks at CTL. An example of the sample geometry in the ASTM standard and a failed test sample can be

seen in Figure 7.

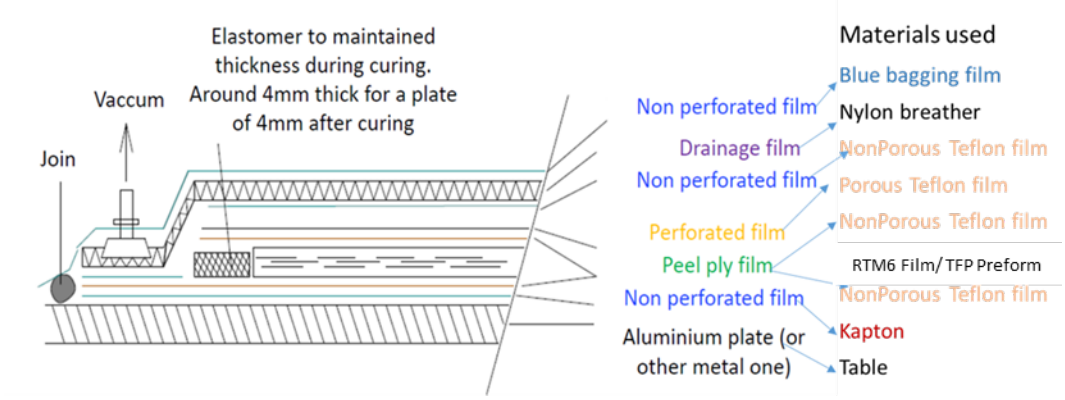

Figure 5. Manufacturer Recommended Bagging Scheme for Autoclave Cure

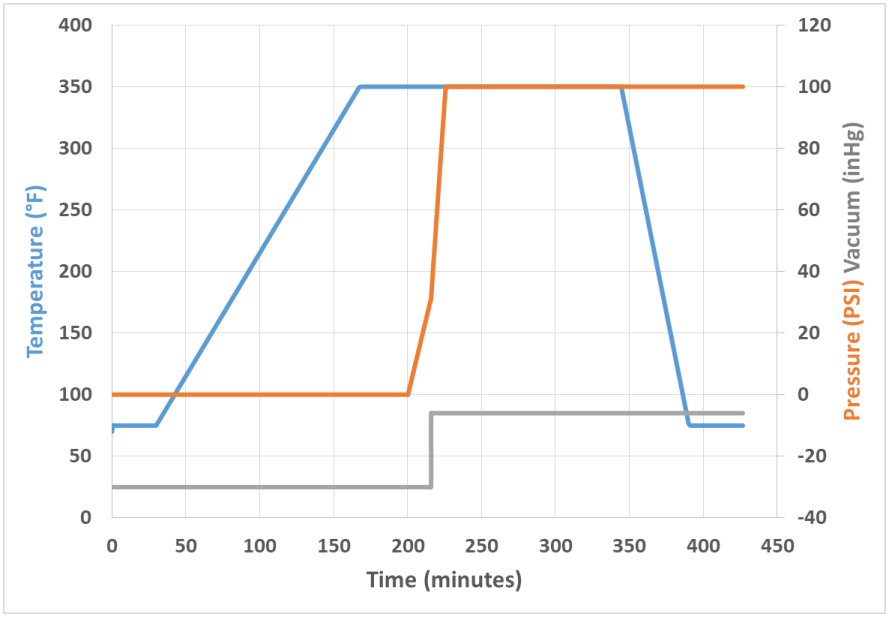

Figure 6. Autoclave Cure Cycle

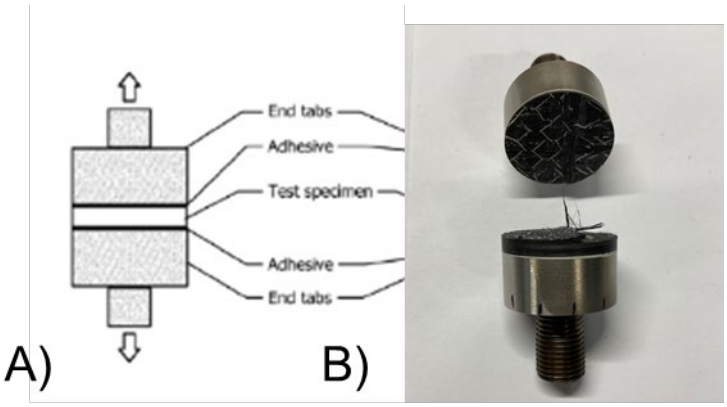

Figure 7. a) Nominal ASTM Standard ILT Sample, b) Example ILT Failure

Test specimens for the nominal (i.e., unstitched), and 8 stitch/cm^2 failed in the specimen cross section. This "valid" failure was the desired mode of failure. However, interlaminar tensile (ILT) test results for 16 and 30 stitches/cm^2 are noted to be "extrapolated values." This is due to the fact that ZSK machine is incapable of stitching through 1" thick carbon preforms specified by the ASTM standard as the size required to taper specimen edges to concentrate load away from the adhesive used to mount the carbon sample to the steel pucks. With this limitation in mind, specimens were fabricated with a uniform thickness assuming that the FM1000 adhesive mounting samples to the steel would be appreciably stronger than the test specimen resin/stitch interfaces. This was shown to be true for baseline, and 8 stitches/cm^2. Problems arose during the testing of 16 and 30 stitches/cm^2 ILT specimens. These specimens all failed at the adhesive interface. It is assumed that the buildup of Kevlar, polyester and glass backing cloth provides a poor surface for adhesion. The stated linear ILT strength value is a linear extrapolation calculated based on the increase in peak average load seen as stitch density increased. Several additional samples were tested at the end of the program to explore how the orientation and type of backing cloth impacted the ILT results. These samples were tested at UDRI and had no through thickness stitching. The sample used Kevlar and Polyester stitching of various densities to increase the buildup of the thread on the edge adhered to the metallic substrate. When this stitch was ground down to the carbon fiber the samples were found to fail in the material verifying the assumption that the reinforcing through thickness Kevlar in the ILT samples resulted in the interface failure for the 16 and 30 stitch/cm^2 samples. An image of the failed adhesive interface is shown in Figure 8. The characterization of change in ILT was critical to capture for the computational model, in order to understand how to scale the cohesive strength between layers of preform in the finite element package. The summary of ILT strengths are included in the final material characterization Table 2.

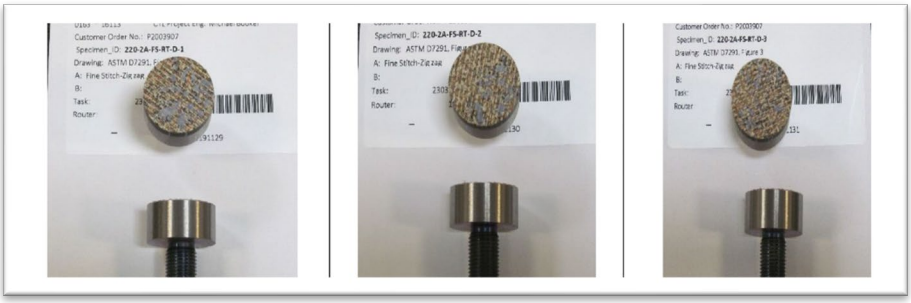

Figure 8. Sample ILT Adhesive Failures at Interfaces

Fracture Toughness

The next round of testing involved the characterization of the improvement in mode I and mode II fracture toughness due to increasing stitch densities. Mode I samples were tested according to the ASTM D5528, while Mode II was tested according to ASTM D7905. Sample geometries are shown below in Figure 9. Samples were fabricated with an initial Teflon insert to produce the mid-plane delamination. The increase in reinforcing stitching was expected to greatly increase Mode I toughness due to the alignment with the load direction of the Kevlar as shown in the work by Huelskamp et al [13]. The impact of Kevlar on the Mode II toughness was not previously explored, but a brief literature survey has found several studies that have found it positively impacted performance [14-15]. A simplified diagram of the stitch locations relative to the Teflon insert is shown in

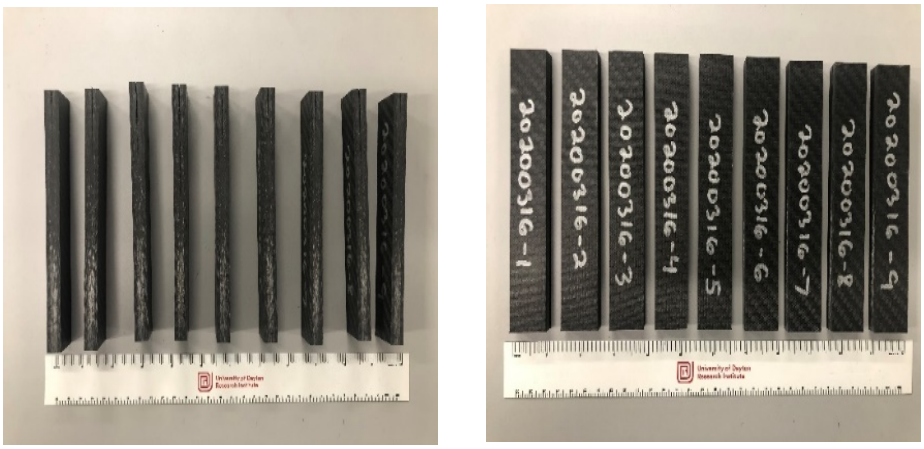

Figure 9. Mode I and Mode II Test Samples

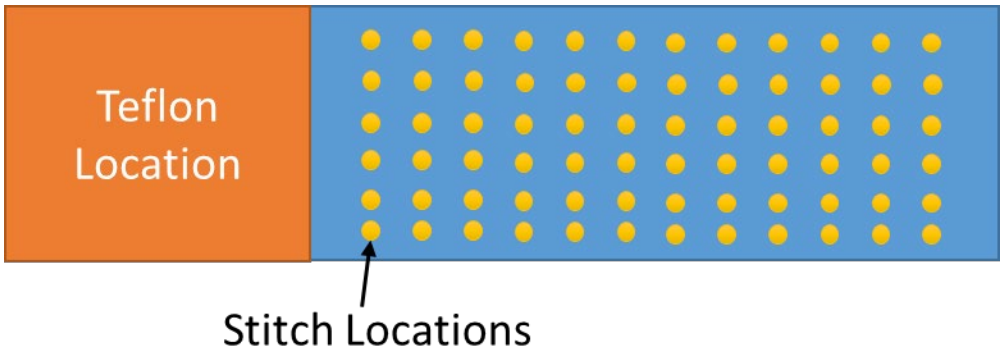

Figure 10. Stitch Location Diagram for Mode I and Mode II Samples

Initial testing of Mode I samples verified the initial assumption that increasing reinforcement led to an increase in toughness. Initial Mode II testing showed a slight improvement in performance, but samples were incorrectly cut too short in the length direction when compared to the ASTM standard. This resulted in samples needing to be moved relative to the loading plane during the testing. This horizontal shift in test configuration was due to a mismarked Teflon insert edge location. Samples were cut to the marked size, and it was later identified that the Teflon insert was shifted slightly after viewing specimens edge on. Concerns

about this horizontal shift led to a second round of Mode II testing. The completion of this second round of testing verified that the incorrect specimen geometry skewed results. The new round of testing showed a significant increase in Mode II toughness at stitch densities of 16 and 30 stitches/cm^2. Whilst ILT strengths were shown to increase by over 60%, the increase in toughness varied between failure modes. Mode I toughness was found to increase by over 1000% (from a baseline of 0.547 kJ/m^2 to 7.85 kJ/m^2), while Mode II toughness increased by roughly 80% (from a baseline of 1.38 kJ/m^2 to 2.54 kJ/m^2). Total results with standard deviations are shown in Table 2. A sample curve showing how Mode I fracture toughness varies as a function of stitch density is shown in Figure 11.

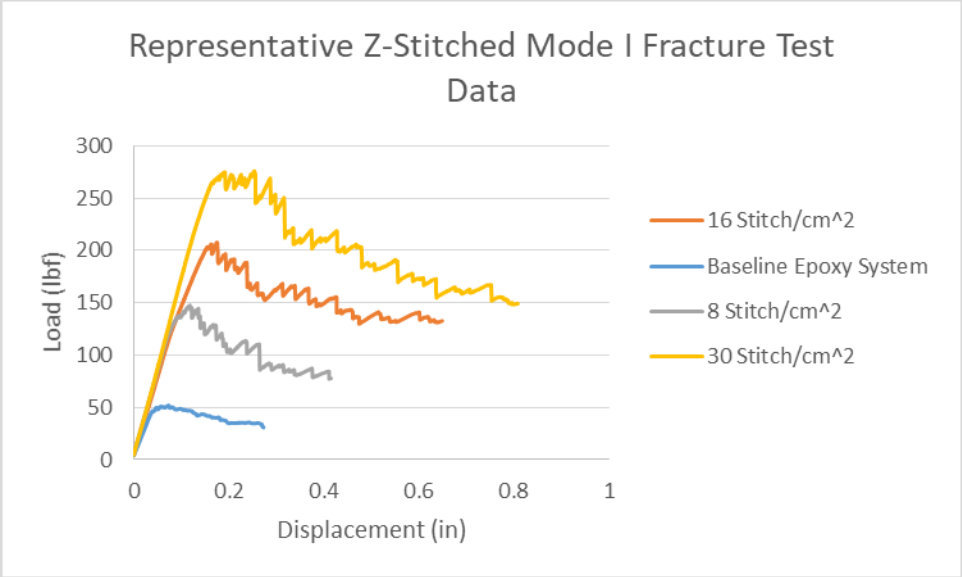

Figure 11. Representative Mode I Fracture Toughness Testing Data as Function of Stitch Density

In-plane Properties

Alongside the characterization of how reinforcing threads improved the ILT and toughness values characterization of the impact stitching had on in-plane mechanical properties was explored. Each of these tests were conducted according to the mechanical characterization table shown above. A sample of test data derived from ASTM D3039 for standard in plane tensile response is shown below. This was conducted for the 0°, or fiber aligned direction, as well as for the 90° material direction. The strength and moduli were measured for both of the test directions. The general trend for the 0° direction is shown in Figure 12a and shows a downward trend in strength and modulus correlating to an increase in fiber misalignment as a function of increased stitch density. This is not a definitive trend due to the high degree of variability in test results shown by the high standard deviation. For the 90° test direction, the strength increases with increasing stitch density, while modulus sees a minor decrease as a function of stitch density. This trend in modulus is shown in Figure 12b. The manufacturer specifies this material having a strength of 400 ksi when prepreged. This form of the material is constructed with a different epoxy resin, and has a much more uniform fiber distribution and alignment. Uni-directional pre-preg is also normalized to a 60% fiber volume fraction. For this standard testing on this program the 0° test specimens have an average volume fraction of 54.8%, while the 90° specimens have a volume fraction of 59.5%. The reduction in in-plane modulus and strength, relative to the uni-directional pre-preg, is a result of the local fiber mis-alignment due to through thickness stitching, and the form factor used for fabrication. For this experimental effort the primary concern is the relative change in performance compared to the baseline (i.e un-stitched) material. As the material is stitched in the through thickness direction it is expected to distort local fiber alignment leading to a reduction in modulus and strength. This trend is verified in the material test data.

This process was repeated for all other stated standard tests to gather a summary of test data. Testing for the actual Kevlar reinforcement thread was also conducted in order to verify the strength of the stitching thread. A summary of the mechanical properties/performance can be seen in Table 2. Data highlighted in blue shows the comparison in Mode II toughness between the original, incorrectly sized samples and the new correct samples. ILT test data at 16 and 30 stitches/cm^2 is highlighted in a shade of yellow to indicate it was linearly interpolated. A key measure taken from this test data is the improvement in mode I toughness, and ILT strength where an improvement greater than 50% is achieved, meeting the program milestone. This improvement in toughness is crucial to improving total performance.

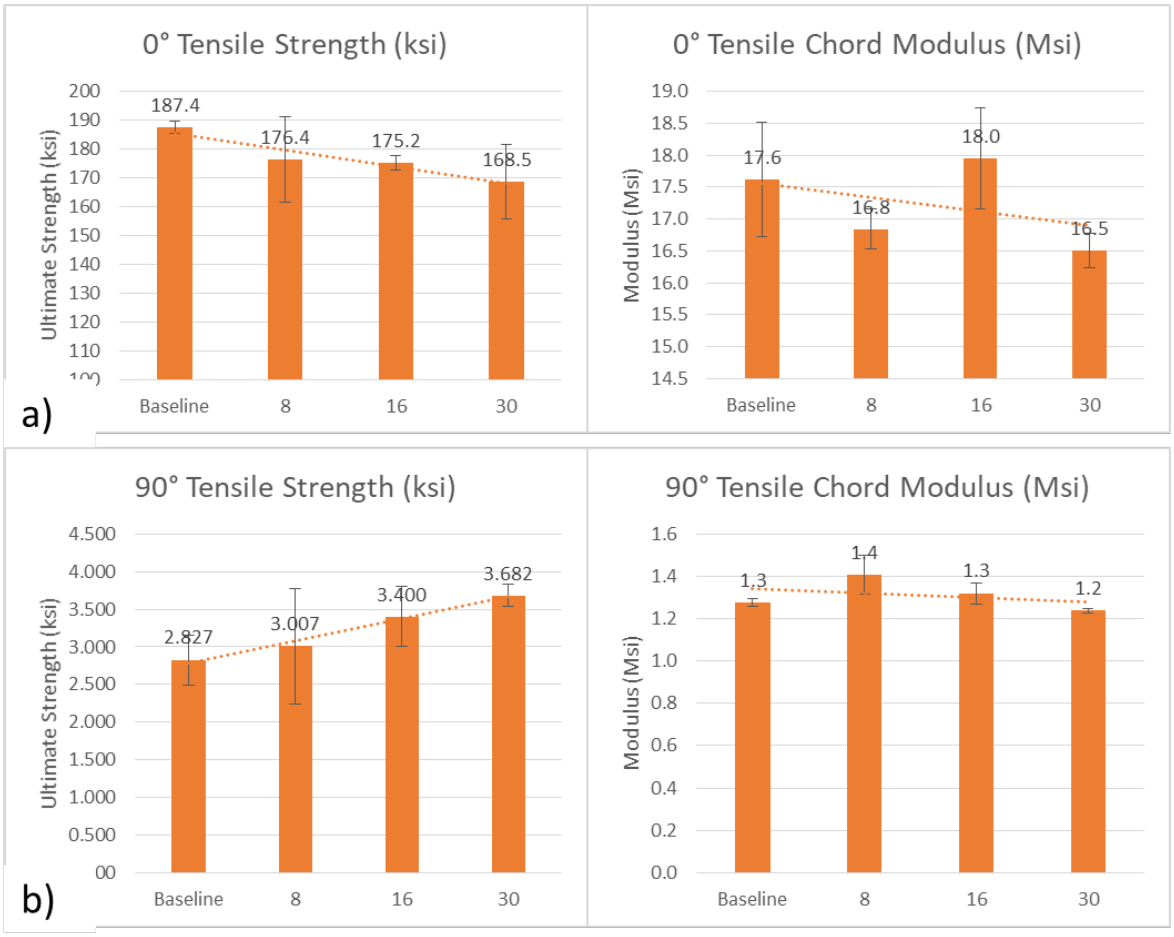

Figure 12. a) 0° Tensile Modulus and Strength, b) 90° Tensile Modulus and Strength

In addition to mechanical testing for characterization, non-destructive inspection was conducted utilizing X-Ray computed micro-tomography (μCT). Small scale samples of stitched material (approximately 0.25”x0.5”) were cut from scrap material and scanned in an Xradia Versa 520. Scans were completed with a voxel size 24.5 microns, using a voltage of 145 kV and a current of 55 amps. Scans took approximately 12 hours to complete and were done over several different sample sizes. These scans were utilized to characterize the “distortion” of fiber directionality as a function of stitching. A breakdown of the characterization process from the CT data is shown in Figure 13. The figure breaks down an initial look at in-plane distortions, followed by high lights of sections that were measured, and finally a breakdown of distortion size throughout the material. In addition to measuring the distortion size, the change in angle relative to principal fiber direction was calculated as well. The principal change in angle was found to be

consistently between 1.2° and 2.4° from the principal fiber direction. This distortion was found to result in an elliptical distortion that is 0.29 mm wide and approximately 4 mm long. It was found that at the interface between plies (especially the 0/90°) ply interface, larger angular distortions (~22°) could occur. These were relatively rare (<5% of stitch locations/interfaces) but were noted for reference as an occurrence. These local distortions reduce the uniformity of the fiber load path due to fibers no longer being perfectly aligned. This local stitch distortion leads to stress concentrations at the stitch locations due to the change in fiber direction during loading. The fiber cannot straighten under load due to the cured epoxy matrix, leading to a reduction in in-plane mechanical performance compared to the baseline data.

Table 2. T700/RTM6 Carbon Epoxy Material Characterization Test Data Summary

	Baseline	St dev.	8 s/cm^2	St dev.	16 s/cm^2	St dev.	30 s/cm^2	St dev.
E11 - Tension (GPa)	121.35	6.14	115.83	2.14	124.11	5.45	113.76	1.86
0° Strength - Tension (MPa)	1292.08	14.89	1216.24	102.66	1207.96	16.48	1161.77	88.87
E11 - Compression (GPa)	106.18	5.28	104.8	2.3	104.11	5.15	108.25	12.23
0° Strength - Compression (MPa)	924.59	8.27	814.27	9.65	586.05	45.51	492.96	81.36
E22 - Tension (GPa)	8.963	0.14	9.653	0.62	8.963	0.34	8.274	0.07
90° Strength - Tension (MPa)	19.49	2.28	20.73	5.24	23.44	2.76	25.39	1.03
E22 - Compression (GPa)	9.101	0.35	9.101	0.25	8.549	0.17	8.825	0.18
90° Strength - Compression (MPa)	188.32	3.43	188.27	2.14	190.04	1.83	201.44	2.65
Mode 1 Toughness (kJ/m^2)	0.547	0.08	2.3	0.14	4.77	0.29	7.85	0.35
Mode 2 Toughness (kJ/m^2)	1.49	0.07	1.77	0.33	1.38	0.42	1.75	0.64
Mode 2 Toughness (kJ/m^2) - Redo	1.38	0.16	1.86	0.06	1.88	0.21	2.54	0.61
ILT (MPa)	19.54	0.43	22.99	1.03	26.3	N/A	32.34	N/A
Kevlar Strength (MPa)	1909.3	28.34						
G12 (MPa)	5311.03	28.96	5028.34	113.07	4955.26	15.17	4962.85	77.91
G21 (MPa)	4382.31	48.26	3860.37	172.37	3758.33	77.91	4149.26	242.01
S12 (MPa)	71.56	1.79	75.02	1.45	73.77	4.27	80.7	3.72
S21 (MPa)	43.98	3.65	36.47	3.03	36.54	1.31	34.61	1.93
IPS 3-1 (MPa)	53.99	2.62	51.5	1.93	52.88	3.03	49.09	1.59
IPS 3-2 (MPa)	60.54	2.41	58.61	1.38	57.78	3.59	57.43	0.83
Newest test data								
Interpolated Value								

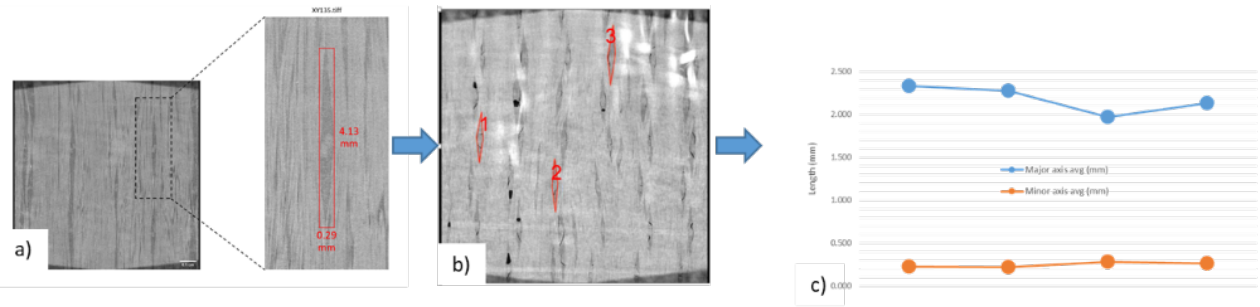

Figure 13. a) In Plane CT Scan of Fiber Distortions, b) Distortion Locations for Characterization, c) Tabulated Distortion Measurement Lengths

Sub-Component Testing

After completing the mechanical characterization testing, two complex comparison tests were derived in order to test the computational predictive capability of the finite element package BSAM. These tests were based on ASTM D5961 (Bearing Shear) and ASTM D6415 (Curved Beam Strength). Bearing shear panels were fabricated using an autoclave process as described for the characterization test panels. Angled bracket samples were fabricated using the same cure cycle, on the tooling shown in Figure 14 below. The tooling has a tool radius of ¼", and was sprayed with a silicone-based release agent, between the Teflon sheets and tool surface prior to specimens being laid up on the tool. These panels were fabricated using the same T700/RTM6 combination. Bearing shear components were fabricated with Layup 1: $[45/90/-45/0]_s$, and Layup 2: $[45/-45/0_2/90]_s$. Each of these bearing panels were uniformly stitched across the entirety of the specimen with a stitch density of 30 stitches/cm^2. Angled bracket preforms were fabricated with Layup 3 $[90/45/-45/0]_s$ and Layup 4 $[45/90/-45/0]_s$. These curved beam samples were stitched at 8, 16, and 30 stitches/cm^2 in the curved beam region. Figure 15 shows the diagram of the 1.5" wide region of stitching on the angled bracket preforms, alongside an image of a polished cross section where Kevlar stitches (at a density of 30 stitches/cm^2 are shown.

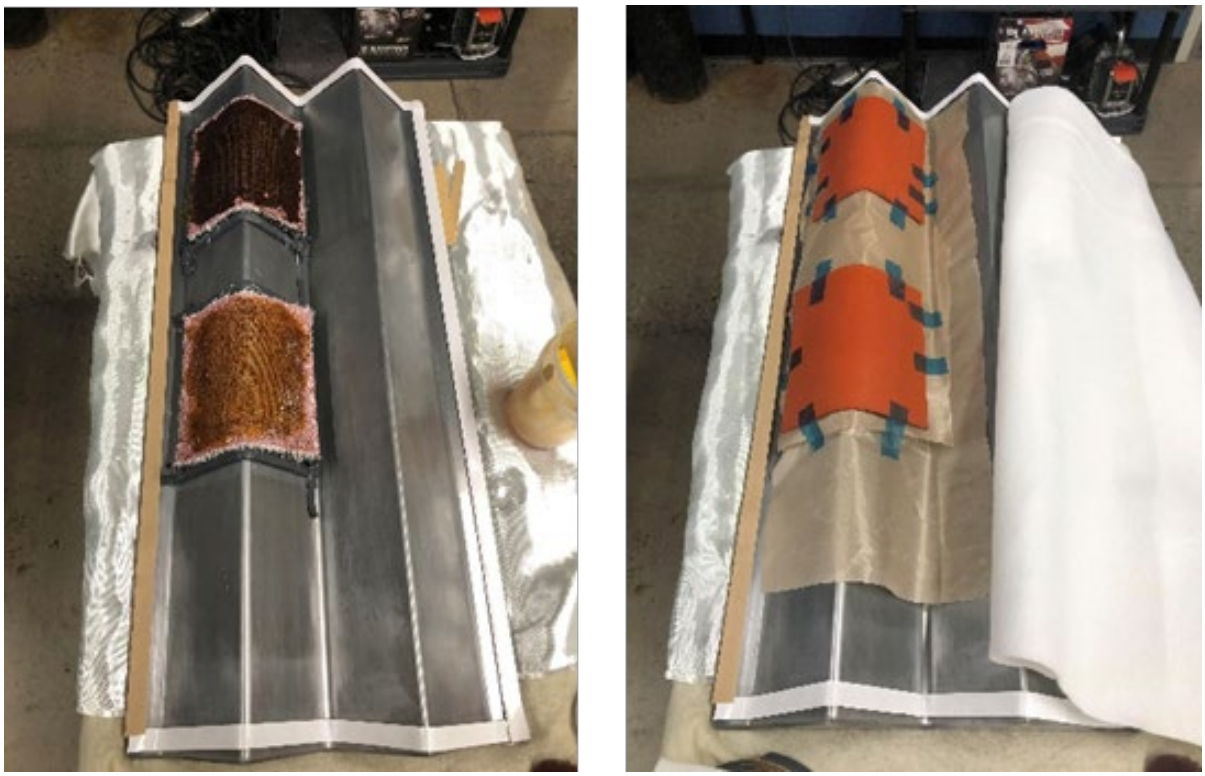

Figure 14. ASTM D6415 Angled Bracket Layup and Tooling

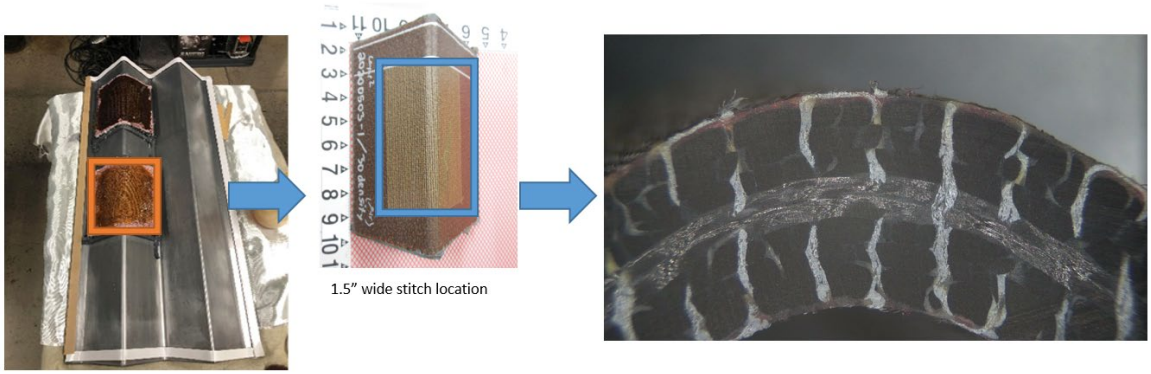

Figure 15. Angled Bracket Stitch Location Diagram with Close up of Stitched Cross Section

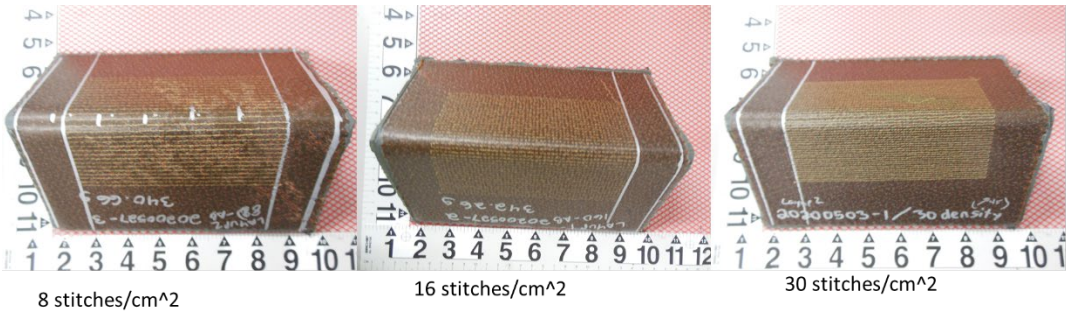

Figure 16. Angled Bracket Coupon Comparison

Laminate 1 $[45/90/-45/0]_s$, and laminate 2 $[45/-45/0_2/90]_s$, which were tested as bearing shear samples, were machined and tested according to ASTM D5961. Five test specimens of each laminate sequence were tested and the results can be seen in Table 3. The results show that laminate 1 ($[45/90/-45/0]_s$), surprisingly had a higher bearing strength compared to laminate Type 2 ($[45/-45/0_2/90]_s$). Since laminate type 2 had two additional zero degree plies it was expected to outperform laminate type 1. Figure 17 shows the nominal stress vs. strain curves for each of the stacking sequences, while Figure 18 shows the failed specimen geometry. An interesting observation is that the failure surface of laminate 1 exhibited significantly higher matrix cracking compared to laminate 2. Both panels ultimately failed in bearing at the hole location.

Table 3. T700/RTM6 Carbon Epoxy Stitched at 30 Stitches/cm^2 ASTM D5961 Bearing Shear Results

Panel 1 Resin Infused, TFP Panel 1 [45/90/-45/0]s (20200514-1)						
Specimen ID	**Max. Load (lbf.)**	**Displ. At Max. Load (in.)**	**Axial Ext. At Max. Load (in.)**	**Bearing Strain at Max. Load (in/in.)**	**Bearing Stress (ksi)**	**Failure Code**
514-1-0-0°-DBS-1	6178.7	0.044	0.03129	0.12516	102.7	B1I
514-1-0-0°-DBS-2	5937.9	0.044	0.03074	0.12247	101.5	B1I
514-1-0-0°-DBS-3	5939.7	0.046	0.03290	0.13030	102.3	B1I
514-1-0-0°-DBS-4	6143.4	0.048	0.03564	0.14171	105.7	B1I
514-1-0-0°-DBS-5	5990.4	0.049	0.03518	0.13988	102.6	B1I
Average:	**6038.0**	**0.046**	**0.03315**	**0.13190**	**103.0**	
Std. Dev.:	**115.0**	**0.002**	**0.00222**	**0.00124**	**1.6**	
COV (%):	**1.9**	**4.9**	**6.7**	**5.4**	**1.6**	
Panel 2 Resin Infused, TFP Panel 2 [45/-45/0_2/90]s (20200514-2)						
Specimen ID	**Max. Load (lbf.)**	**Displ. At Max. Load (in.)**	**Axial Ext. At Max. Load (in.)**	**Bearing Strain at Max. Load (in/in.)**	**Bearing Stress (ksi)**	**Failure Code**
514-2-0-90°-DBS-1	7070.3	0.048	0.03510	0.13929	97.8	B1I
514-2-0-90°-DBS-2	6798.6	0.042	0.03053	0.12139	96.3	B1I
514-2-0-90°-DBS-3	6906.7	0.055	0.04090	0.16230	98.6	B1I
514-2-0-90°-DBS-4	6743.3	0.041	0.02866	0.11350	96.3	B1I
514-2-0-90°-DBS-5	6763.9	0.063	0.05065	0.20059	96.5	B1I
Average:	**6856.6**	**0.050**	**0.03717**	**0.14742**	**97.1**	
Std. Dev.:	**135.1**	**0.009**	**0.00889**	**0.00077**	**1.0**	
COV (%):	**2.0**	**18.6**	**23.9**	**3.2**	**1.1**	

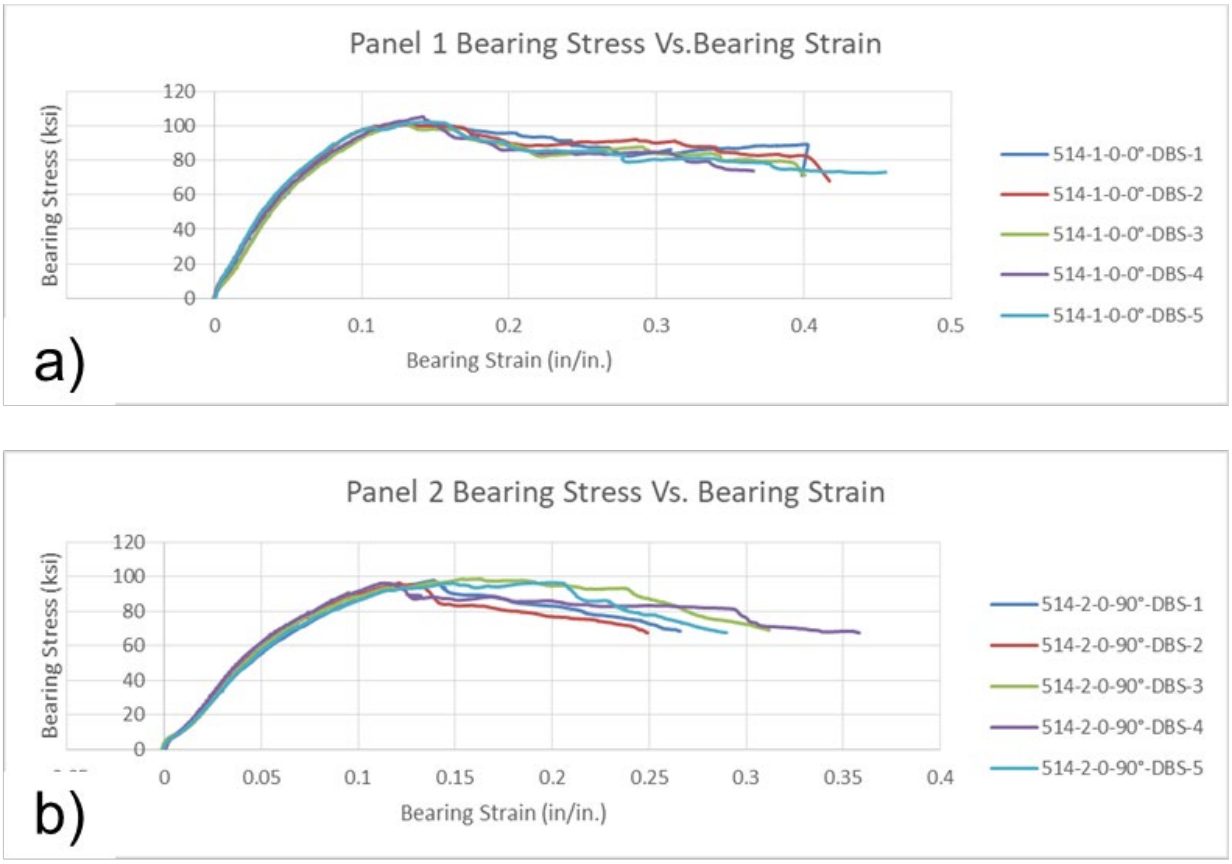

Figure 17. Nominal Bearing Stress vs Strain for TFP Preforms a) Laminate 1, b) Laminate 2

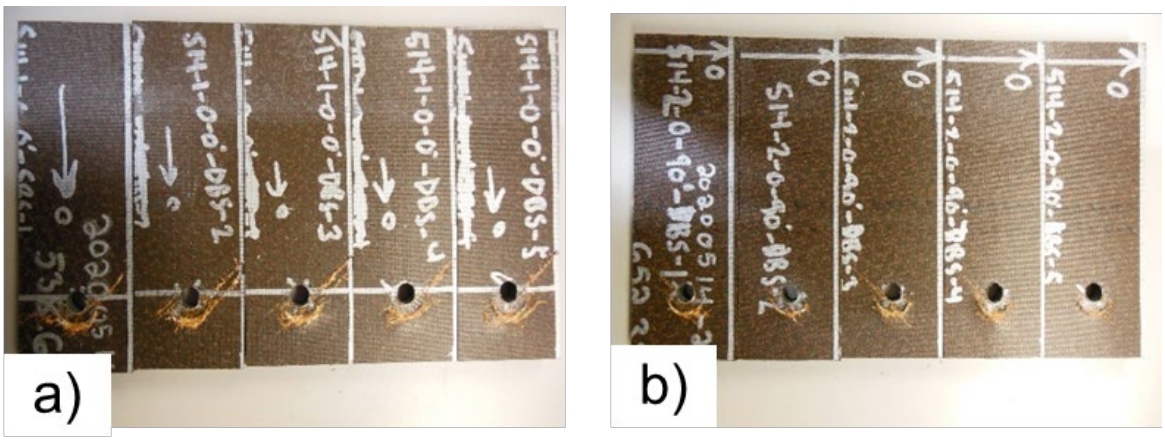

Figure 18. Test Specimen Geometries A) OCC Specimen, B) OCT Specimen

Angle brackets were fabricated and tested according to ASTM D6415. Test results showed that an increase in

stitch density led to an increase in curved beam strength. Failure of both test laminates was concentrated in radius of curvature. During loading, damage accumulated in the specimens until total failure occurred at the onset of widespread delamination. This can be seen in Figure 20, where the edge on view of each test specimen is shown to provide an image of delamination growth and matrix cracking. For each labeled section layup 3 ($[90/45/-45/0]_s$) is the upper image, while laminate 4 ($[45/90/-45/0]_s$) is the bottom image. Table 4 shows the summary of test results from the experimental testing. An additional outcome of this testing is that layup 4 exhibits increased stiffness compared to layup 3. In the radius of curvature fiber failure can be seen on the inner radius of the post failure test specimens.

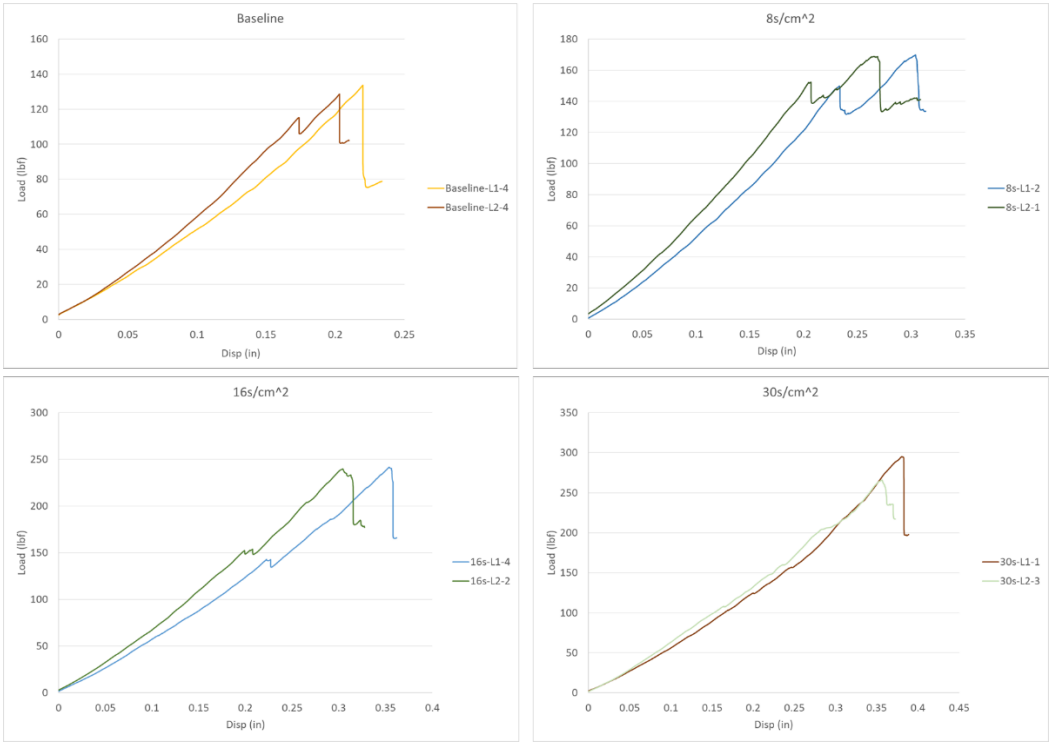

Figure 19. T700S/RTM6 Angled Bracket Comparison of Layup 3 and 4 at Various Stitch Densities

Table 4. T700/RTM6 Carbon Epoxy ASTM D6415 Curved Beam Strength Results

IACMI 5.7 Curved Beam ASTM D		AVERAGE RESULTS			
Layup	**Specimen**	Curved Beam Strength	σ_r^{max}, radial stress component in curved segment, (Ksi), Eq.7	σ_r, radial stress component in curved segment, (Ksi), Eq. 4	Average Load (lbs.)
Layup 3	513-2-0-L1-CBS-1	79.67	1.85	1.83	126.27
	422-1-8-L1-CBS-1	95.31	2.04	2.01	161.35
	527-2-16-L1-CBS-1	127.90	2.55	2.46	235.65
	422-2-30-L1-CBS-1	140.61	2.91	2.85	293.33
Layup 4	513-3-0-L2-CBS-1	80.92	1.89	1.88	122.77
	527-3-8-L2-CBS-1	106.19	2.18	2.12	169.69
	527-1-16-L2-CBS-1	144.78	2.82	2.74	247.51
	503-1-30-L2-CBS-1	140.26	2.98	2.90	281.72

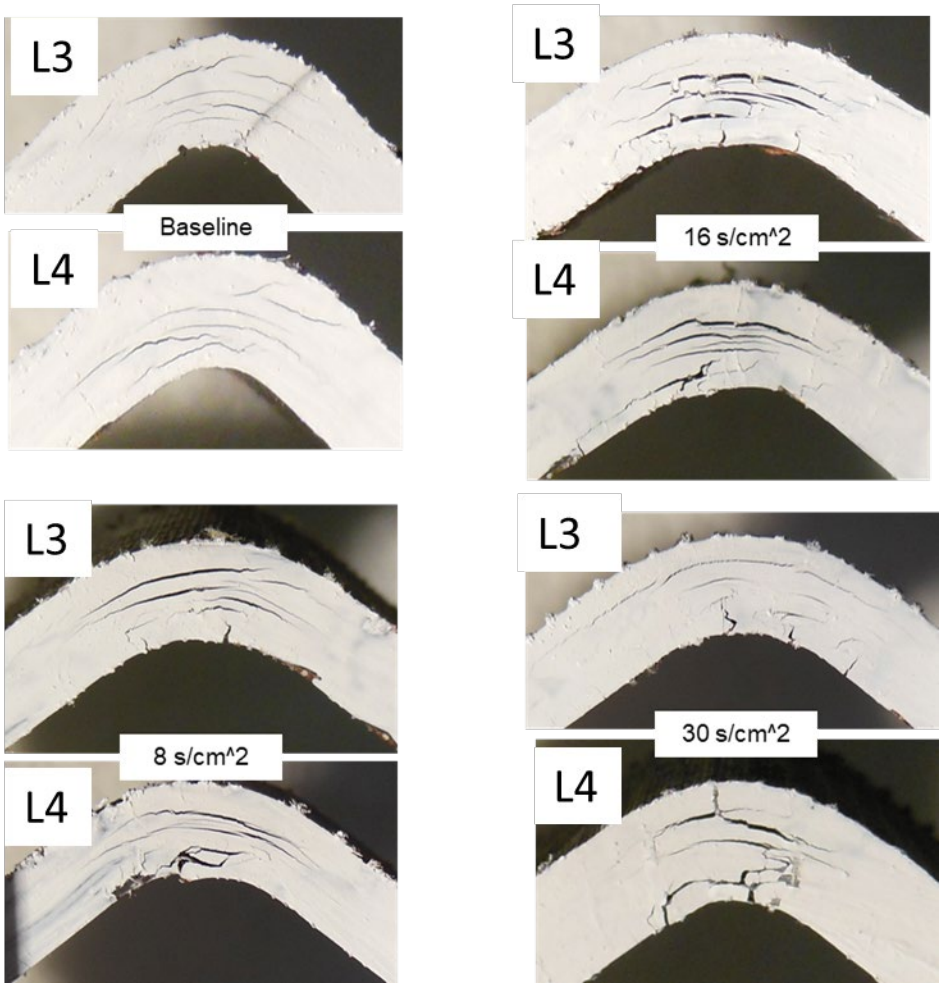

Figure 20. Curved Beam Strength Failed Test Specimens

TFP Inserts

Alongside the fabrication of components using only TFP preforms, UDRI explored the use of TFP inserts to provide local reinforcement at desired locations. This design was proposed after discussions with Lockheed Martin's Robert Koon. His stated interest led to the exploration of using TFP inserts to provide local reinforcement. Initial designs can be seen in Figure 21 below, where sample designs vary from a radial stitch to circular loops of decreasing diameters. The spiral design was quickly eliminated from contention due to large increase in thickness driven by the sharp turn around as material laid down increased. This thickness resulted in a non-uniform thickness increase and was expected to produce difficulties during testing. After eliminating the initial radial spiral design UDRI began building a variety of circular designs, using 24k, 3k, and 1k carbon fiber tows. Designs explored mounting on glass fiber backing cloth as well as on carbon veils. The desired stress design limit for a quasi-isotropic prepreg unidirectional laminate was given by Lockheed as 141.36 ksi (974.64 MPa) for a quarter inch bearing hole, with ratios of t/D = 0.53, w/D =6, and e/D = 3 (from the ASTM standard).

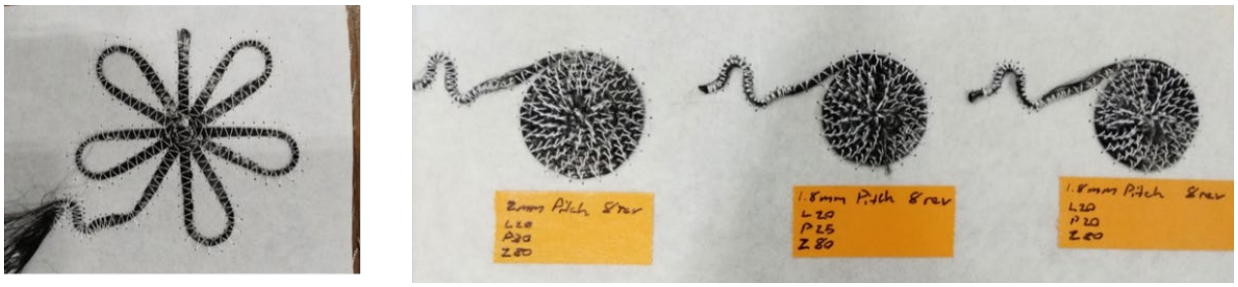

Figure 21. Preliminary Stitched TFP Insert Designs

Samples tested for this work can be seen in Table 5 below. Several different stacking sequences were fabricated and tested, including baseline samples and those without doily inserts. Not only were there different laminate stacking sequences, but the individual laminate, doily insert type and failure loads can be seen. Baseline samples were constructed for comparison against doily inserts. Several stacking sequences were explored, as were different doily designs. Three different TFP insert types were constructed, 1 using 24k tow and two using 3k tow. These bearing samples were constructed from IM7/MTM45-1 unidirectional prepreg provided by Lockheed Martin. TFP inserts were constructed using T700 (for the 24k tows), and IM7 fibers (for the 3k tows). The table references an "optimized" design for the last doily insert. The development of the optimized design is discussed in detail in the modeling section. The principal difference between the TFP designs is the shape of the preform inserted into the prepreg stack. The 24k circle, and 3k tow circle also did not utilize any additional resin to ensure total wet out of the preform stack. A close up view of the 3k tow circular doily is seen in Figure 22. These inserts relied on excess resin flow from the prepreg only. The optimized elliptical design included neat MTM45 resin film inserts at 160 gsm to ensure proper wet out. This resin was provided as neat resin film to test doily wet out by the resin manufacturer.

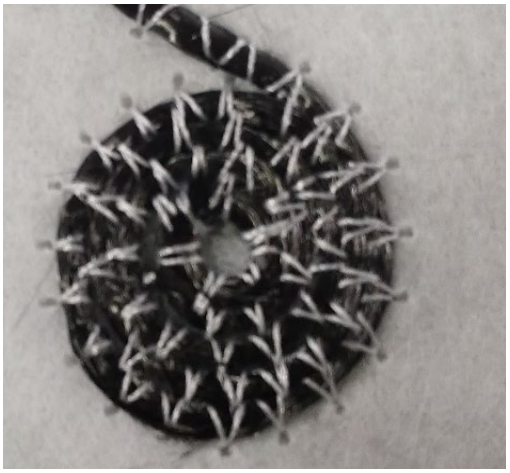

Figure 22. E34k Circular Doily

Table 5. Bearing Shear with TFP Insert Results

Bearing Layup	TFP Insert Type	Experimental Peak load (N)	Model Failure Stress (MPa)	%Change Load	%Change Thickness
$[45/0/-45/90]_{3s}$	N/A	16785.71	920.60	N/A	N/A
$[45/-45/90/0/0]_{2s}$	N/A	14136.45	896.64	N/A	N/A
$[45/-45/90/0/0/Doily/45/-45/90/0/0]_s$	24k Tow circle	24681.80	790.40	74.60	76.6
$[45/-45/90/0]_{2s}$	N/A	14852.39	930.82	N/A	N/A
$[45/-45/Doily/90/0/45/-45/90/0]_s$	3k Tow Circle	15482.04	773.70	4.24	44.5
$[45/-45/Doily/90/0/45/-45/90/0]_s$	3k Tow Ellipse (from Optimization)	15675.53	839.26	5.54	29.3

As can be seen in Table 5, the inclusion of the 24k tow led to a massive increase in part thickness and total peak average load, however the total percentage increase in thickness exceeded the increase in load bearing capability. This increase in thickness produces a reduction in bearing strength. Figure 23 and Figure 24 show the comparisons of load vs. displacement for each insert type against the relevant baseline. These show that not only do the inserts increase the total load required to reach failure, but they also increase the initiation strength and toughness (area under curve). This increase is desirable from a designer standpoint as it leads to slower failure and increases the design space, while being able to directly place reinforcement without the traditional ply build up or metallic inserts. Discussions were conducted with Lockheed to determine if the increase in load is used to calculate stress based on the local thickness at the hole (which results in decrease in stress due to thickness build up), or if stress is more appropriately calculated based on far field thickness. After discussions with Robert Koon, it was determined that the local thickness build up was to be used resulting in a decrease in bearing stress. At this time Lockheed has decided not to pursue this approach further.

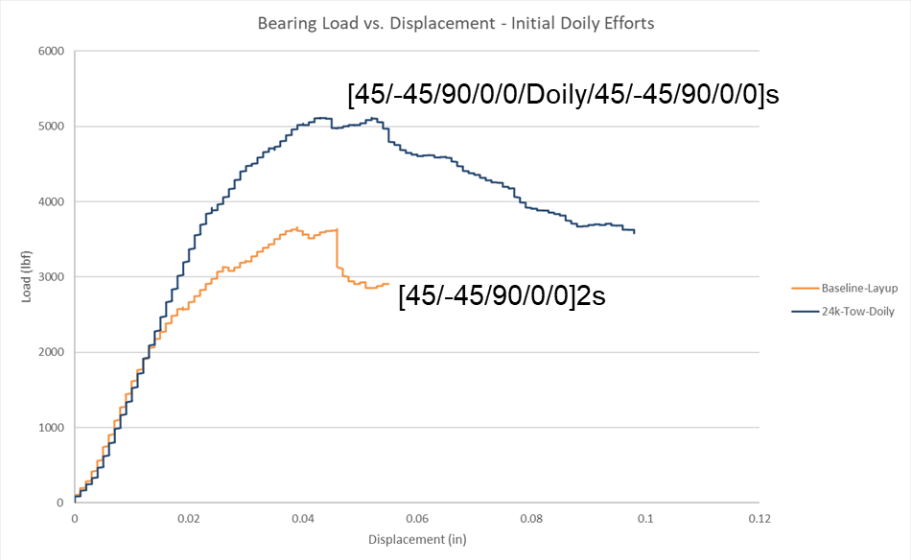

Figure 23. Comparison of Baseline Laminate to a 24k Tow Circle TFP Insert Laminate

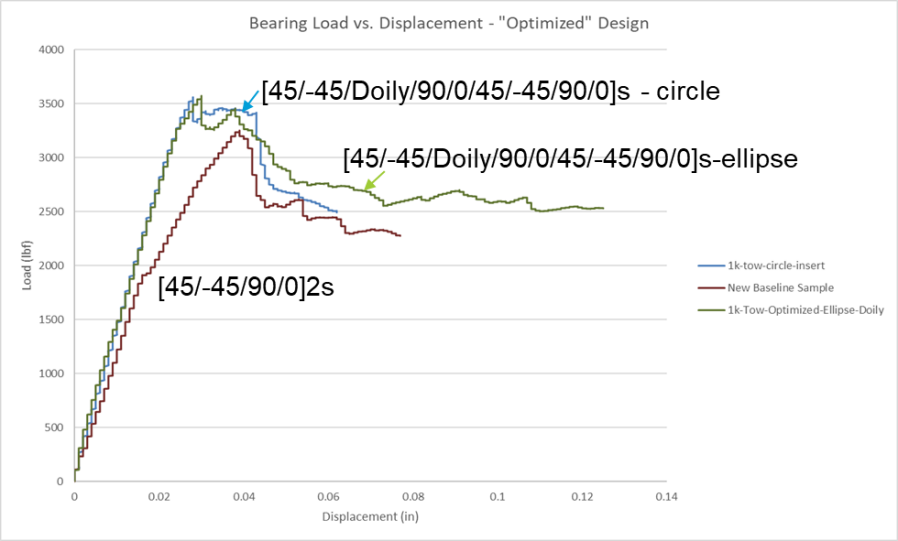

Figure 24. Comparison of Baseline Laminate to a 1k Tow Circle and 1k Tow Ellipse TFP Insert Laminate

Post failure analysis of the large doily inserts was conducted by sectioning to understand if the inserts properly wet out. Figure 25 shows a cut diagram of the sample of the 24k tow sample cross sections from the 24k preform insert. Figure 26a shows a far field of the sample corresponding to cut plane between location 2 and 3 on the cutting diagram. This shows the extent of delamination during loading, as well as capturing the fiber distortion due to the insert. Figure 26b shows what UDRI believes to be a void formed during fabrication. It is not clear what lead to void formation, but it was assumed that the large tow size of the doily insert led to the lack of fiber wet-out producing the void. This large void was part of the reason a smaller tow size and neat resin film was used on later design iterations. Failed sample images from the baseline laminate corresponding to the 24k tow circle are shown in Figure 27a, the damage from the baseline sample shows matrix cracks on the surface with fiber breakage on the surface due to the compression of the surface by the bolt washer. In Figure 27b the failure shows a large delamination coupled to the matrix split on the surface and fiber breakages. Failure images for the bearing samples with 3k tows are shown in Figure 28. The 3k ellipse and circular inserts show similar failure modes as the large two insert. This is shown in Figure 28 as the annotated matrix cracks, delaminations and fiber breakage.. The major takeaway from this effort is the delay in damage onset and massive improvement in toughness.

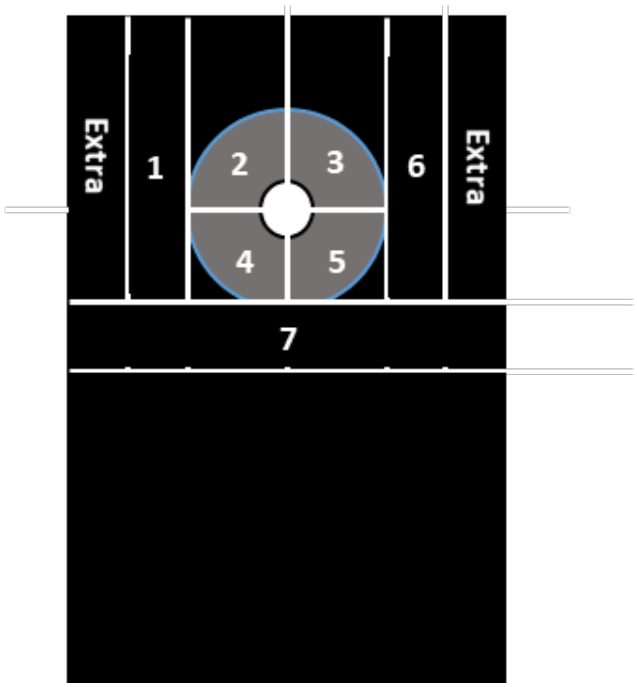

Figure 25. Cut Diagram for TFP Insert Sample (Blue Circle Corresponds to Nominal Doily Location)

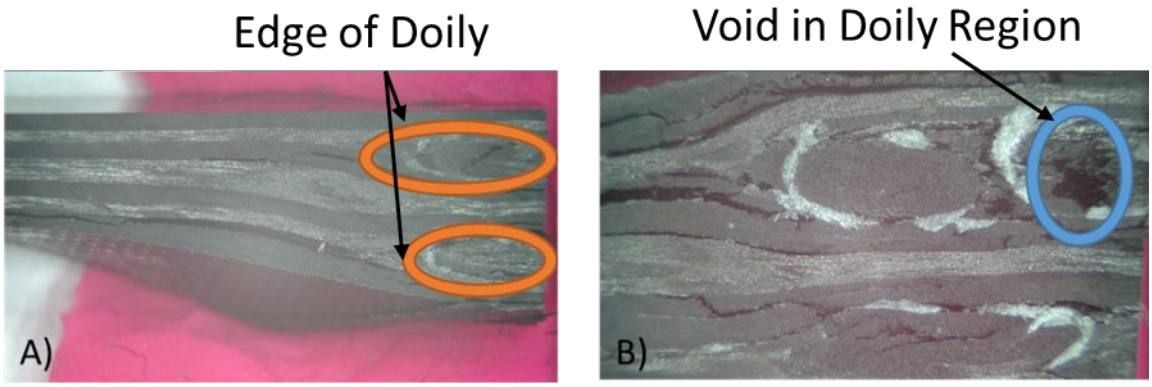

Figure 26. a) Sample Cut Plane 2-3, b) Void Formation Cut Plane 3-5(Orange Shows Doily Location, Blue Indicates Void

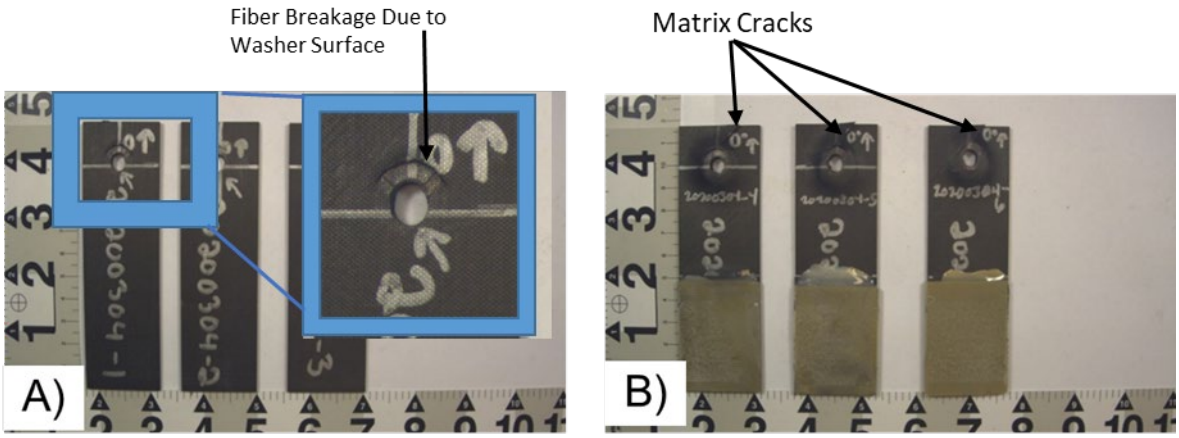

Figure 27. a) Baseline Sample – No TFP, b) 24k Tow TFP Insert Failure

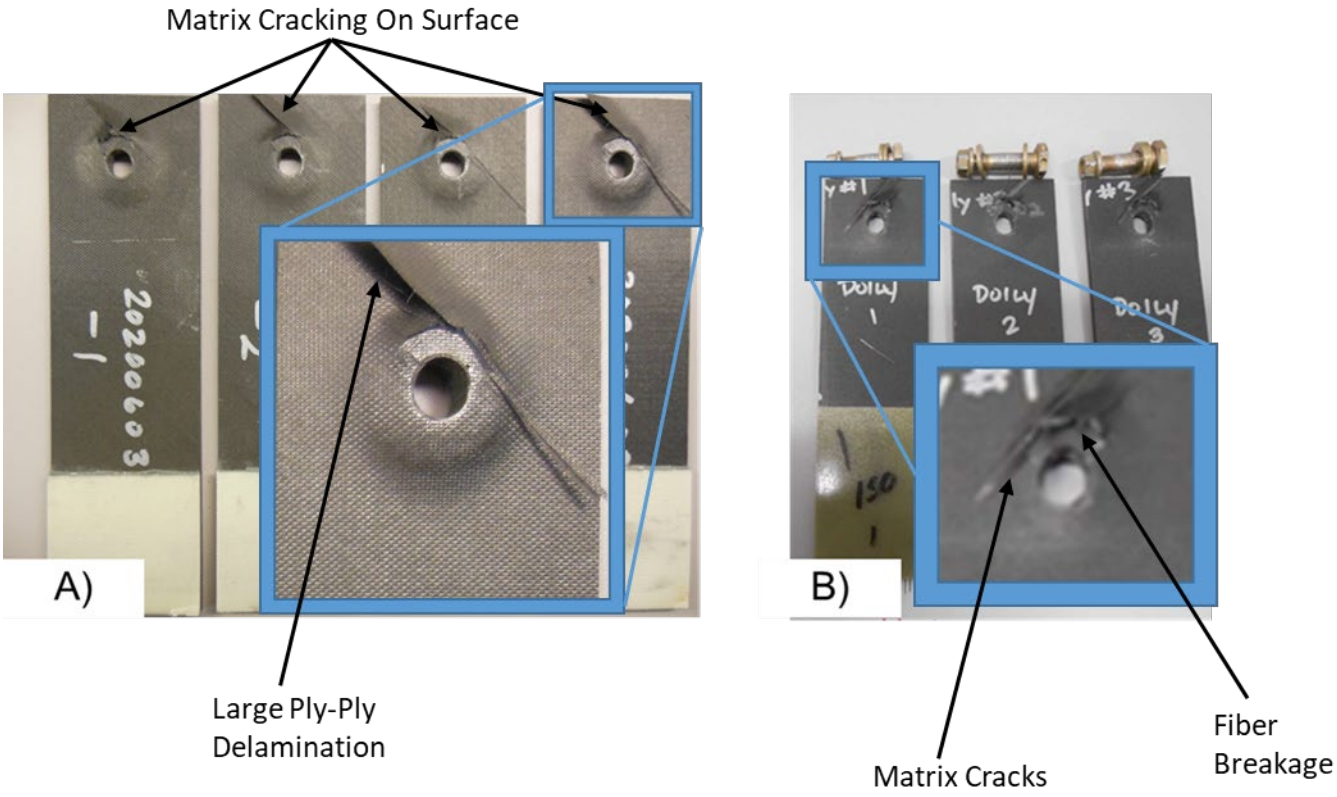

Figure 28. a) 3K Tow Circle Insert Bearing Failure, b) 3K Tow Ellipse Insert Bearing Failure

Lug Testing

The next phase of manufacturing and testing involved the fabrication of the large-scale lugs for tensile loading. These lugs were originally based on a paper [18] that explored the failure of a woven textile lug. The given part thickness in this paper was deemed too large for the available load frames at UDRI so the nominal thickness was cut from 38.2 to 19.1 mm as the target thickness. A drawing of the part geometry with the

locations where strain gauges were placed during testing can be seen in Figure 30. The nominal part dimensions were consistent between all specimens, while the inner diameter of the lug bearing surface changed depending on whether a hard point was inserted. This metallic hard point was bonded into the sample and therefore needed additional clearance in order to still fit the loading pin used to apply load. This resulted in the diameter of the bearing surface varying from 76.2 mm up to 81.2 mm for the hard point insert construction infused by Michigan State. This results in two distinct lug geometries fabricated on this program, the "nominal" construction with an inner diameter of 76.2 mm, and a "hard point" construction with an inner diameter of 81.2 mm. The additional clearance was required for the carbon sleeve that was part of the hard point construction as shown in .

The nominal lug component was fabricated using two different sub-laminate structures, where each ply was a pre-impregnated (RTM6 epoxy) twill weave fabric (Hexcel G986, that were then co-cured together. The sub laminate stacking sequences were laminate a: $[0/45/45/45/0]_{so}$, laminate b: $[0/45/0/45/0]_{so}$, and laminate c: $[0/45/45/45/0]_{so}$. The final part stacking sequence was: [(laminate a)/(laminate b)$_{11}$/(laminate c)]. Using the nominal lug design from the work by Wallin et al. [18], and recreated in Figure 29, as a starting point UDRI constructed several computational simulations to explore potential stacking sequences. These simulations explored 4 different stacking sequences, which are constructed of several sub-laminates. When stitching through parts using the TFP process, there is a limit to how thick of a part that can be stitched through without breaking the needle. The current best practice on the TFP machines utilized required each part to have a maximum thickness of 8 layers of the T700S fiber. For clarity each sub-laminate used in the part stacking sequence is enclosed in parentheses, while the total stacking sequence is enclosed in brackets. The first stacking sequence explored was $[(0_2/\pm45/90_2)\ (0_2/\pm45/90_2)(90_4)(\pm45/0_4)]_s$, and consisted of 8 sub laminates as indicated by the parenthesis. This stacking sequence failed in the simulation at a load of 290.1 kN. This was below the nominal design load of 298 kN needed to "meet" the performance of the woven preform in the reference paper. Stacking sequence two ($[(\pm45_3)\ (0/90)_4(0/90)_4]_s$) failed at 331.5 kN, while sequence three ($[(\pm45_3)\ (0/90)_3(0/90)_3(0/90)_2]_s$) increased that load even further to 335.1 kN. Due to machine limitations on the thickness of material that can be stitched through, stacking sequence two was not manufacturable, and stacking sequence four was found to fail sooner than any other construction and was excluded from consideration. It was decided that both stacking sequences one and three from the discussion above would be fabricated for testing. These sample stacking sequences are subsequently referred to as part lug laminate 1 and 2.

Each of these preforms is stitched on a glass fiber backing cloth that is fitted into the tooling mold as seen in Figure 32. In the mold resin flow channels can be seen for the 2 injection ports allowing resin to flow from both sides. An example of the constructed lug preforms is shown in Figure 33, where 4 of the different lug "sub-laminate" preforms are shown, alongside a diagram indicating stitch regions. Figure 33 shows the Kevlar stitch locations corresponding to the yellow threads seen on the sub-laminates. This stitching is not "joining" any part but used as a through thickness reinforcement for each of the sub-laminate preforms as described at the end of the first page of the "Lug Testing" section. This through thickness stitching passes through several layers of TFP fibers that correspond to plies within the sub-laminates, of which there are several stacking sequences (such as the sub-laminates $(0_2/\pm45/90_2)$, $(0_2/\pm45/90_2)$, (90_4), or $(\pm45/0_4)$). Each sub-laminate has stitching through all plies within the sub-laminate but no stitching crosses between sub-laminates due to limitations on the thickness that can be stitched through. All sub-laminate preforms are stacked in the tooling mold according to the prescribed laminate stacking sequence, with Figure 32 showing a singular sub-laminate in the tooling mold prior to the placement of all other sub-laminates (sub-laminates were stacked one on top of the other). After placing the sub-laminates in the mold the parts were infused with resin (sub-laminates are connected solely by the infill of resin during the RTM process).During final infusion and fabrication stitched "sub-laminate" preforms (described above as the "stacking sequences in parentheses) were stacked in the tooling mold without any additional stitching. Bearing inserts were purchased and hard point bolts/washer/nuts were fabricated as well. These can also be found in Figure 27. The bolts were fabricated out of a hardened steel in order to avoid any failure in the bolt during loading. The washers/nuts

were fabricated using sheet stock aluminum since their purpose was to simply contain excess resin flow during infusion of the hard point.

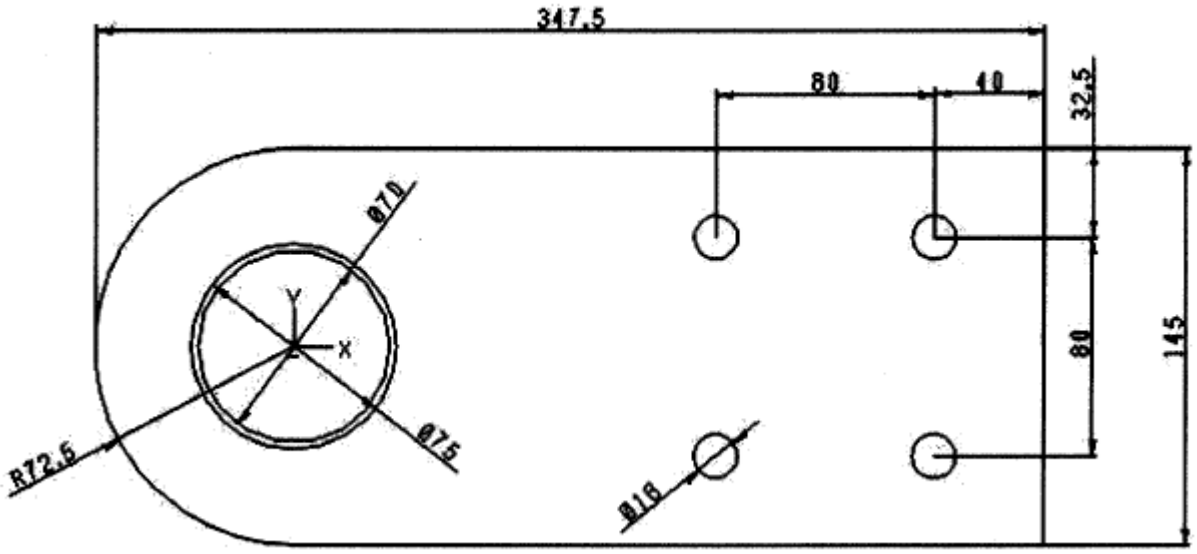

Figure 29. Nominal Lug Schematic Taken from Wallin Et. Al [18]

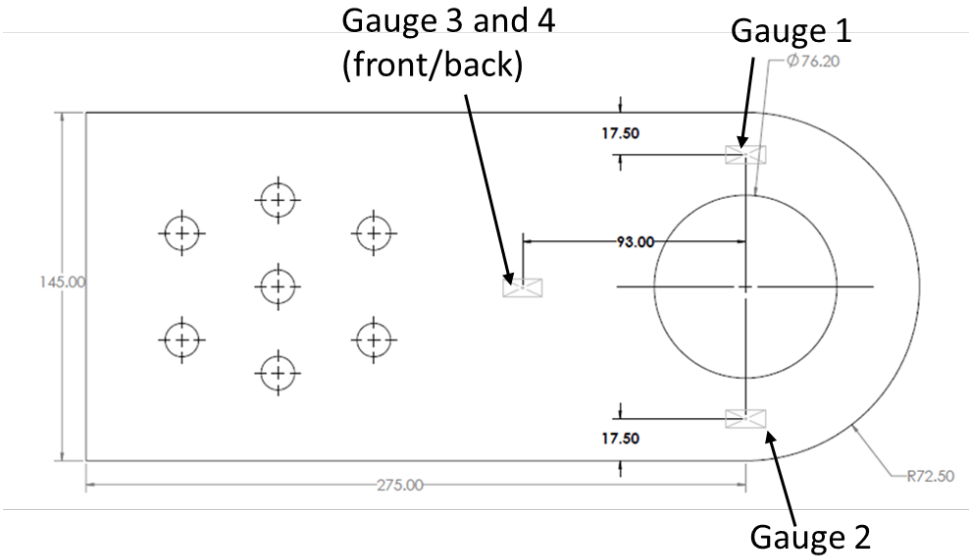

Figure 30. Nominal Lug Design with Tooling Mold Diameter set at 76.2 mm

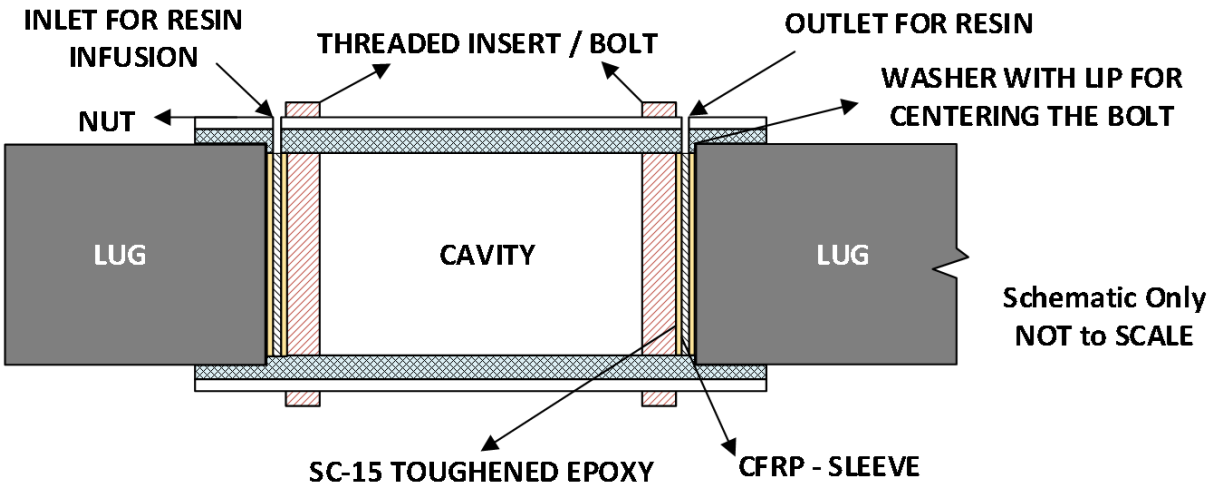

Figure 31. Diagram of the Hard Point Insert Construction for TFP Lug

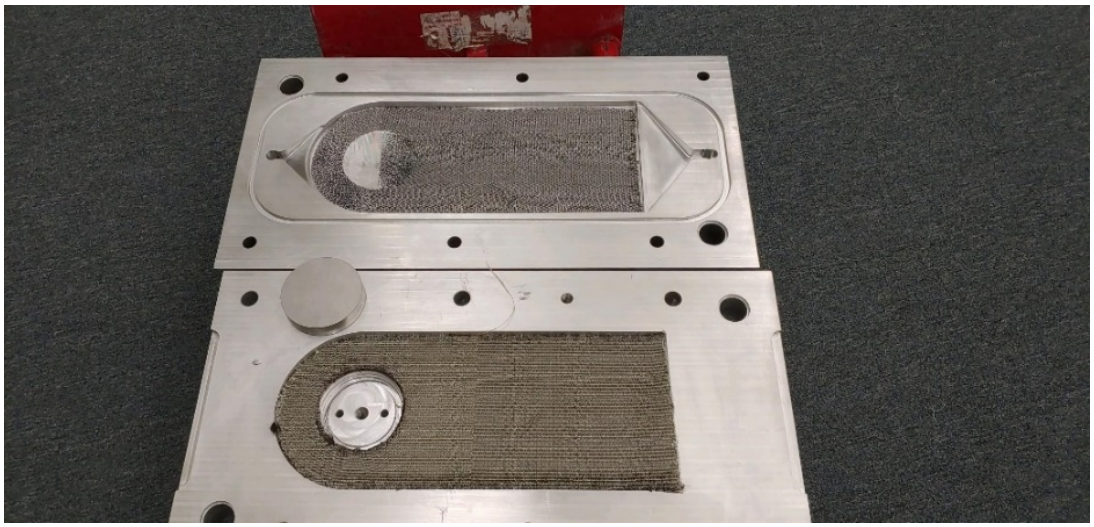

Figure 32. Lug Component Tooling Mold

Figure 33. Example Lug Sub-laminate Preforms, and Stitch Density Diagram

Initial efforts to construct the lugs focused on parameters that minimized any gaps or overlaps during layup on the ZSK. Depending on what tow is used, the necessary spacing between each tow varies significantly and other parameters, such as stitch length, width, and tension, were used to reduce gaps and spacing in the preforms during fabrication. Lugs were fabricated using IM7 fiber initially after a carbon fiber roll was mislabeled. This resulted in UDRI fabricating lugs from both IM7 and AS4 fiber. The AS4 was chosen due to its similarity to the T700 fibers used to measure the mechanical properties for the computational model. Since there is a density and cross-sectional area difference between IM7 and AS4 tow, both tows used a slightly different parameter set for their layer designs. The tow to tow spacing for the IM7 and AS4 variants was 0.8mm and 1.1mm respectively and was determined experimentally (Figure 34-Figure 35 show how the optimized TFP fabrication parameters discussed reduced any gaps/spaces during fabrication). This spacing was optimized to minimize any gaps or overlaps that develop between carbon fiber tows during fabrication of the samples (tow-tow spacing, and polyester stitch spacing parameters are described in Figure 3. This polyester thread is used to hold the carbon fiber to the glass backing cloth for each sub-laminate. Similarly, the stitch width was changed from 1.8mm for IM7 to 3.0mm for AS4 to help spread them to similar layer thickness. This stitch width refers to the distance (side to side) between polyester stitching used to hold carbon tows in place, and was increased to allow for maximum spread of the carbon tows, ultimately resulting in a per ply thickness close to that of the IM7 fiber. Figure 35 shows how the original parameters optimized for the IM7 fiber produces gaps when used with the AS4 fiber, whilst the optimized parameters reduce or eliminate those defects. For both materials, a stitch length (distance along the carbon tow length) of 3.0mm was used. In this figure, the left side shows the non-optimized fabrication parameters that produce gaps between fiber tows, while the right minimizes and essentially removes these gaps.

The Kevlar through thickness stitching spacing/density was kept consistent, at a stitch density of 16 stitches per square cm based on several factors. The first was the desire to improve local toughness and strength, based on the ASTM standard test data it was clear that 16 stitches/cm^2 would improve the local strength and toughness, while minimizing the potential knockdown on in-plane properties compared to a stitch density of 30 stitches/cm^2. The second design consideration was based on the time required to stitch at higher densities through parts this thick. Given the thickness of the part the reinforcing stitching process was slowed to minimize fiber breaks and fabrication issues. When determining the appropriate stitch density for the lug component, it was determined that 16 stitches/cm^2 would be used since it was still shown to produce

significant improvements in the desired mechanical properties, while minimizing the time needed for part fabrication. Fiber path locations were designed using concentric semicircles around the bearing hole, with tangent lines in the desired load direction, based on previous bearing testing of coupon level components showing improved strengths with the addition of concentric cylinder fiber paths near the bearing surface. Fiber centerlines were chosen based on the minimum tow to tow spacing to ensure maximum fiber content, while minimizing any gaps or spaces in between tows. Stitch spacing was based on computational models showing that a stitch spacing of 16 stitches/cm^2 would reduce delamination growth leading to failure while minimizing in-plane reductions of properties. Fiber tow bundles that passed in to the bearing lug surface location were cut and removed prior to infusion to ensure preforms fit the tooling mold.

Figure 34. Optimized Parameters for IM7 Lug (Shown with Parameters optimized to reduce defects)

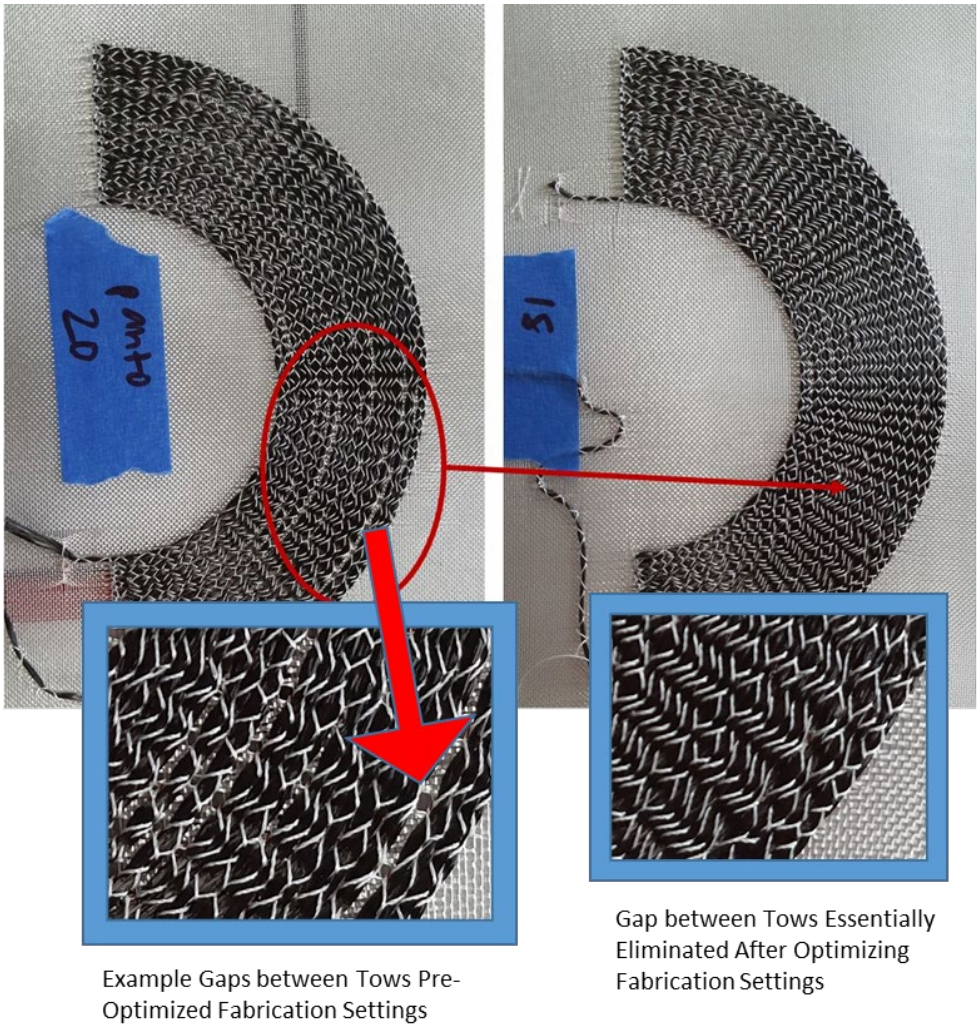

Figure 35. AS4 Parameter Optimization for TFP Construction Near Bearing Surface: Left is Non-Optimized Producing Spacing Defects, Right Shows Optimized Parameters Eliminating These Defects

After the completion of the fabrication of each preform stack samples were sent for RTM infusion. The first lug infusions went well; however, the parts appeared to have surface porosity that detracted from the surface finish of the finished part. There were also isolated areas along the tool seam that collected surface porosity. These blemishes were not anticipated to affect overall mechanical performance, but they were not desirable. The first lugs were infused with full part cavity vacuum and no backside pressure on the resin pot, with 50 psi pressure being added after full infusion. The infusion took approximately 10 minutes. In an effort to improve the part finish, a partial vacuum was placed on the resin pot for subsequent infusions so that the pressure differential pushing the resin into the part cavity was halved. This resulted in a slower part infusion, 15 to 20 minutes, and more chance for full fiber wet-out. After infusion, cavity pressure was increased to 50 psi for the duration of the cure. This change, coupled with the addition of a thin fiberglass veil on the part surface, yielded a very nice part with a significant reduction in surface blemishes. Example images of the sample porosity before and after the modifications to the infusion process are shown in Figure 36. The upper right section of Figure 36b has some surface roughness that is exaggerated by the reflection of light off the

surface but did not have the surface blemishes seen in Figure 36a.

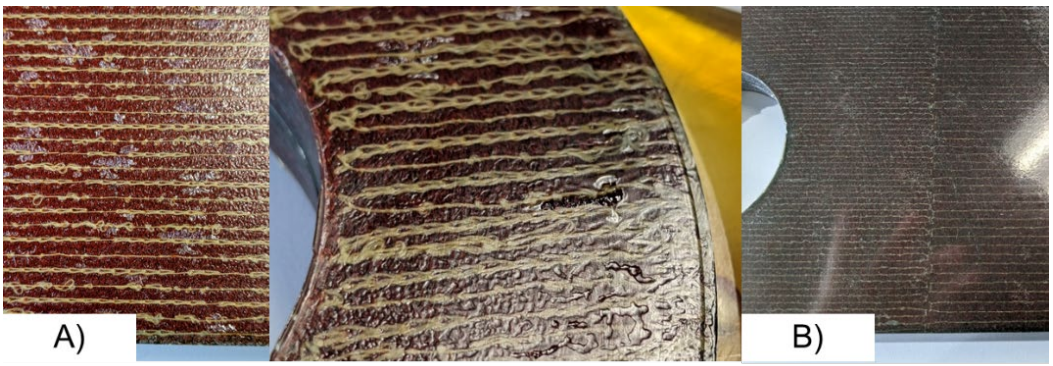

Figure 36. a) Lug Preforms Fabricated With Surface Blemishes Post Resin Infusion, b) Lug Preforms after Infusion Process Modifications with Improved Surface Finish

Lugs were designed to have bolt holes away from the lug feature in order to properly secure the sample in the test fixture during tensile loading. An example image of the lug hole locations for the test fixture can be seen in Figure 37 below. The MTS hydraulic load frame used to test the samples is shown with the test fixture in place.

Figure 37. Lug Preform Test Fixture

Alongside the fabrication of the nominal lug, samples were sent to Michigan State in order to introduce a mechanical hard point. This mechanical hard point uses the threaded steel bolt, a woven carbon fiber sleeve and structural resin to form a strong structural reinforcement at bolt locations [© Cloud, G.L., Hybrid Fastener, U.S. Patent 10,400,813 B2. (2019) & U.S. Patent 9,464,658. (2016)]. This patented approach has been shown to be highly effective. A diagram of the part construction is shown in Figure 38. . This design eliminates bolt slip, lowers stress concentrations, and prevents matrix cracking from initiating at the bolt location by turning a brittle failure into a ductile failure [17]. Hard point inserts were fabricated using a

biaxial carbon sleeve (V56L300X) from A&P Technologies and infused using SC-15 resin at a weight ratio of 10:3 (Part A to Part B). Samples were cured at room temperature for 24 hours followed by a post cure at 94°C for 4 hours. An example image of the assembly prior to infusion and cure is shown in Figure 38.

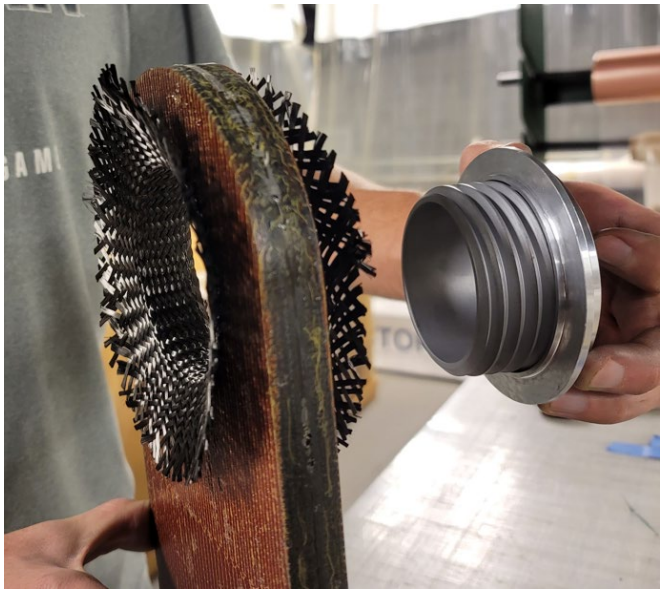

Figure 38. Image of Hard Point Assembly Prior to Infusion

Tension tests were performed on eight Resin Transfer Molded (RTM) composite lugs in a servo-hydraulic MTS load frame with a 220 kip actuator. The load was measured with a 220 kip MTS load cell. Four quarter inch strain gages were placed in selected locations to measure the strain at those particular spots. A drawing of the lug with gauge locations was provided above (Note that the fourth gage is on the backside of the lug, back-to-back with the gage on the opposite surface). Each lug was placed in the load frame vertically with the large hole upward. Each of the seven smaller holes had bolts in them that were torqued to 150 ft lbs while the large hole was pin loaded. Each strain gage was wired into a Vishay 2311 Amplifier and output to a general data plotter along with the load and displacement data. Before the beginning of each test, a straight edge and level were used to ensure alignment and avoid bending. The test setup is pictured below in Figure 39 with a

sample loaded in place.

Figure 39. Image of Test Specimen in MTS Hydraulic Load Frame Prior to Testing

Lugs constructed from both AS4 and IM7 fiber were tested. Samples using a metallic hard point were fabricated following lug laminate 1 ($[(0_2/\pm45/902)\ (0_2/\pm45/90_2)(90_4)(\pm45/0_4)]_s$) using IM7 fibers. The samples can be broken into fiber and laminate type. The nominal reference from the paper that was originally intended to be compared against would have a failure strength of 298 kN. The stated milestone requires the TFP preform to improve on performance by 10%, with an increase in performance using the hard point of an additional 10%. A summary of the test results for the lugs can be seen in Table 6. The table breaks the objects into relevant groups and summarizes the results.

Table 6. Lug Test Results

	Specimen	Experimental Load (kN)	Average Load (kN)	% Change from Nominal
IM7 Lug Laminate 1	Lug 4	269.3	259.8	N/A
	Lug 3	250.3		
	Lug 1 - HP	308.97	315.2	18.92
	Lug 2 - HP	321.47		23.73
IM7 Lug Laminate 2	Lug 5	263.3	261.7	0.73
	Lug 6	260.09		
AS4 Paper Reference		298	N/A	N/A
AS4 Lug Laminate 2	Lug 1	244.4	249.85	N/A
	Lug 2	255.3		

The results of this show clearly that the inclusion of the hard point increases failure strength by over 20% on average. This increase in failure load is driven by the delay in onset of fiber breakage, while each part still appears to experience the same failure mode. This massive increase allowed UDRI to check off the relevant milestone. Concerns about samples having porosity or voids led to concerns about the "reference" load being overly optimistic. In order to ensure UDRI met the project milestone of improving performance of the TFP insert compared to the woven preform UDRI purchased IM7 woven fabric. This was used to layup a sample using the following laminate stacking sequence: $[(0/45/45/45/0)(0/45/0/45/0)_{15}(0/45/45/45/0)]$. This would build up to the nominal part thickness of 19.1 mm, while getting close to approximating the same percentage of fibers in each direction as seen in the TFP preform. A post failure image of a lug that was constructed using woven fabric preforms with the stacking sequence $[(0/45/45/45/0)/(0/45/0/45/0)_{15}/(0/45/45/45/0)]$, can be seen in Figure 40. Experimental failure was found to concentrate at the bearing surface tangent points as predicted by the model. Failed TFP samples constructed from IM7 can be seen in Figure 41, where construction type is indicated by the text to the right. Failed Images of the AS4 TFP preforms can be seen in Figure 42. Sample 1 from the AS4 lugs was found to fail at a lower load compared to the second sample. This sample shows failure away from the bearing location, with a matrix split following the nominal arc of the fiber geometry indicating a failure due to a massive resin rich area with the sample. This resin rich region is likely formed by the development of a gap between fiber bundles. This gap was formed by the failure to properly develop the optimized fabrication controls with the AS4 fiber due to the time constraints at the end of the project. As mentioned previously the carbon fiber roll was improperly labeled leading to the fabrication of components using the wrong fiber (IM7) until the error was discovered. At this point the project deadline was approaching and AS4 samples were fabricated rapidly without the appropriate time needed to optimize

fabrication procedures used to reduce defect formation.

Figure 40.Failed IM7 Plain Weave Lug Geometry

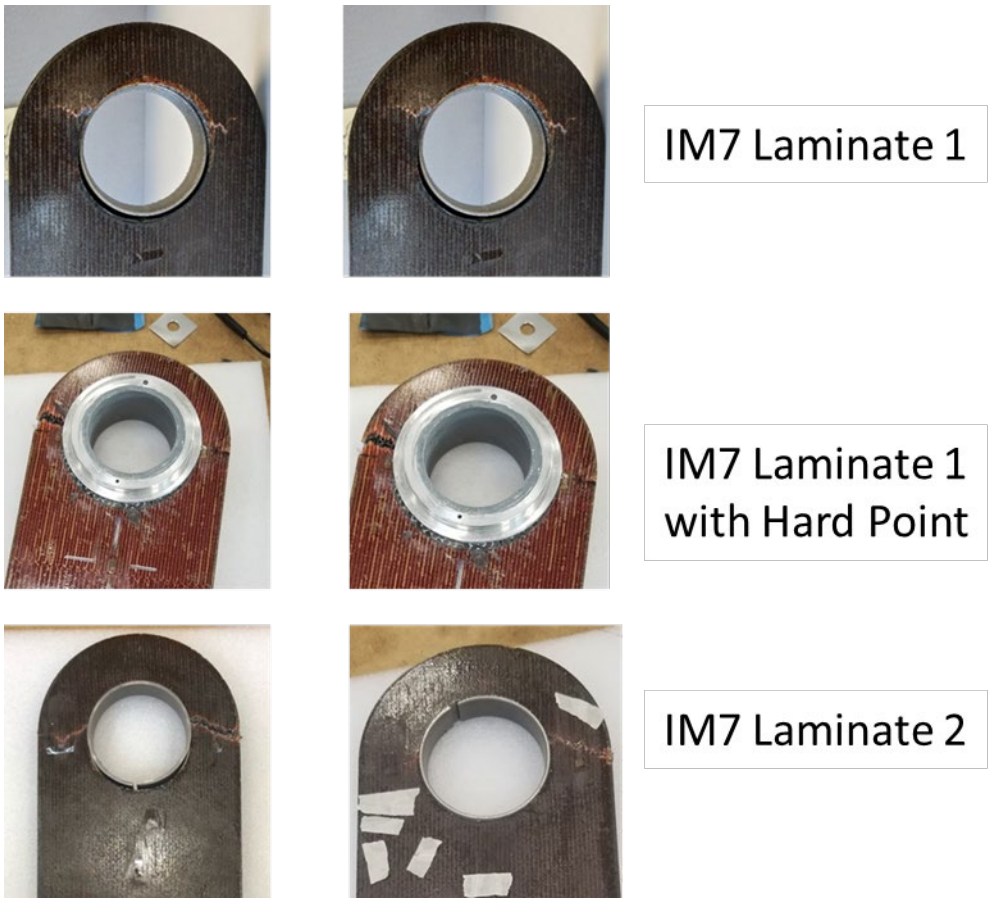

Figure 41. IM7 TFP Lug Sample Failure Images

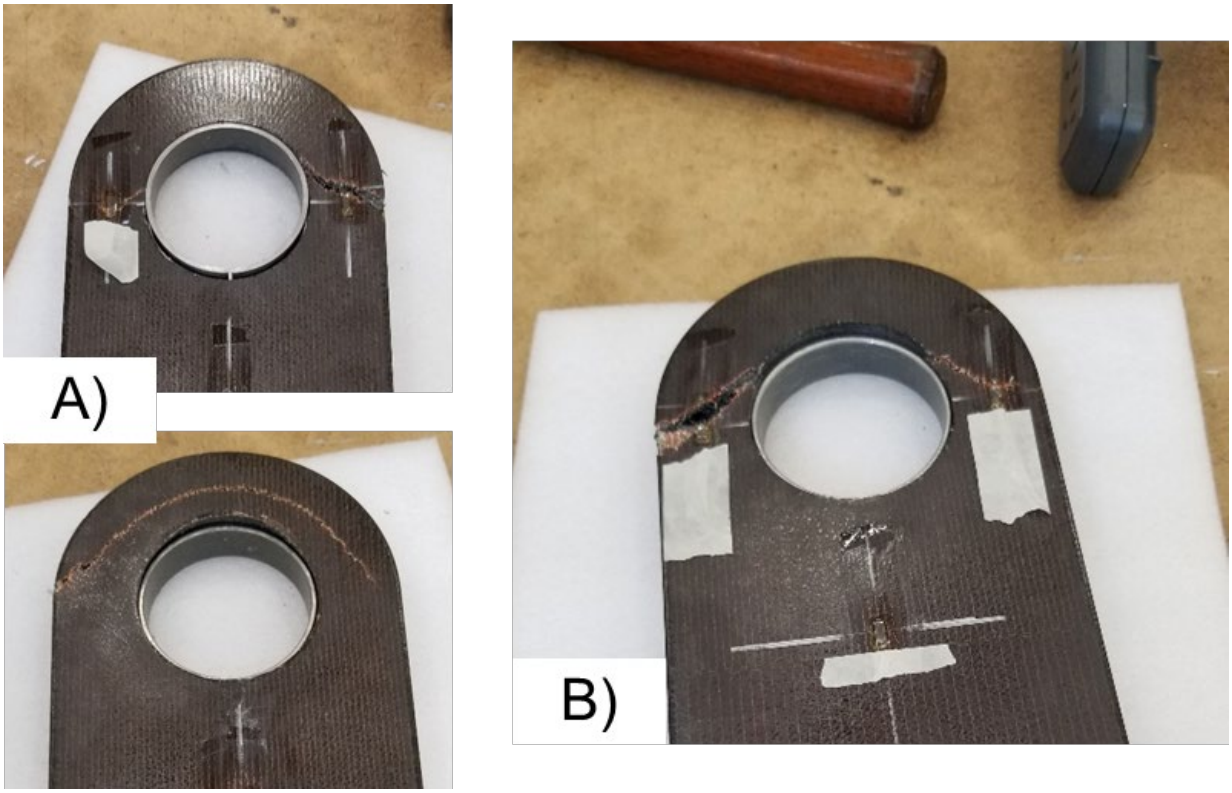

Figure 42. a) Failed AS4 Lug Laminate 2 Sample 1 (Front and Back), b) Failed AS4 Lug Laminate Sample 2

Test data for the IM7 TFP preforms can be seen in Figure 43. Blue lines correspond to IM7 lug laminate 1, without any hard points. Green lines correspond to the IM7 lug laminate 2 preforms without hard points. Orange lines corresponds to the hard point models of IM7 lug laminate 1. There is significant deviation in load frame compliance due to variations in the pre-load applied to samples (the first test samples had no standardized pre-load, while later samples were all preloaded to 10,000 N). This compliance variation is easily seen in how much variation is required to begin loading the sample in a linear-elastic fashion. Failure in all IM7 fiber preforms was found to occur at roughly the same locations. The deviation in load to failure is driven by the hard point insert. A map of the strain contours from the left and right side of a test specimen can be seen in Figure 45. This comparison includes the model results as a point of reference. Strain gauge data from the back-to-back gauges below the lug hole were used to ensure that no out of plane bending occurred.

This comparison can be seen in Figure 44.

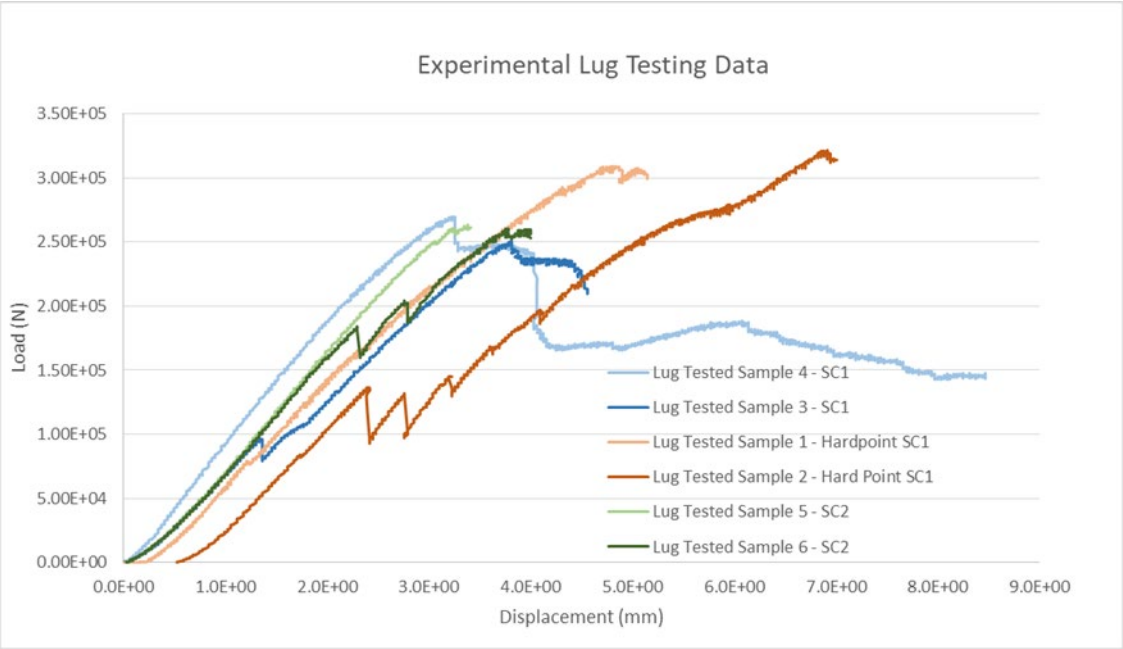

Figure 43. IM7 Fiber Lug Load vs. Displacement Data

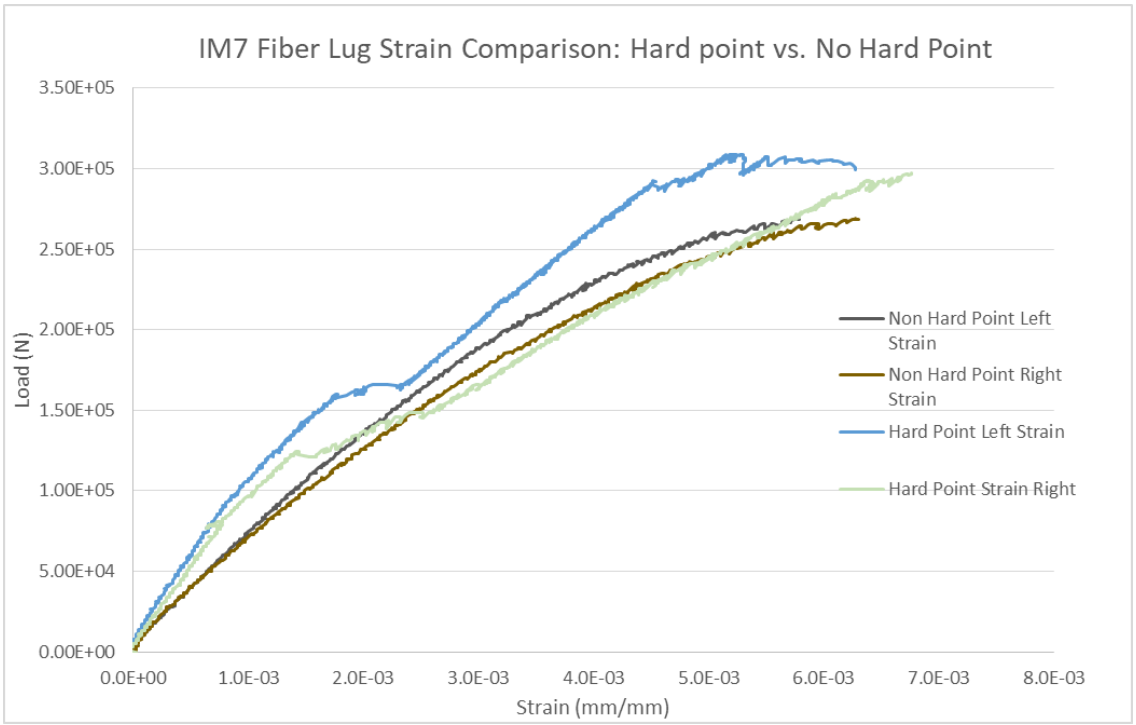

Figure 44. IM7 Fiber Strain Comparison: Hard Point vs. No Hard Point (gauge on the left and right)

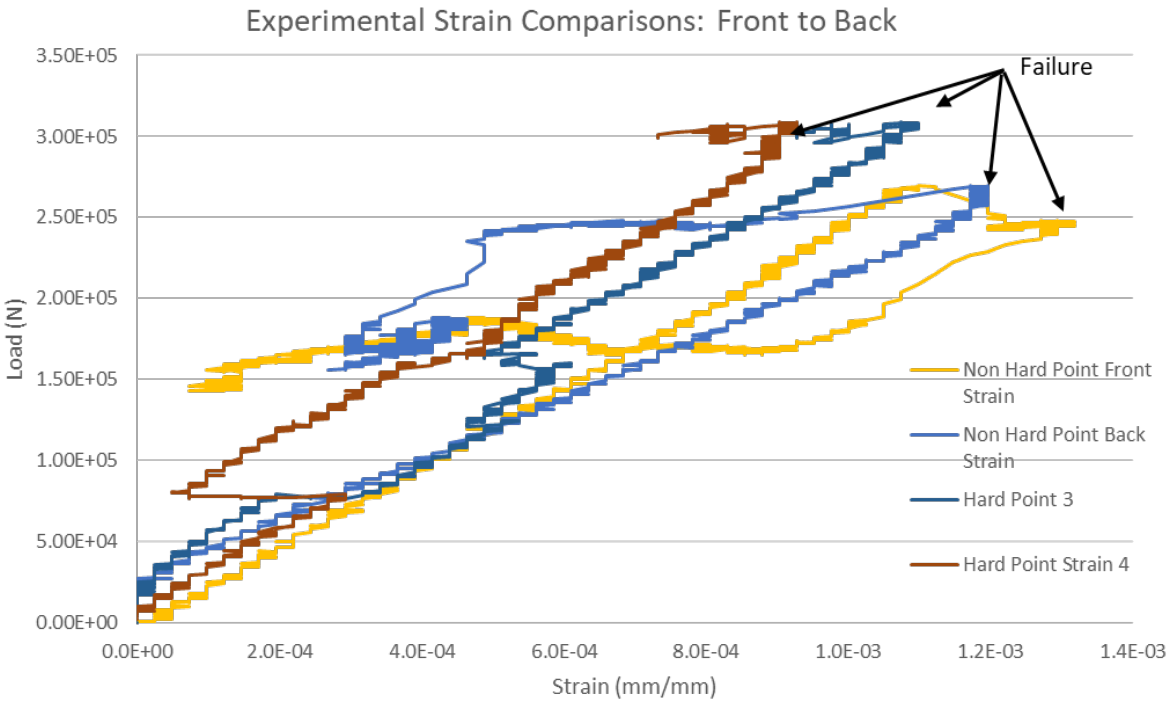

Figure 45. IM7 Fiber Lug Strain Comparisons Hard Point vs. No Hard Point (gauge on the front/back)

In an effort to further understand variation in the material behavior additional comparisons were broken down by laminate stacking sequence and fiber type. Figure 46 shows a comparison between IM7 fiber preforms with and without hard point inserts. The major takeaway is that the hard point increases part stiffness and leads to delayed onset of damage (in Sample 1). This massive increase in peak load is vital to showing the value of this program. Figure 47 shows the comparison of laminate 2 between AS4 and IM7 fibers. These samples were quickly fabricated at the end of the testing program, when time was running out and were not optimized for fabrication.

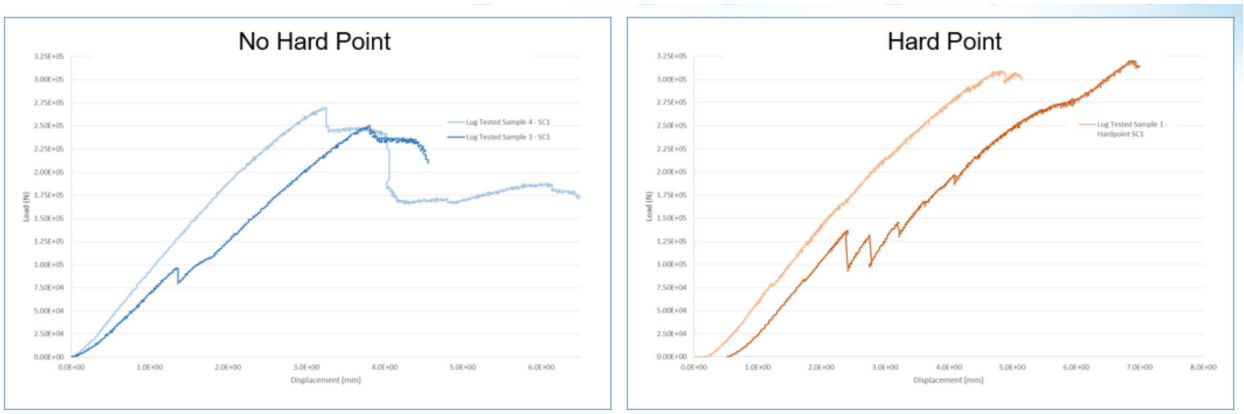

Figure 46. IM7 Fiber Lug Comparisons between Standard Fiber and Hard Point Samples Laminate Stacking Sequence 1

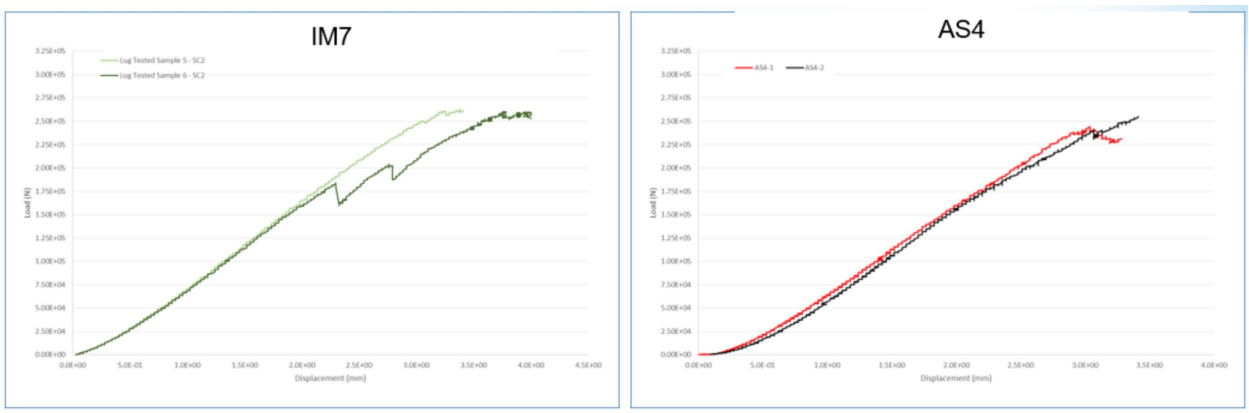

Figure 47. IM7 Fiber Lug Comparisons between IM7 and AS4 Fiber Lugs (Stacking Sequence 2)

UDRI purchased IM7 plain weave fabric and constructed a lug using the same tooling mold. This part was fabricated with the same sub-laminate stacking sequence discussed previously [18] and repeated here: $[(0/45/45/45/0)/(0/45/0/45/0)_{15}/(0/45/45/45/0)]$. In this stacking sequence each "sub-laminate" is separated by parenthesis. This part was infused and found to have a fiber volume fraction of 59.92%. The nominal TFP preforms averaged a fiber volume fraction of 52.43% when calculating the v_f using the mass of preforms pre- and post-infusion. The non-normalized peak load of the IM7 woven preform was 310.6 kN, while the fiber volume fraction normalized peak load was found to be 271.8 kN. The average IM7 TFP lug constructed with the stacking sequence identified earlier as laminate 2, was found to have a peak average load of 261.7 kN. While the TFP preforms failed to exceed the woven preform fabricated by UDRI, the TFP preforms showed a much later damage onset compared to the woven lug fabricated and tested.

The lack of statistically relevant test samples for the woven lug (only one sample was tested), and TFP fabricated lugs samples makes a statistical analysis impossible. The significant variation in damage onset is difficult to understand given the small number of samples. Without additional time to produce a statistically relevant number of samples it cannot be explored further at this junction. Given the massive increase in performance by the hard point, and the computational results showing the potential for improvement the milestone was considered "completed."

Clip Bracket Testing

The final component fabricated on this program was complex geometry provided by Airbus (Nathan Ball and Jeff Nangle). This "clip bracket" geometry was provided after much discussion with the OEM Airbus. The geometry is shown in Figure 48. The design limit load is 10kN and is expected to experience out of plane loading as well as in plane loading. This geometry is small and currently fabricated using an aluminum alloy. This alloy is expected to weigh approximately 44 grams. The stated design is to reduce weight by at least 25% or cost by 10%. The part geometry (i.e. shape of the clip bracket) was provided to UDRI by Airbus in a CAD file. Given the complexity of the part UDRI outsourced the tool design for infusion to the projects' RTM partner and began designing the laminate construction required to fit the tooling mold. The original

tooling mold designs are shown in Figure 49.

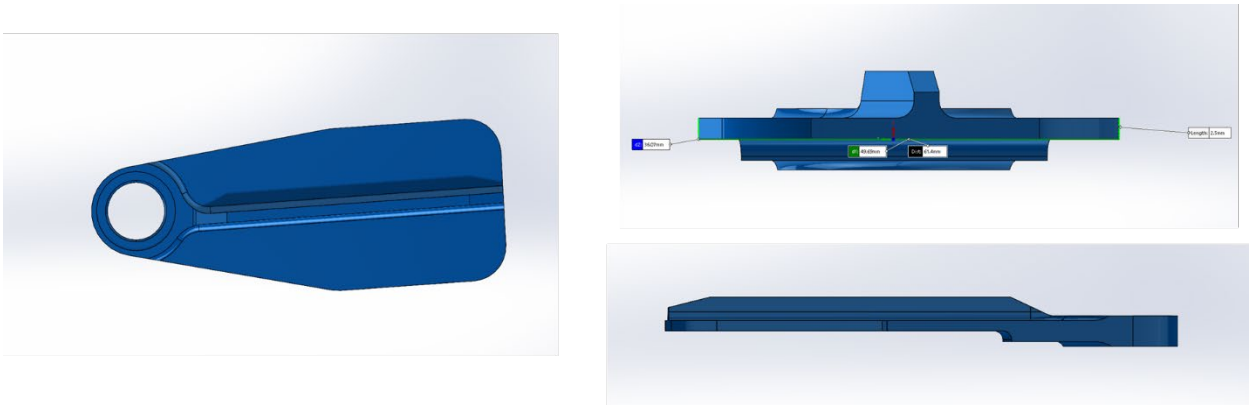

Figure 48. Clip Bracket Geometry from Airbus

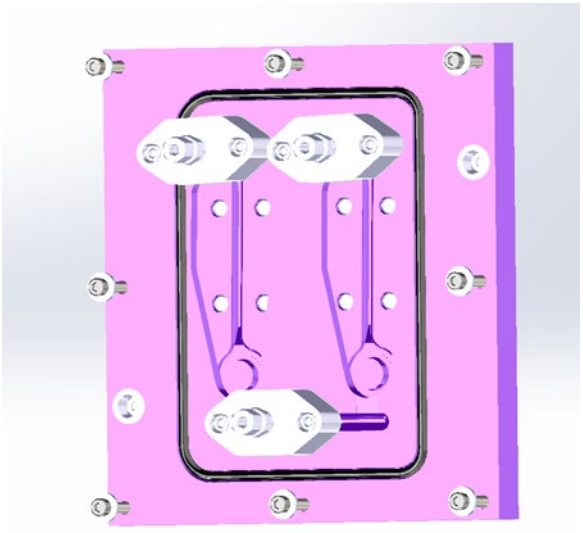

Figure 49. Clip Bracket Tooling Mold for RTM Infusion

Initial efforts at fabricating the clip bracket were based on input from the computational model (discussed in the modeling section 5.2 under the "Clip Bracket" Sub-heading). Assuming a purely unidirectional load case, a clip bracket laminate was fabricated according to the following stacking sequence: [(B/0/0/0/0/0),(B/0/0/0),(B/0/0/45/0/90/-45),(-45/90/0/45/0/0/B), (0,0,90,90,0,0/B)]. Where each "B" corresponds to a backing cloth the carbon layers are stitched to. This design can be seen in Figure 50, where the blue spine corresponds to the first preform of all 0 plies.

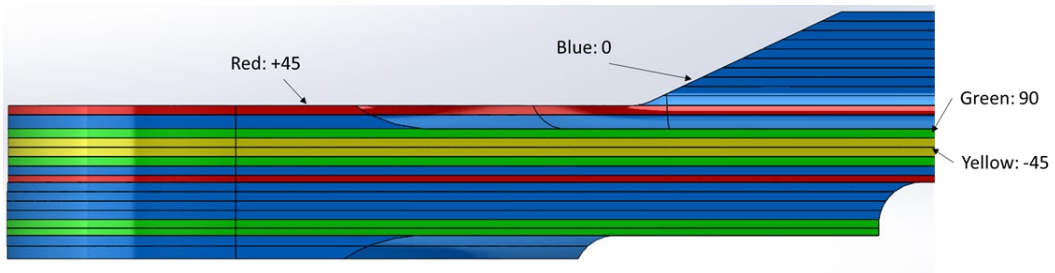

Figure 50. Clip Bracket Design Schematic

The first attempt at getting the bracket to fit in the mold encountered issues. The principal problem was swelling of the fiber during layup at the lug (hole) feature. There were also issues in fitting the "spine" to body transition, but the general dimensions of the first preform were good. The print path designs were modified to reduce build up at thickness transition locations to prevent fiber swelling. To correct for this led to the additional loops being dropped off and the backing location being changed in a few locations resulting in a final layup of [(0/0/0/0/0/B),(0/0/0/B),(0/0/45/0/90/-45/B),(-45/90/0/45/0/0/B), (0,0,90,90,0,0/B)] An image of the first attempts at the construction of the spine are shown in Figure 51. After making several modifications to the design a successful fit test was completed. The sample was infused using the nominal tooling mold. The lug feature of the bracket proved to be very difficult to demold. The part hung-up in the part cavity, and the jack bolts were not sufficient for driving out the part. The first two bracket parts were damaged beyond usefulness during the demold process. The mold was modified by machining down the boss feature in the tool that fills in the lug during molding. A removable boss was machined that would demold with the bracket and be subsequently removed after the bracket was outside of the mold cavity. With this change, the parts easily demolded from all subsequent infusions. An image of a cured sample is shown in Figure 52.

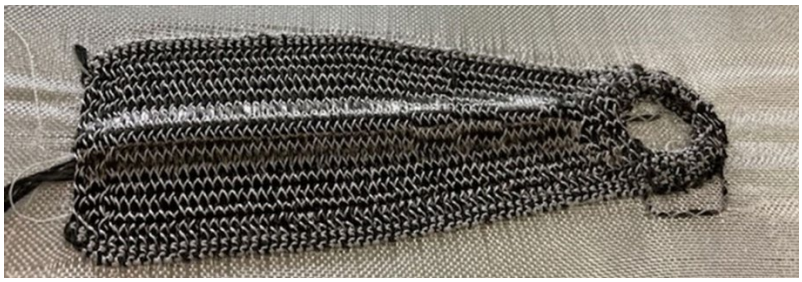

Figure 51. Clip Bracket Spine TFP Preform

Figure 52. Clip Bracket after De-Molding and Machining

Samples were prepared for testing by touching up the lug surface and drilling bolt hole locations. These bolt hole locations are seen in the sample above. This spacing was provided by Nathan Ball. Samples were tested in tension using an Instron load frame at a tensile rate of 0.05 in/minute. The average failure load of the test samples was 17.73 kN. Each sample failed at the lug location during loading. No damage was found to occur at the bolt locations. An image of the test set up is seen in Figure 53, while a close up of the failed surface is seen in Figure 54. Load vs. displacement curves are shown in Figure 55. Samples were found to have an average mass of 25.4 grams compared to the metallic weight of 44 grams. This ~43% reduction in weight well exceeds the design milestone.

Figure 53. Clip Bracket in Instron Load Frame

Figure 54. Failed Clip Bracket Surface

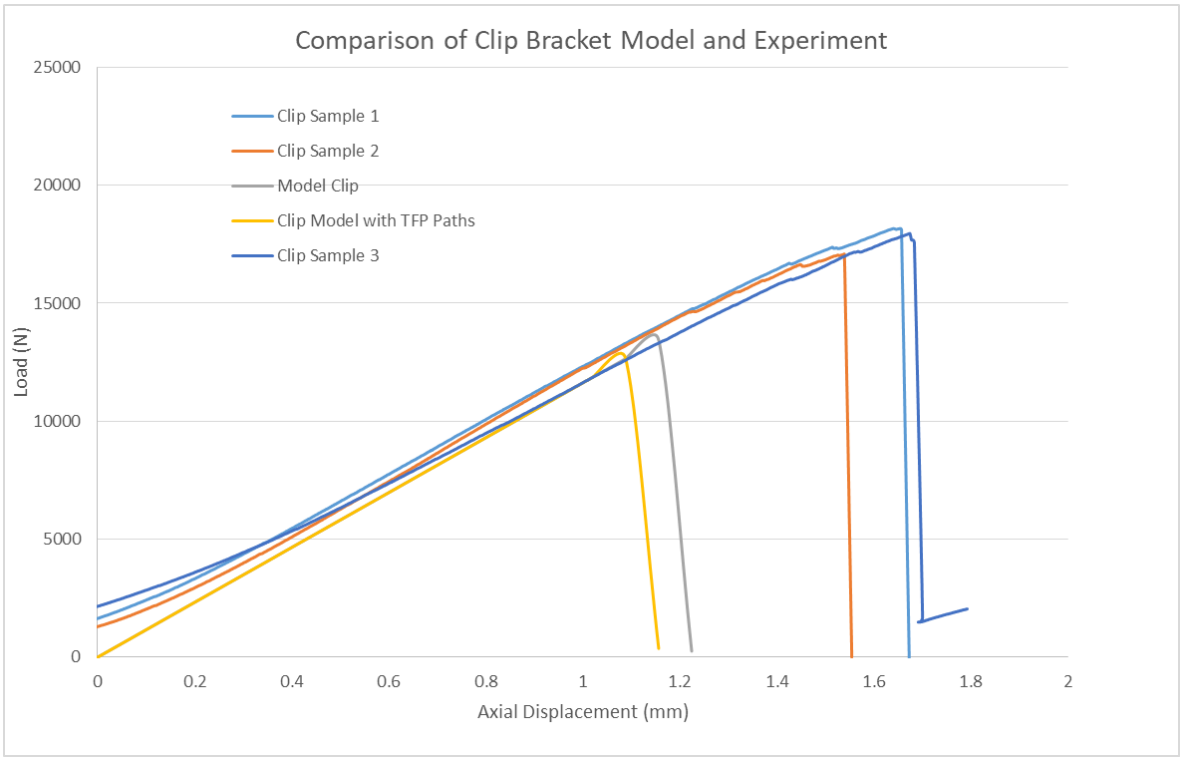

Figure 55. Comparison of Clip Bracket Load vs. Displacements

5.2 Modeling Section

Material Property Models

When starting the modeling efforts on this program several different mechanisms were discussed as possibilities for capturing the impact of stitching on the mechanical performance of the test coupons. The first method discussed was the construction of models that discretely modeled the all of the stitches and fiber. This would require the use of the Virtual Textile Morphology Suite (VTMS) to generate a realistic

approximation of the tows and stitches from each preform, and then generate a complex finite element mesh for analysis. This method was quickly discounted due to the difficulty in accurately representing the geometry, in addition to this method producing models too large to solve in a timely fashion. The second method discussed was the inclusion of 1D rod elements at locations of stitches, but this was excluded because it would require the modification of the current finite element code in BSAM.

Ultimately it was decided to explore the modeling of two first order approximation methods. Method one would utilize standard cohesive surfaces between plies that was governed by a traction separation law [18]. This traction separation law is characterized by the release pressure or strength, and area under the curve or fracture toughness. The model could then have the cohesive surface strength and toughness modified to match experimental data. This would simplify the model complexity greatly but is limited by the over simplified response. An additional limitation is the requirement of measuring the change in the mode I and II fracture toughness of every potential variation in stitch density. The second methodology discussed was the modeling of stitch locations as separate cohesive zones compared to the "nominal" cohesive zone governing the standard ply interface. This method utilizes an automated search algorithm to generate node sets used to create cohesive surfaces based on an x/y/z coordinate list of the stitches produced by the ZSK machine utilized to fabricate the preforms. This method presented the potential benefit of simply needing the effective strength/facture toughness of the local material interface in the region surrounding a Kevlar stitching. This effective strength and fracture toughness would account for the strength of the Kevlar in the through thickness load direction (i.e. reinforcement direction), and epoxy interface as a homogenized response. In addition, this method allows the user to create "effective" stitch radii, or "spatial tolerance" within some dimensional tolerance of the stitch center point that can capture the distortion in the in-plane fiber direction caused by the stitching fiber. This allows the model to change the in-plane fiber direction, as a function of fiber distortions due to Kevlar through stitches. Models of the mode I fracture testing were constructed and modeled with both methods described above. This approach was described in length in the previous work presented at SAMPE [19].

Models with cohesive zones at each stitch location were run with effective radii varying from 0 mm (i.e. only within the element the stitch falls within) up to 1.4 mm, with a mock schematic of various cohesive surfaces shown in Figure 56. This schematic shows how the midplane interface of a Mode I fracture toughness coupon is explicitly simulated with stitch locations, Teflon inserts, and the nominal epoxy properties. A screen shot from the software GUI shows how stitches are inserted in the model, and the impact on the number of nodes captured by the change in "effective" radius in *Figure* 57. The center point of the yellow dots corresponds to the Kevlar stitch locations, while the diameter of the circle can be varied to tune material properties as a function of mesh density. The homogenized version of the model did not have any locations corresponding to stitches (i.e. yellow circles) and simply had two cohesive surfaces the Teflon starter delamination and the nominal interface where the effect of stitches is smeared onto the entire interface. The models consisting of a totally homogenized interface showed good agreement with the average peak experimental load for the mode I (i.e. DCB) testing of each of the preforms simulated. The models showed linear increase in load until the onset of delamination at the mid-plane and showed uniform growth of the delamination as the load was applied. This produced a very "smooth" response compared to the experimental data. Initial modeling of the discrete cohesive zones' interlaminar strength was an estimate, as no data on the strength of the Kevlar stitching thread had been collected yet. This, unsurprisingly, resulted in a failure to match the experimental peak average load (shown as a dashed line in Figure 58a) of the experimental data for mode I fracture testing. The homogenized results consists of the totally homogenized interface models for all three stitch preforms in addition to the baseline test data; the average experimental peak is highlighted in the red box, and corresponds to dashed lines. Figure 58b consists of the test data for stitched preform 2 in blue/grey/yellow, while the computational model is in shades of orange. This shows that the un-calibrated model that was using material data sheet values under-predicted the response, but showed the ability to capture the complex load displacement curve that increased and decreased as damage propagated through

stitch regions.

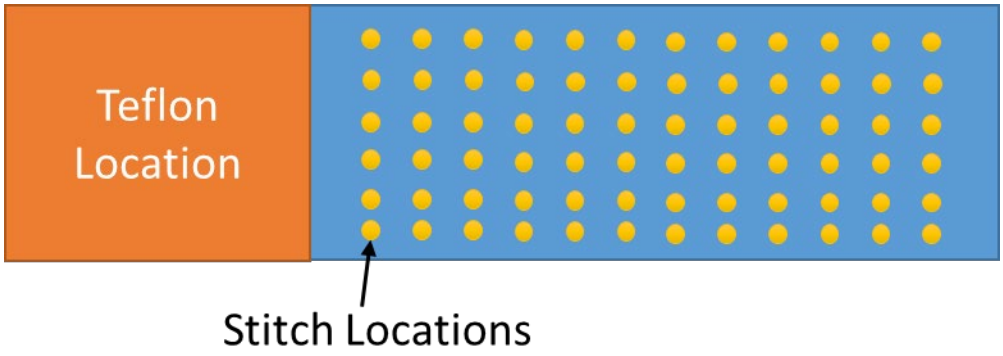

Figure 56. Schematic of Model with Stitch Regions Discretely Modeled for Mode I Fracture Testing

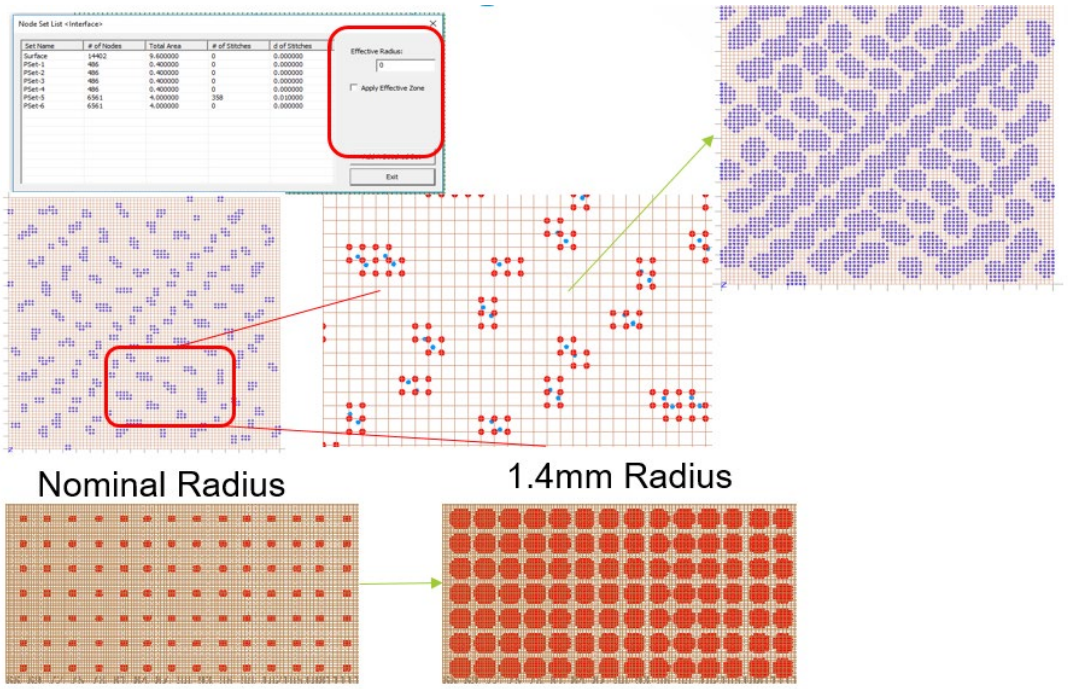

Figure 57. VTMS Screenshot of Stitched Cohesive Surface Selection as a Function of Effective Radius

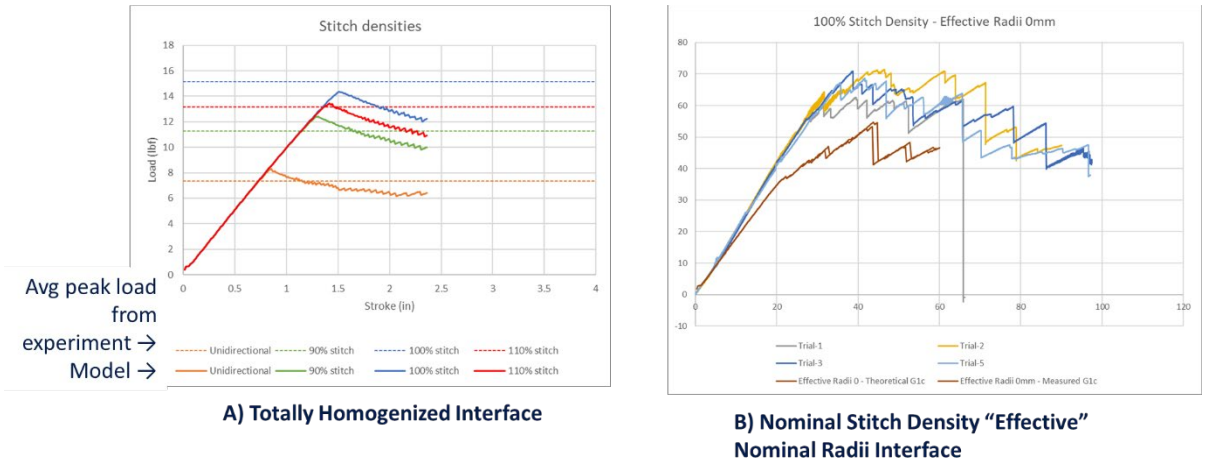

Figure 58. a) Homogenized Interface Results, b) Discrete Stitch Locations

In order to improve the discrete stitch model results the strength of the Kevlar thread was tested. With the strength data on thread collected a method of estimating the improvement in fracture toughness was devised. This method was devised in order to estimate the potential improvement in toughness for any variation on stitch density. The analytical model starts at the assumption that each Kevlar thread is uniformly strained in conjunction with the top layer of composite material. Crack growth in the matrix is assumed to be self-similar within the Kevlar, in other words the crack at the matrix interface also grows across the Kevlar fiber diameter. The Kevlar is assumed to exhibit a linear-brittle fracture, where the fracture of Kevlar leads to release of all strain energy. Equation 1 shows the analytical method used to estimate the fracture toughness associated with Kevlar thread stitches. This calculation considers the failure strength and strain of each fiber, in addition to the total cross-sectional area of fibers in the laminate. Equation 2 shows that the total estimated fracture toughness for the stitched area is the summation of the toughness due to stitches coupled and baseline resin. Table 7 shows a comparison of the analytical predictions with the measured toughness values. A principal driver of the difference is the assumption in the analytical method that there are no defects present and strain is uniformly applied. This is done to estimate the theoretical upper bound possible with a variety of stitch densities. The table is labeled as Preforms 1-3, with the annotation of the relative "percentage of stitching" added to provide reference to Figure 58.

$$G_{IC-Eff\ Fiber} = \sigma_{Stitch} * \varepsilon_{Stitch} * \frac{\#\ Fibers}{Unit\ Area} * A_{Fiber} * t_{laminate} \quad [1]$$

$$G_{IC-Total} = G_{IC-Eff\ Fiber} + G_{IC-Resin} \quad [2]$$

Table 7. Comparison between Analytically Calculated and Experimentally Measured Toughness

Comparison of Fracture Toughness Values (kJ/m^2)		
Preform	Measured	Calculated
Baseline (unstitched)	0.718	N/A
Preform 1 (90%)	1.686	2.272
Preform 2 (100%)	2.288	2.464
Preform 3 (110%)	1.986	2.677

Using the analytical estimate of toughness of a specified stitch density models were used to tune the strength of each stitch cohesive surface. Models were constructed to determine how to scale the failure strength of the discrete stitch cohesive zones as a function of effective radii. This "calibration" of cohesive strength was completed for each effective radius. Each effective radii model had the cohesive strength scaled as a function of area captured by the cohesive zone compared to cross sectional area of Kevlar fibers. Models were run until peak load was within 1% of average peak load from the experimental test data. This process can be seen by moving from left to right in Figure 59, where the cohesive strength (Yt) is varied until the model has honed in on the appropriate value. After determining the appropriate cohesive strength for the stitch region, fracture toughness in that region is varied in order to qualitatively fit the experimental data. This process is completed across all the effective radii in order to produce a calibration curve for fitting cohesive strength to each effective radii.

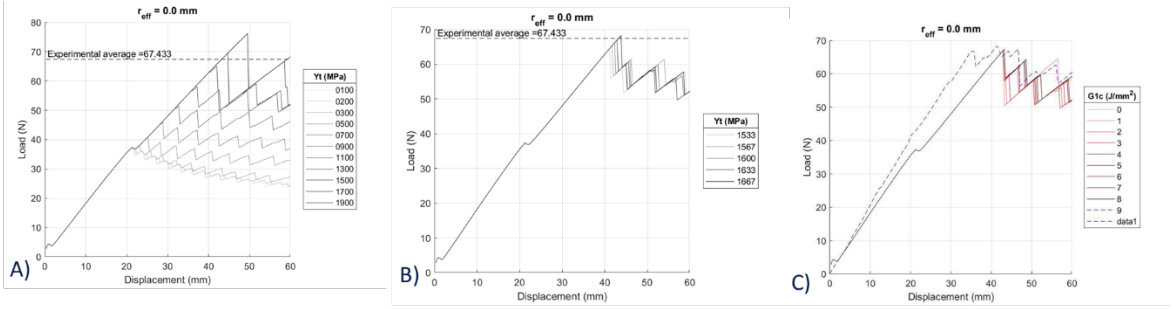

Figure 59. Calibration of Cohesive Strengths, A) Initial Variation of Cohesive Strengths, B) Finely Tuned Cohesive Strengths, C) Calibrated Cohesive Strengths

After this was completed for each of the varied effective radii a rough "calibration curve was developed (Figure 60). This calibration curve shows consistent values at some effective radii changes, indicating that the relative change in the number of elements captured by the cohesive surface did not change appreciably. This is due to the fact that the increase in effective area did not increase the total number of elements that approximated the stitch region. This would be taken into consideration if mesh density of the models was continuously increased until every subtle increase in effective radii changed the number of elements represented by the stitch region. This data was fit with a linear trend in order to produce a mechanism for determining what cohesive strength should be utilized as a function of effective stitch area. The trendline indicates that the effective strength of the "stitch" cohesive surface should decrease as it is used to simulate a large area. This makes intuitive sense as the toughness is constant over each cohesive surface so lowering the strength as you increase area helps to keep a consistent peak load response.

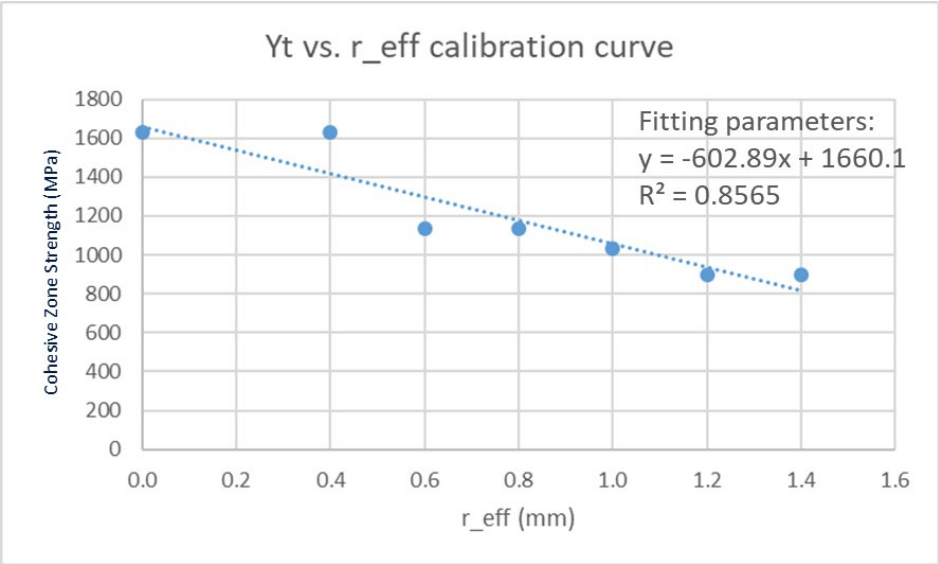

Figure 60. Sample Calibration Curve for Effective Stitch Cohesive Zone Strength

The next step was to focus on the development of methods to account for fiber distortions due to reinforcing stitching. This method took into account the measured distortion from the CT data by overlaying element by element orientation vectors. A MATLAB script was developed that would account for stitch locations and provide a "distorted" map of the fiber paths. Each fiber path was then converted into a "fiber" or "tow" that is overlaid onto the mesh geometry. A nearest neighbor search then finds elements in the vicinity of the fiber centerline and assigns an orientation vector based on the fiber normal direction. These orientation vectors are then used to calculate the local element coordinate system, resulting in variations in material properties designed to capture the impact of stitching on the TFP preform. Using a X-Ray CT, fiber path distortion was characterized as a function of stitch location. This characterization resulted in an elliptical distortion based on the stitch center point. The distortion is characterized by a major and minor axis length. A Matlab program was written to plot the theoretical straight line fiber paths associated with the fiber tow centerlines, and overlay stitch locations on the fiber path and "perturb" the center lines according the CT characterization of the fiber distortion. These new fiber paths are used to produce theoretical fiber tow geometries, that are overlaid on the finite element mesh representation of the geometry and local element orientations are assigned on an element by element basis. This allows the FE program to capture the change in local stiffness as a function of the fiber distortion. Figure 61 shows how the semi-manual method is used to implement these orientation vectors into the finite element program BSAM with the image showing the initial fiber centerlines being distorted by a stitch location and how the adjusted fiber or tow centerlines are output to a file used to assign orientations. The final portion of the figure simply shows a close up of a ASTM standard model of 0° tensile strength test coupon, showing how the fiber distortions are mapped to the part on an element by element basis.

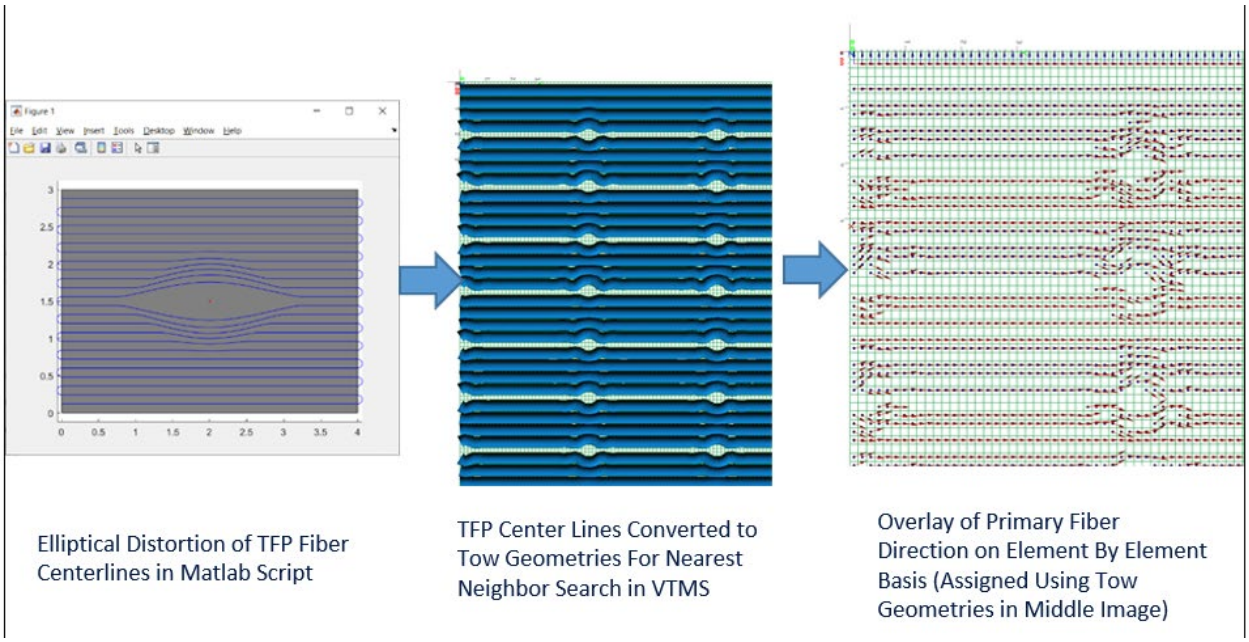

Figure 61. Semi-Automated Method for Implementing Fiber Distortions due to TFP Stitching

Using this method to introduce fiber distortions, models were constructed in order to compare against the ASTM D3039 and ASTM D6641 mechanical data developed on this program. Tension test models were constructed to utilize a Weibull statistics approach for a critical failure volume (CFV) [8]. Compression models utilized a continuum damage mechanics (CDM) [11-12] approach for predicting fiber failure. Test models were constructed for all stitch densities and orientations (0° and 90°). Models were run using displacement control and results are tabulated in Table 8. Using this approach, the fiber distortions resulted in stress concentrations at distortion locations leading to changes in the model predicted strength. These strengths change as a function of the number of stitches as seen in the experimental data. In all test cases, model predictions were within 25% of the experimental strengths and moduli, while the majority of simulation results were within 15%. The models were found to over predict the tensile strengths. The experimental and simulation results for 90° tension at a stitch density of 8 stitches/cm^2 showed the largest difference when compared to other stitch densities. This test data had a high degree of variability as shown in Table 8, so it is difficult to interpret why the results were so low compared to the computational model.

Table 8. Computational Model Comparison to ASTM Standard Mechanical Tests

	0° Tensile, Modulus (GPa)			0° Tensile, Strength (MPa)			90° Tensile, Modulus (GPa)			90° Tensile, Strength (MPa)		
	Analysis	Exp.	% Difference	Analysis	Exp.	% Difference	Analysis	Exp.	% Difference	Analysis	Exp.	% Difference
Baseline	121.51	121.35	0.13	1387.60	1292.08	7.39	8.98	9.1	-1.32	19.80	19.49	1.59
8 Stitch/cm²	114.94	115.83	-0.77	1332.60	1216.24	9.57	9.67	9.65	0.21	25.89	20.73	24.89
16 Stitch/cm²	123.10	124.11	-0.81	1326.50	1207.96	9.81	8.98	8.96	0.22	24.04	23.44	2.56
30 Stitch/cm²	111.61	113.76	-1.89	1098.55	1161.77	-5.44	8.29	8.27	0.24	22.21	25.39	-12.52
	0° Compression, Modulus (GPa)			**0° Compression, Strength (MPa)**			**90° Compression, Modulus (GPa)**			**90° Compression, Strength (MPa)**		
	Analysis	Exp.	% Difference	Analysis	Exp.	% Difference	Analysis	Exp.	% Difference	Analysis	Exp.	% Difference
Baseline	99.32	106.18	-6.46	943.79	924.59	2.08	8.89	9.1	-2.31	170.30	188.32	-9.57
8 Stitch/cm²	103.22	104.8	-1.51	812.37	814.27	-0.23	9.37	9.65	-2.90	164.07	188.27	-12.85
16 Stitch/cm²	99.35	104.11	-4.57	563.71	586.05	-3.81	8.40	8.96	-6.25	177.45	190.04	-6.63
30 Stitch/cm²	97.02	108.25	-10.37	493.68	492.96	0.15	8.71	8.27	5.32	178.96	201.44	-11.16

Angle Bracket Models

Angle bracket models were constructed with a nominal per ply thickness of 0.645 mm, and a nominally perfect radius of curvature. This resulted in models that have slight geometric variations compared to the experimentally tested coupons. This was done to avoid the need to make every test specimen individually, both for each laminate and stitch density. The nominal stitch region for the curved bracket was simulated using various cohesive zones as describe in the work by Huelskamp et al [13] and Rapking et al [19]. These cohesive zones had properties scaled according to this method to account for various stitch densities. Baseline mechanical properties were input as laminae level properties prior to accounting for fiber distortions using the semi-automated method. Displacement boundary conditions were used to simulate the applied displacement via the loading pins. An important distinction to make is that BSAM does not have a true contact method so the rotation/sliding in the actual test fixture could not be captured. Models were run for all laminate sequences and stitch densities. Load vs. displacement curves were generated for all models and are shown in Figure 62.

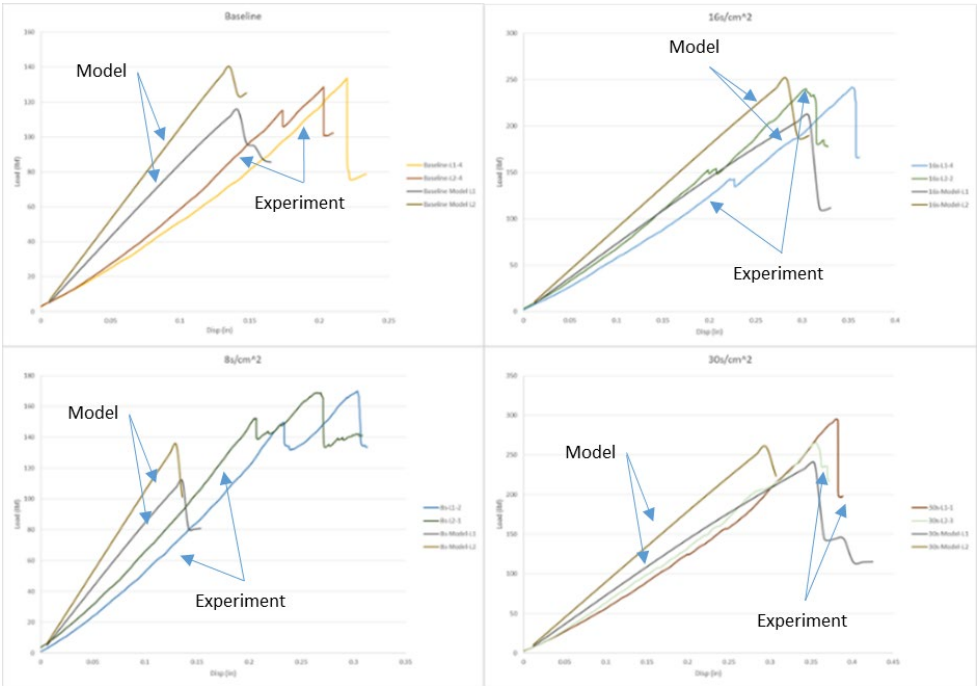

Figure 62. Load vs. Displacement Data for Comparison between Angled Bracket Models and Experimental Data

Computational models are seen to be stiffer than the experimental data due to the direct loading of the surface with displacement controls compared to the sliding contact in the test fixture. This also explains the linear model response compared to the nonlinearity seen in the experimental data. All models were found to have a load drop that occurred once widespread delamination developed in the model. Figure 63 shows a comparison of the edge on delamination coupled with matrix cracks. Table 9 shows the comparison between model predicted strengths and experimental data. Data in Table 9 in yellow corresponds to the computational model. The experimental data shows variation in the performance of each stitch density prediction. For laminate stacking sequence 3 the baseline model and 8 stitch/cm^2 model under predict the strength compared to the experimental data, while the 16 and 30 stitches/cm^2 models over predict performance compared to the experimental data. For laminate stacking sequence 4 the model over predicts for all models except the 8 stitch/cm^2 experimental coupon. All but one of the model results is within 20% of the experimental data. Given the modeling approach is not able to capture sliding contact of the loading pins used to experimentally load the part it is not unexpected to have deviations from the experimental data. Additional code development would be required to explicitly simulate the sliding contact of the experimental set up.

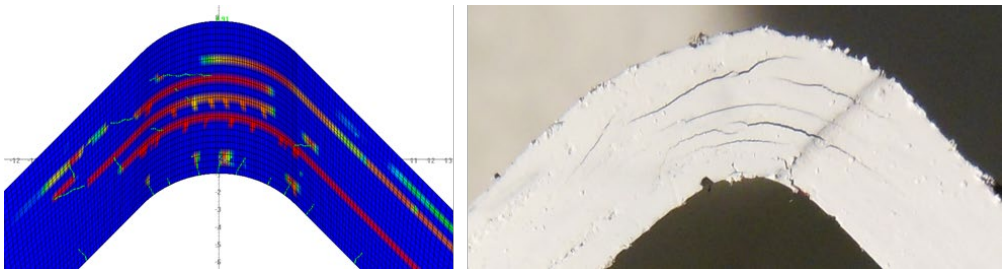

Figure 63. Model Predicted Damage in Baseline Laminate 3 Compared to Experimental Damage

Table 9. Computational Model Prediction of Curved Beam Strength Compared to Experimental Data

ASTM D6415		Results		
Layup	**Specimen**	Curved Beam Strength	Average Load (lbs.)	% Diff CBS
Layup 3	Basline Exp	79.67	126.27	
	Baseline Model	79.12	115.41	-0.69
	8 Stitch Exp	95.31	161.35	
	8 Stitch Model	77.23	111.77	-18.97
	16 Stitch Exp	127.9	235.65	
	16 Stitch Model	143.42	210.83	12.13
	30 Stitch Exp	140.61	293.33	
	30 Stitch Model	156.58	239.21	11.35
Layup 4	Baseline Exp	80.92	122.77	
	Baseline Model	96.72	139.89	19.53
	8 Stitch Exp	106.19	169.69	
	8 Stitch Model	93.95	134.2	-11.53
	16 Stitch Exp	144.78	247.51	
	16 Stitch Model	170.12	250.7	17.51
	30 Stitch Exp	140.26	281.72	
	30 Stitch Model	177.11	260.34	26.27

Bearing Models

Bearing models were constructed according to the ASTM standard and used rigid components to simulate the bearing pins and steel fixturing. Samples were loaded using displacement control, and damage accumulated using CDM and matrix cracking. Models were constructed using a symmetry plane shown in Figure 64. This allowed the model to be cut in half in order to reduce computational time. Figure 65 shows the accumulation of damage in the 0° and 45° plies and shows that the model is capable of capturing the accumulation of damage at bearing locations, as well as capturing failure strengths. For laminate one $[45/90/-45/0]_s$ the model predicted failure at a bearing strength of 612.033 MPa, and a strain of 0.1065 mm/mm. This compares to the experimental data of 710.16 MPa and a failure strain of 0.1319 mm/mm. Laminate two $[45/-45/0_2/90]_s$ predicted failure at a bearing stress of 670.19 MPa and strain of 0.1326 mm/mm, while experimental failure occurred at a bearing strength of 669.48 MPa and strain of 0.147 mm/mm. The computational model predicted premature failure in 0° plies due to CDM damage evolution. This was only a major problem in laminate 1 due to the lowered presence of 0° plies. The increase in 0° plies for laminate 2 resulted in a distribution of loading that resulted in reduced damage accumulation in the 0° plies. This led to a more accurate damage prediction.

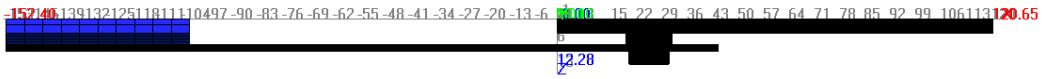

Figure 64. Symmetric Model of TFP Laminate in Bearing

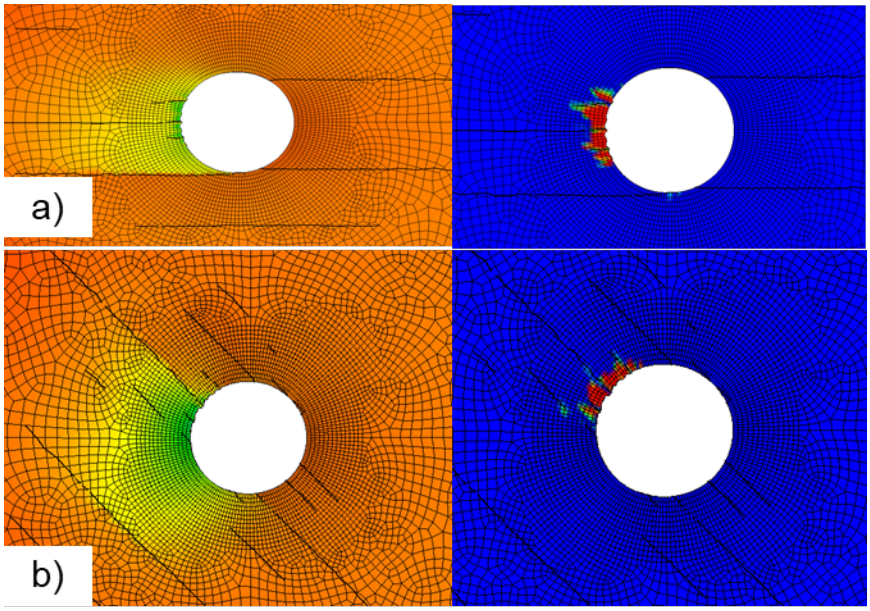

Figure 65. Damage Accumulation Maps from Computational Model a) Displacement Gradient and CDM Damage in 0° Ply b) Displacement Gradient and CDM Damage Accumulation in 45° Ply

TFP Insert Models

After simulating the TFP bearing shear models, work began to simulate the TFP insert's impact on behavior for the Lockheed MT45 prepreg. The goal was to capture the distortion on the prepreg due to the TFP insert, and how it impacts mechanical performance. This analysis utilized a topology optimization routine shown in Figure 66. This workflow took a given mesh input and minimized the ratio of axial to transverse stress. This algorithm defines local orientations on an element-by-element basis, Figure 67 shows an example of the assigned orientation field. The topology optimization utilizes a non-dominated sorting genetic algorithm in order to modify the orientation field of the TFP insert, the resulting change in stress state during a linear elastic simulation is used to calculate the new stress state. This process is repeated in order to produce a Pareto front showing the optimization process. In addition to modifying the in-plane orientations the NGSA-II algorithm used a cubic spline fit along the surface vector of the TFP outline. This radial distortion was based on photomicrograph measurements of the distortion produced by TFP inserts. The result of the optimization, in the form of the Pareto front is shown in Figure 68, with the chosen design criteria specified by the blue circle. This location is a combination of efforts to minimize the Tsai-Hill stress criterion while keeping the part compliance as high as possible. This optimized design results in an ellipse orientated 90° from the load direction, with an eccentricity ratio of 0.7119 and a major axis radius of 6.274 mm. The resulting model prediction using this orientation is found to be 861.7 MPa, and reduces to 839 MPa when accounting for the change in thickness due to the doily insert. Experimental failure was found to be 741.9 MPa. The model is found to over predict the impact on performance. While the model accounts for some local fiber distortion due to the doily insert, it is likely under predicting the total fiber distortion due to the insertion of the doily geometry.

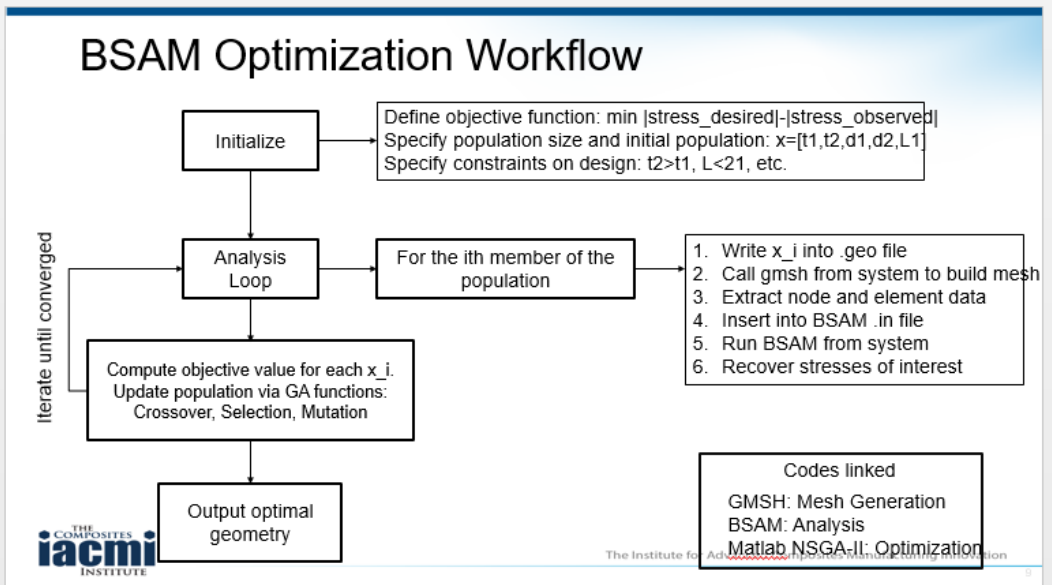

Figure 66. Topology Optimization Routine for TFP Insert

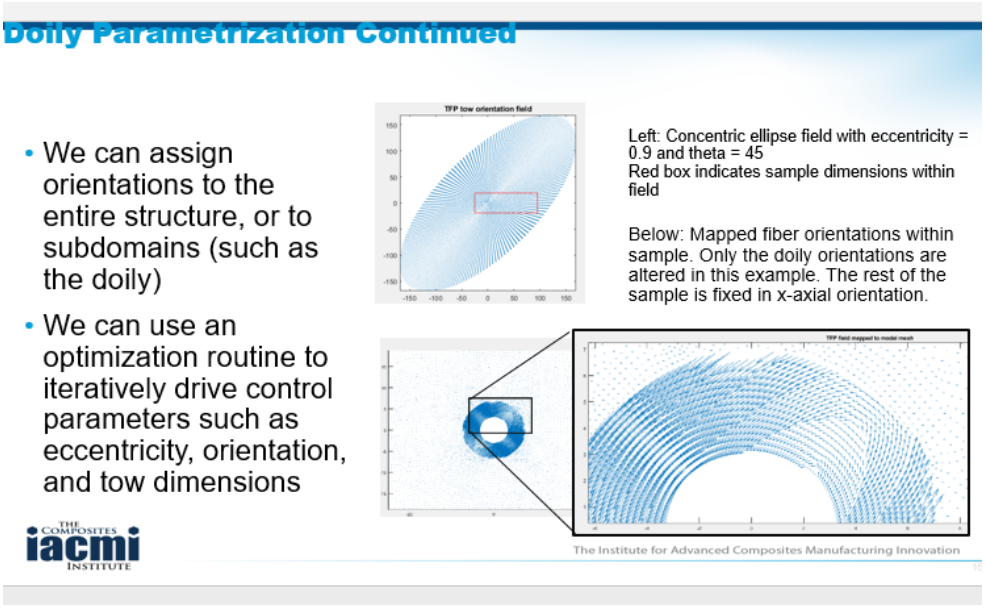

Figure 67. Method of Defining and Element by Element Orientation for TFP Optimization

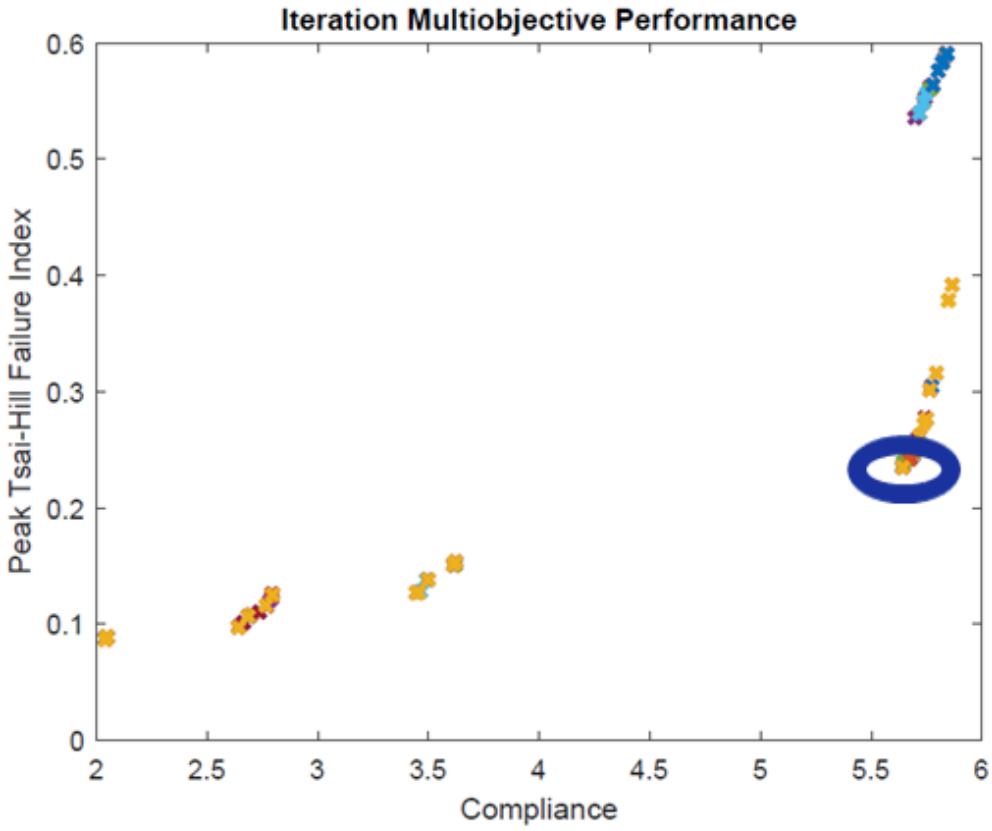

Figure 68. NGSA-II Pareto Front from TFP Insert Optimization

Lug Models

The next step was simulating the behavior of the TFP lugs. UDRI built a computational model using the same framework used to simulate the other test coupons. The fabrication team worked to produce fiber print paths for each layer direction (0/45/90°). These layer directions were converted to DXF file types and read into the GUI for BSAM Export. This allowed UDRI to overlay the element-by-element orientations (Figure 69). This Figure gives an example of the fiber print path DXF and how it overlays fiber orientations on a homogenized ply.

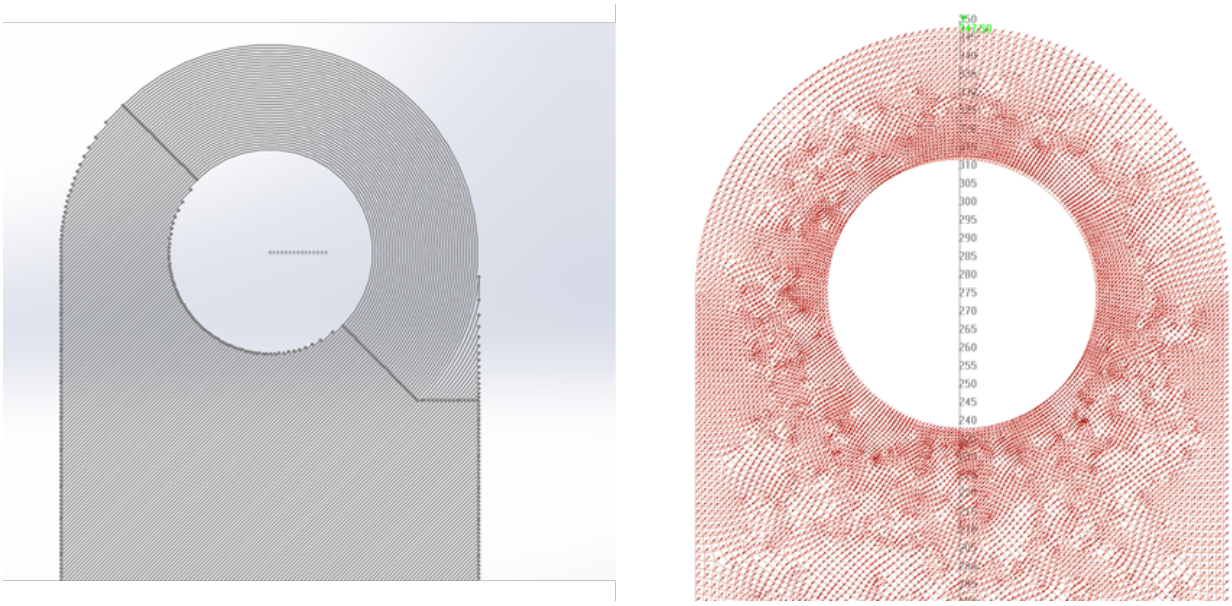

Figure 69. DXF Print Path for 45° Ply and Resulting Element by Element Orientations

Computational models of four lug laminate stacking sequences were constructed in order to determine which sample would reach the desired design load. The nominal target load was 298 kN. Model results were desired to improve performance by 10 percent relative to this. Laminate 1 was $[(0_2/\pm45/90_2)(0_2/\pm45/90_2)(90_4)(\pm45/0_4)]_s$, Laminate 2 was $[(\pm45_3)(0/90)_4(0/90)_4]_s$, Laminate 3 was $[(\pm45_3)(0/90)_3(0/90)_3(0/90)_2]_s$, and Laminate 4 was $[(0/90)_2(+45/0/90/-45/0/90)_3]_s$. Each sample was constructed so that preforms bracketed by parentheses were stitched through with a uniform stitch density of 30 stitches/cm^2 in the region near the lug feature, once you get an inch below the lug the stitch density changes to 8 stitches/cm^2. An example of this stitching is shown in Figure 70, where the yellow is Kevlar stitching. The lower density is the left side of the preform, while the right side has the higher stitch density. This shift was captured by modifying the cohesive zone strength between layers of each preform according to the local stitch density. Results of the models were discussed above but are repeated here. Laminate 4 was the weakest failing at 287.6 kN, while laminate 3 and 2 failed at 331.5 and 335.1 kN, respectfully. Laminate 1 was predicted to fail at 290.1 kN. These model results are plotted in Figure 71, where the different model load vs. displacement curves are shown together. In all cases damage onset is pretty rapid, and there is matrix cracking near the lug feature that propagates outward quickly. An example of the predicted matrix cracks in a 45 and 90° ply are shown in Figure 72 (from the outermost 45 and 90 ° ply in laminate 3). Fiber failure was predicted to occur in locations shown in red in Figure 59. From these original model approaches laminate 1 and laminate 3 were picked to fabricate (and subsequently referred to as Laminate 1 and 2). In addition to simulating the nominal lug, an extremely simplified model of the hard point insert was completed. This model ignored the carbon sleeve, and threaded bolt by simply inserting a metallic sleeve matching the

nominal thickness of the total hard point assembly. This model predicted an increase in failure load by 12.6% and 10.2% for the 2 chosen fiber schematics (laminate 1 and 3 from the modeling section). An example comparison of the predicted model failure can be seen against the part failure in Figure 73. In this damage model the color green corresponds to delamination between layers, while red is matrix cracks and black is fiber failure. In general, the model shows good agreement capturing the large spread damage accumulation at the tangents of the lug moving outward.

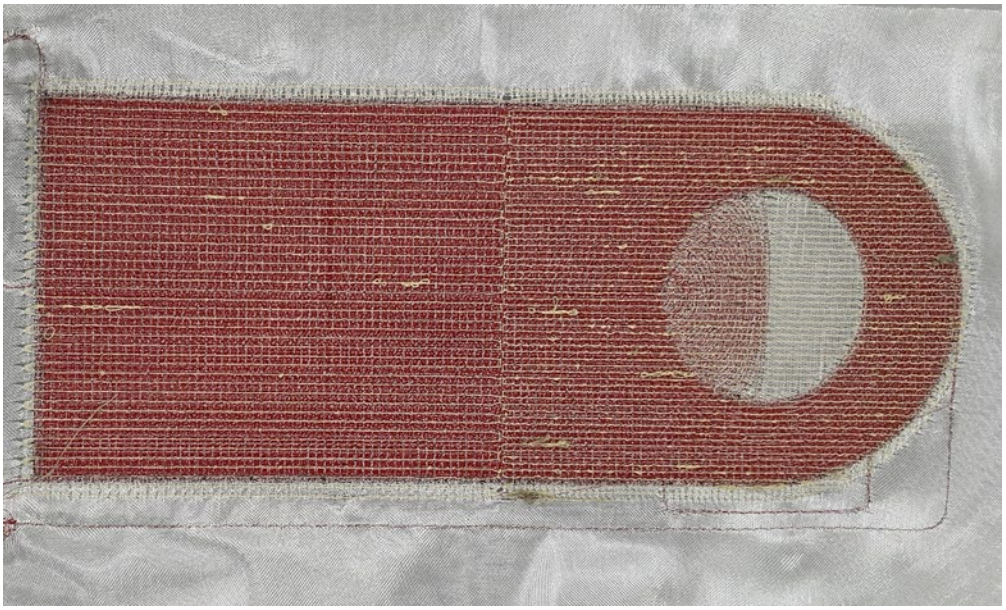

Figure 70. Stitch Locations of Lug Component (Kevlar in Yellow)

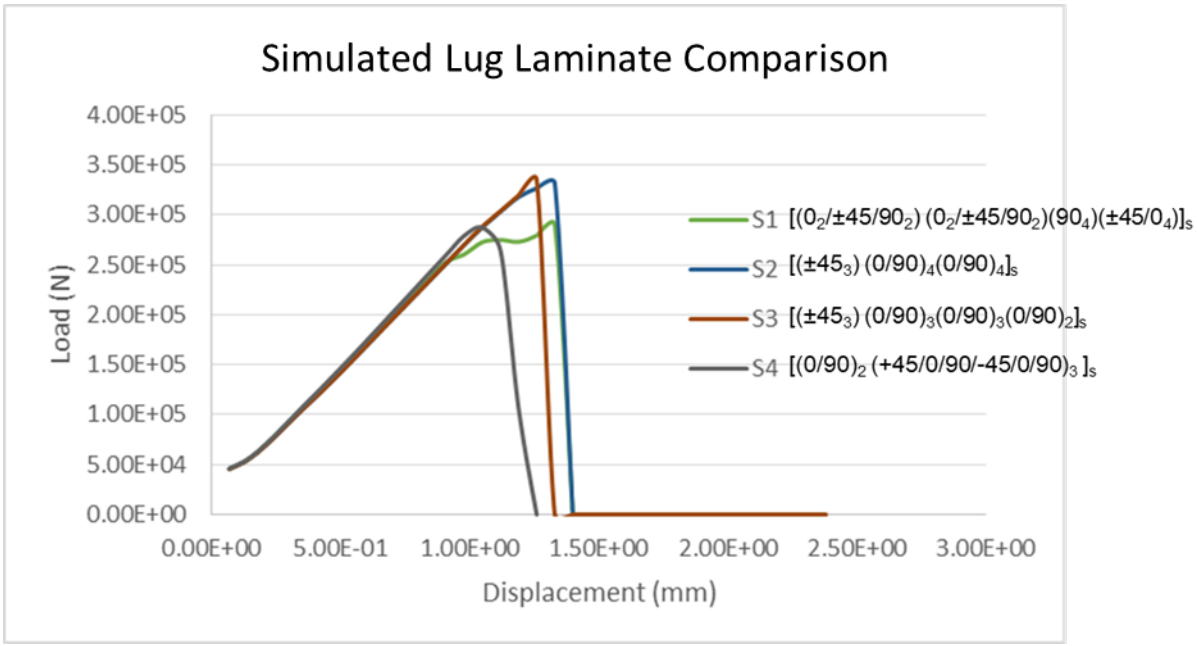

Figure 71. Computational Model Results of TFP Lugs

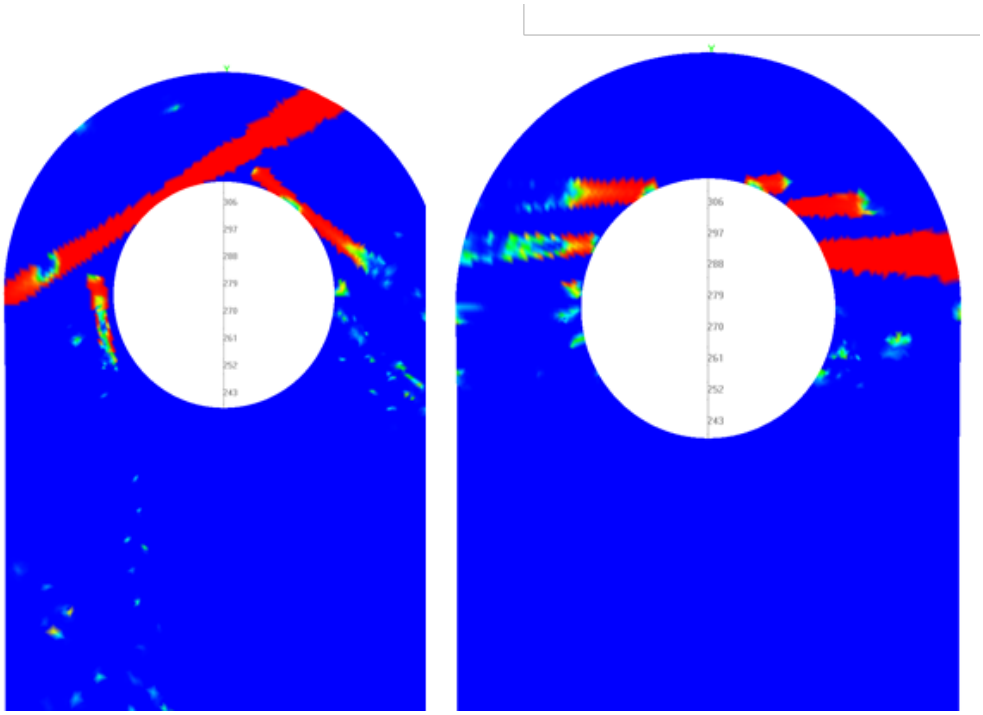

Figure 72. Computational Model Predicted Matrix Cracking in 45 and 90° Plies (Laminate 3)

Figure 73. Computational Model Predicted Failure of a Hard Point Model against Experimental Failure

Clip Bracket Model

The next step was to simulate the clip bracket. The laminate stacking sequence was picked after discussion about simulation results. UDRI then fabricated the TFP preforms that form the clip bracket, with the intention of localizing stiffness as needed, while still being able to fabricate the sample. The sample laminate stacking sequence follows where "B" corresponds to the location of a fiber glass backing cloth used to hold fiber in place. Each "sub-laminate" is indicated by parentheses. The stacking sequence of ([(B/0/0/0/0/0),(B/0/0/0),(B/0/0/45/0/90/-45),(-45/90/0/45/0/0/B), (0,0,90,90,0,0/B)]) was originally

simulated without any "steering" of the fiber or impact of reinforcement. This was completed as an initial effort while the fabrication group modified the TFP design to ensure a proper fit in the tooling mold. Figure 74 shows initial damage locations from the "unidirectional" model. Damage quickly accumulates in the lug location and is expected to produce some delamination at the "ridge" on the back surface. This delamination under the matrix crack is not surprising either. Once the TFP print paths were verified to fit in the tooling, mold print paths were provided to the modeling team. These print paths were overlaid on a ply-by-ply basis. The simulation fixed the surface of the part with an out of plane constraint, and displacement constraint at bolt holes. The applied displacement at the loading pin was applied in uniform step sizes. The applied boundary conditions can be seen in Figure 75, where Figure 75a shows the out of plane constraint, and Figure 75b shows the in-plane constraint and displacements (red = constraint, blue dot = applied displacement).

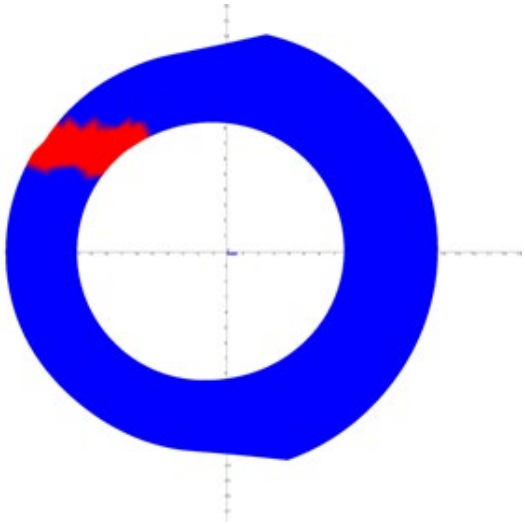

Figure 74. Matrix Crack Accumulation in Clip Bracket

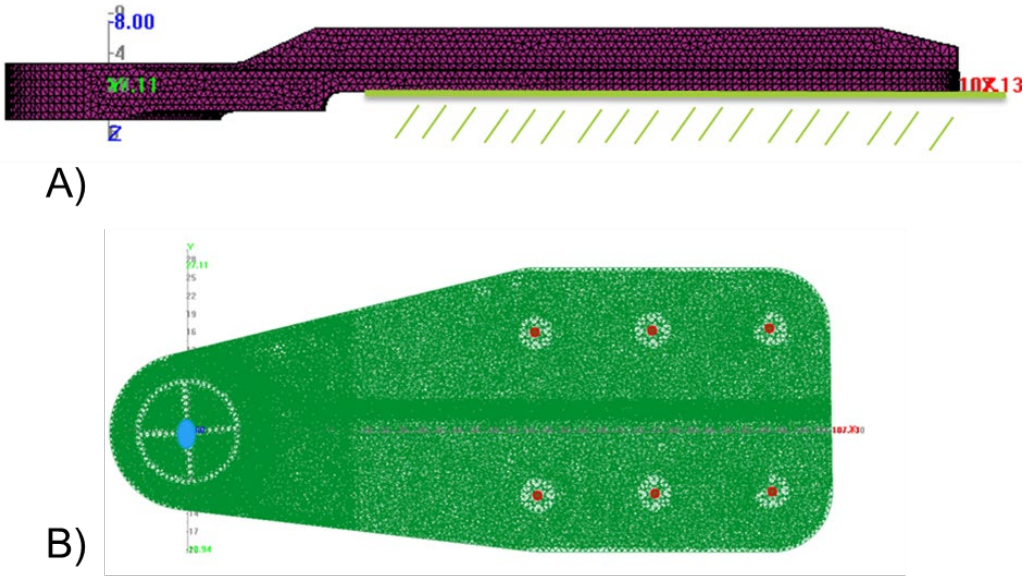

Figure 75. a) Clip Bracket Model Out of Plane Constraint, b) Clip Bracket Model In-Plane Constraints

The load vs displacement data from the unidirectional clip bracket model and TFP "steered" model are compared against the experimental data in Figure 76. The experimental data has been shifted horizontally in order to remove the mechanical slop from the testing. What jumps out immediately is how the model captures the part stiffness well, while under-predicting the total displacement required to fail (i.e. load to failure). In this case UDRI believes the "rigid" nature of the loading pin and boundary conditions results in the premature stress concentrations leading to failure compared to the experimental data. This could be further explored with additional modeling efforts if there was time left on the program. The main take-away is the model showed excellent agreement with the failure location and stiffness, while providing a conservative estimate of performance.

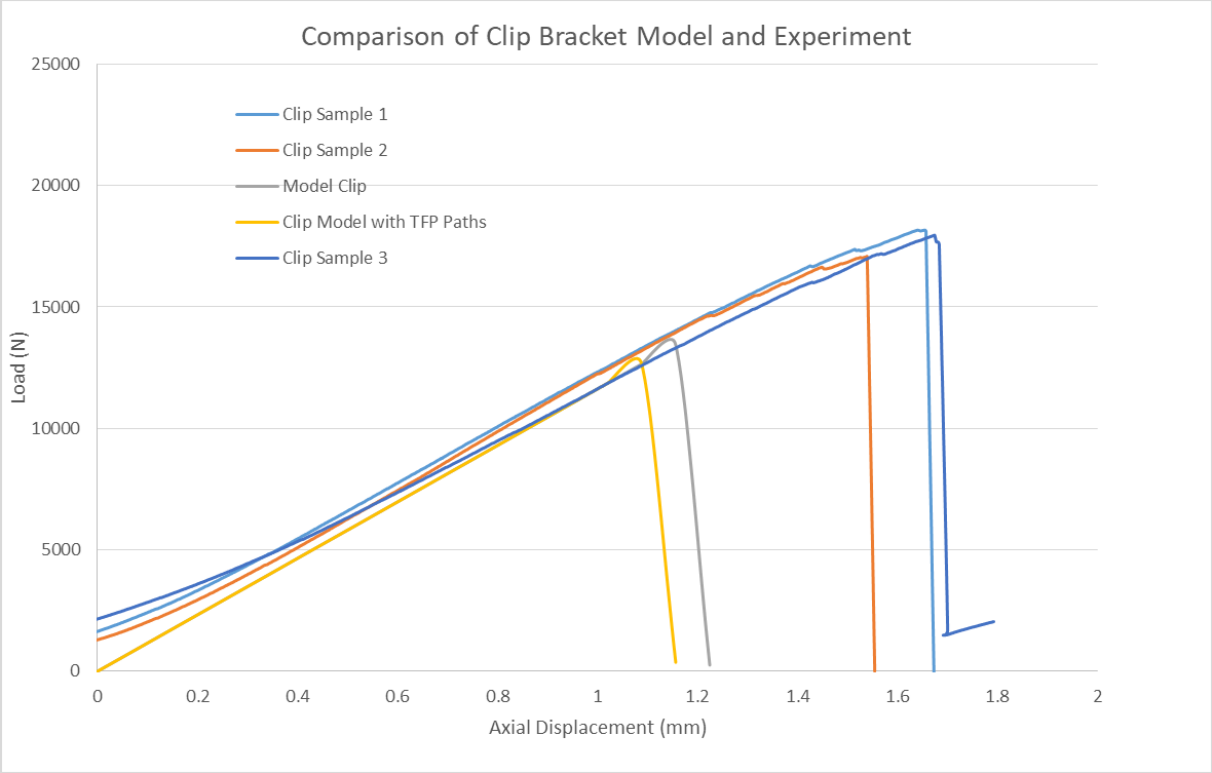

Figure 76. Clip Bracket comparison of Model and Experimental Data

6. BENEFITS ASSESSMENT

Tailored fiber placement (TFP) is a manufacturing technique that automatically lays down fiber bundles (of various sizes) at specified locations, with the ability to provide out-of-plane reinforcement via localized stitching. This process offers a novel approach to optimize fiber architecture for the fabrication of complex structural parts not traditionally suitable for advanced composites. This process promises to improve mechanical performance and reduce component weight by laying down fiber reinforcements in a strategic and geometrically optimized manner. This not only offers routes for component weight reduction by substituting for traditionally metallic components, but it also offers cost reductions through the minimization of material scrap and reduced manual labor. This reduction in component weight leads to increased fuel efficiency, and reduced production energy consumption.

The team used the clip bracket as a cost model test since the baseline cost for the metallic component is well-understood, at $150 per part. The cost of the bracket constituents is $40.95/lb for the resin and $25/lb for the carbon tow. Using fiber volume measurements from the actual parts, this equates to $2.10 per part for materials. Although this cost does not account for scrap (wasted resin in fill lines, scrapped preforms, etc.), for the sake of this cost model, it is assumed these costs are offset by the use of low-volume material costs in the study.

Time studies indicated that one hour is needed to stitch one complete bracket preform. Per ZSK, one technician can run two, 8-head machines concurrently. If a fully burdened hourly rate of $80/hr is assumed, the 16 preforms made on the two machines per hour would cost $5 per preform ($80 divided by 16 parts). Using three shifts, the equipment could make almost 100,000 preforms in a year.

Trimming of the preforms from the backing material would also be needed. If a roll-to-roll TFP machine is used, these rolls could be loaded onto an automated cutter, and be cut out very inexpensively. This cost is estimated to be $0.50 per preform.

Figure 77. Commercial Scale ZSK TFP Fabrication Setup

Other manufacturing costs, such as overhead, equipment depreciation, operational costs, maintenance, etc. are not well understood by the team. An estimate of $200,000 annually for the work cell was used for the sake of this study. At roughly 100,000 preforms per year, this cost amortizes to $2 per preform.

Tallying up these costs, the cost to generate a preform is just under $10. UDRI consulted with Spintech to determine molding costs. These were estimated at $68 per unit. This puts total manufacturing cost at $78 per unit, almost half the cost to manufacture the bracket from aluminum.

7. COMMERCIALIZATION

Tailored Fiber Placement (TFP) offers a novel approach to optimize fiber architecture for the fabrication of complex, structural parts not traditionally suitable for advanced composites. Equipment partner ZSK has a number machines in operation across the US and Europe. Although Airbus has been an early adopter of the technology, the majority of machines in operation support the automotive industry. A yet-to-be named US automaker has just recently made a very large investment in the technology to support the manufacture of composite auto components.

Lockheed and Airbus have a principal interest in this technology for primary structure in UAV's, and

non-flight critical commercial aircraft components. Composite fuselage-to-wing and fin to hull attachments and other, thick, complex shaped structure, would offer lightweight, fatigue resistant, distributed stress transitions for joinery where present components are currently made exclusively with metals. Next generation airframe and seaframe designs would benefit from this light-weighting/stress-distributing option. Pending successful test and manufacturing trials, Lockheed Martin would likely pursue qualification and certification of these new composite applications. Part demonstrations were conducted under Task 5 of this project, and it is expected to take 1-2 years following successful completion for commercialization.

UDRI is in the process of formalizing their partnership with Spintech, who will serve as the commercialization partner for this technology. Initially, Spintech will provide molding services in their AS9100 facility and deliver finished components to the end user. UDRI will continue to produce the preforms until the economics allow Spintech to procure its own TFP equipment or lease UDRI equipment, at which point UDRI will step away from manufacture and serve as the engineering and design lead on product development.

Regarding commercialization, low risk applications such as sporting goods are historically an early entrant for new composite applications. Qualification and certification efforts can take one or more years. Application of the technology, however, is more dependent on the arrival of new aircraft and naval programs that would benefit from the lightweight composite option. For instance, certain structures related to specific submersible programs could host applications during an emergent time-frame. Immediate potential includes submersible prototype and surface combatant (LCS/Frigate) seaframe and control structures aligned with short-term applications. Long-term impacts are associated with new development and production aircraft programs. Taking full advantage of the technology by aerospace and automotive would take about 5 years.

Short-term impacts may also include some implementation of new “beam design” on legacy aircraft. In the long-term, this project could lead to redesign for new aircraft manufacturing, with a positive lasting ripple effect on the entire supply chain.

8. ACCOMPLISHMENTS

The completion of this project allowed UDRI to show the full potential of the TFP process for successfully designing parts with improved strength and toughness. This project provides a verified template for using the software packages BSAM and VTMS to successfully predict a wide variety of load cases with differing design parameters such as fiber path, and stitch placement. As part of this project UDRI submitted **three** conference proceedings that are detailed below.

- Daniel Rapking, Eric Zhou, Bert Liu, Michael Braginsky, Gyaneshwar Tandon, “A Computational Design Methodology for Tailored Fiber Placement Preforms,” presented at the IACMI Winter Members Meeting, Jan, 2020

- Daniel Rapking, Eric Zhou, Bert Liu, Michael Braginsky, Gyaneshwar Tandon, Scott Huelskamp, “On The Development of a computational Design Methodology for Tailored Fiber Placement Prefroms, “ Proceedings SAMPE, 2020

- Daniel Rapking, Bert Liu, Michael Braginsky, Eric Zhou, Scott Huelskamp and Gyaneshwar Tandon, “Computational Tool Development for Tailored Fiber Placement (TFP) Design Optimization,” Proceedings of the American Society for Composites—Thirty-fifth Technical Conference, Sep 2020

The completion of this project resulted in the completion of milestones listed below:

Milestone 5.7.2.1: Achieve an optimum stitch design that increases the cohesive strength by at least 50% over unstitched baseline laminate

This milestone was easily achieved where both the mode I and II toughness values were significantly increased, while also improving on the interlaminar tensile strength. The relative improvements shown as a function of stitch density are discussed in Table 2.

Milestone 5.7.2.2: Predict the ultimate strength and stiffness within 25% of the actual mechanical properties of the test element

This milestone was achieved on several different components in this program showcasing the versatility and capability of the modeling tools developed by UDRI. This can be seen looking at the modeling results of the bearing shear test components, curved beam samples, and even the simplistic ASTM standard coupons shown in Table 9.

Milestone 5.7.3.1: Demonstrate that at least one sub-element TFP preform exceeds the strength of a traditional component by at least 10%

The angled bracket preform with stitching was shown to improve performance over the baseline unstitched bracket. Table 4 shows that the curved beam strength improved by more than 76% for layup 3 and by 73% for layup 4 as the stitch density was increased from 0 (unstitched) to 30 stitches/cm^2.

Milestone 5.7.3.2: Predict the ultimate strength and stiffness of the sub-element within 25% of the actual mechanical properties of the tested sub-element

The angled bracket components were used to compare against the computational model predictions and the toolset showed excellent agreement with the experimental failure loads and damage locations. Figure 50 compares the load vs. displacement data for comparison between angled bracket models and experimental data. As shown in Table 9, curved beam strength predictions are within 19% for both layups 3 and 4 for unstitched and all stitch densities (8, 16 and 30 stitches/cm^2) with the exception of one simulation for the highest stitch density for which the difference is 26%.

Milestone 5.7.4.1: Validate that the analytical models can predict the location of initial failure and predict the failure strength within 25% of measured value

The angled bracket components were used to compare against the computational model predictions and the toolset showed excellent agreement with the experimental failure loads and damage locations. Figure 51 shows comparison of model predicted damage in baseline laminate 3 compared to experimental damage showing widespread delamination in the curved region of the laminate. Table 9 compares the curved beam strength from simulations with the experimental data for various stitch densities.

Milestone 5.7.5.1: Demonstrate that a properly designed TFP part exceeds the tensile strength of a textile based preform by at least 10%

This milestone is stated as completed by the project completion, as the original design goal had been

to compare against the lug component in [18]. Due to a mix-up in the fabrication process of the lugs the incorrect carbon fiber was originally used. This resulted in the fabrication of lugs with IM7 fiber, when they should have been fabricated from a standard modulus fiber such as T700s or AS4. This mix up lead to delays in the fabrication time line near the end of the project. With a month left to complete the project there was not enough time to fabricate lugs with optimized fabrication parameters. This resulted in components with gaps and laps in the fiber placement, alongside voids formed during the RTM process. However, the numerical model results showed a 12% increase in performance with TFP Laminate 2 over the theoretical woven baseline. Given the time constraints for fabricating additional components, UDRI is using the modeling predictions as the completion of the milestone.

Go/No-Go 5.7.1: Demonstrate that an element TFP preform can exceed bearing strength of a textile based preform by at least 10% and a hardpoint insert provides an additional 10% increase over the TFP preform

The modeled hard point inserts showed 10.17 and 12.62% improvement in failure loads for Laminate 1 and Laminate 2, respectively. The inclusion of the hard point was a massive success resulting in an increase in the peak average load by ~23%. Thus, the stated Go/No-Go criterion was satisfied via a combination of computational modeling and experimental testing.

Go/No-Go 5.7.2: Demonstrate that the TFP preforms for the complex parts with yield a 10% cost reduction or 25% weight reduction compared to a metallic part

This final milestone proved to be a resounding success for UDRI. The fabricated clip bracket resulted in a 43% decrease in part weight, and 32% reduction in part cost, while recording a 70% increase over the design load. The traditional clip bracket is a metallic component (aluminum alloy) with a mass of 44 grams, while the TFP preform results in an average mass of 25.4 grams for the clip bracket utilizing the tooling mold for RTM infusion. Three clip brackets parts were successfully tested and had an average sustained peak load of 17.73 kN with a very low COV (2.3%), which exceeds the design limit load while being considerably lower in both cost and weight.

9. CONCLUSIONS

The results of this project demonstrated that the TFP process of laying down fiber bundles (of various sizes) at specified locations, with the ability to provide out-of-plane reinforcement via localized stitching, offers a novel approach to optimize fiber architecture for the fabrication of complex structural parts not traditionally suitable for advanced composites. This project developed the analytical tools to support the design of composite parts made with TFP preforms, and provide a design methodology for parts fabricated using the TFP process.

An analytical toolset was developed and demonstrated as a way to predict TFP performance alongside a building block approach using coupons/sub-elements in order to optimize the design process and validate the analytical performance of the developed toolset. While this data was used to validate the computational approach it simultaneously generated performance and cost data. This project focused on experimental characterization via standardized ASTM testing, and testing of representative service components such as a curved beam, bearing shear, a large scale TFP lug, and a clip bracket that were used to compare against the computational model predictions. The predictive toolset showed excellent agreement with the experimental failure loads and damage locations. The insertion of a hard point insert in a composite lug and the fabrication/performance of a clip bracket demonstrated beyond doubt the advantages which the TFP methodology presents. These studies have clearly demonstrated how analytical methods can be utilized to develop approaches for designing structures and have given the

industry sponsors the confidence to take advantage of TFP's ability to fabricate primary, highly loaded structures.

10. RECOMMENDATIONS

As part of this program UDRI built a ground up characterization process that generated a material properties database that was used to predict material performance in a variety of mechanical configurations. This program was able to build a complex non-structural component that far exceeds the design limit load while significantly cutting part weight and cost. The potential impact of this weight savings is not fully explored at this point and requires further collaboration with project partners from Airbus. As part of these discussions Nathan Ball identified an area of potential interest that could be explored in follow up efforts: As part of the design allowables, the impact of high temperature/moisture exposure or saturation during loading would need to be explored. It is difficult to determine computationally how the TFP preforms would behave due to moisture/temperature exposure. There are several things that would need to be explored as part of this continuing research, such as moisture uptake of the material system, of particular interest is the uptake in the glass/carbon backing cloths and the Kevlar reinforcing threads. A preliminary look at the impact of hot/wet properties of the resin are shown in the appendices.

During the initial month of the project Lockheed Martin asked how UDRI intended to track the impact of stitching needle wear on the performance of parts during the program. Given the need to massively increase the total number of parts fabricated and tested to fully characterize the impact of needle diameter and wear would have on performance it was excluded from analysis. Stitching needles were simply removed and replaced every 200,000 stitches. Every needle utilized was labeled and kept for potential analysis as part of a follow up program. Alongside this needle replacement UDRI developed a "tracker" shown in the appendices that details the fabrication procedures utilized for each and every preform. Another area of interest for follow up research based around needles is characterizing the maximum size needle that could be used without reducing preform performance significantly. At this moment the TFP machine utilized on this program and produced by ZSK has a maximum part thickness that can be stitched through. This limitation is partially due to the diameter of the needle utilized for the reinforcing thread. Given its small diameter it is possible to break when stitching through large numbers of layers of carbon fiber. UDRI would like to explore options for increasing the total allowable part thickness that can be stitched through as part of follow up work. This would expand the potential range of applications that parts could be produced with TFP preforms. This would also reduce any impact on performance that occurs at interfaces of preforms due to reinforcing thread buildup.

The final area of interest identified as potential follow up research would be the continued exploration of using TFP preforms as local reinforcement at areas of bearing or complex loading. UDRI was able to show that by using TFP preforms the total bearing load could be significantly increased, while simultaneously increasing the load at damage onset. Couple this with the ability to generate large preforms on carbon veils and it quickly becomes attractive for providing local reinforcement at specified locations without the significant increase in human labor associated with prepreg layup where buildups are completed manually. If an improvement in mechanical performance is not desired, these preforms could be used to simply indicate drill locations allowing precise and repeatable drill spot marking. UDRI believes that given follow up research there could be use cases for TFP inserts to improve part performance and achieve the desired increase in the stress allowable. Another area recommended for further development is topology optimization of components by tow steering.

11. REFERENCES AND/OR BIBLIOGRAPHY

[1] G. Gardiner, "Tailored Fiber Placement: Besting metal in volume production," CompositesWorld, 2 September 2013. [Online]. Available: http://www.compositesworld.com/articles/tailored-fiber-placement-besting-metal-in-volume-production. [Accessed 05 06 2017].

[2] Sankar, Bhavani V., and Suresh K. Sharma. "Mode II delamination toughness of stitched graphite/epoxy textile composites." Composites Science and Technology 57.7 (1997): 729-737.

[3] A. Mouritz and B. Cox, "A mechanistic approach to the properties of stitched laminates," Composites: Part A, pp. 1-27, 2000.

[4] E. Koricho, A. Khomenko, T. Fristedt and M. Haq, "Innovative tailored fiber placement technique for enhanced damage resistance in notched composite laminate," Composite Structures, vol. 120, pp. 378-385, 2015.

[5] "Fiber reinforcement forms," CompositesWorld, 1 January 2014. [Online]. Available: http://www.compositesworld.com/articles/fiber-reinforcement-forms. [Accessed 21 05 2017].

[6] Iarve EV, Mollenhauer DH and Kim R. Mesh-independent modeling and More´ interferometry studies of damage accumulation in open-hole composite laminates. Mechanics of Composite Materials 2004; 40(5): 419–426.

[7] Iarve EV, Gurvich MR, Mollenhauer DH, et al. Mesh independent matrix cracking and delamination modeling in laminated composites. Int J Numer Meth Eng 2011; 88: 749–773

[8] Iarve EV, Mollenhauer D and Kim R. Three-dimensional stress analysis and Weibull statistics based strength prediction in composite laminates with open holes. Compos A 2007; 38: 174–185.

[9] Iarve EV, Gurvich MR, Mollenhauer DH, et al. Mesh independent matrix cracking and delamination modeling in laminated composites. Int J Numer Meth Eng 2011; 88: 749–773

[10] Turon A, Camanho PP, Costa J, et al. A damage model for the simulation of delamination in advanced composites under variable-mode loading. Mech Mater 2006; 38: 1072–108

[11] Maimı´ P, Camanho PP, Mayugo JA, et al. A continuum damage model for composite laminates: Part Iconstitutive model. Mech Mater 2007; 39: 897–908.

[12] Maimı´ P, Camanho PP, Mayugo JA, et al. A continuum damage model for composite laminates: Part IIcomputational implementation and validation. Mech Mater 2007; 39: 909–919.

[13] Huelskamp, S., C. Tanner, and J. Stonecash. "Effects of Z-Stitching in Heavy Tow Carbon Laminates via Tailored Fiber Placement (TFP)." SAMPE JOURNAL 54.1 (2018): 44-52

[14] Turon, A., et al. "A damage model for the simulation of delamination in advanced composites under variable-mode loading." Mechanics of materials 38.11 (2006): 1072-1089.

[15] Jain, Lalit K., Kimberley A. Dransfield, and Yiu-Wing Mai. "On the effects of stitching in CFRPs—II. Mode II delamination toughness." Composites Science and Technology 58.6 (1998): 829-837.

[16] Rapking, D, Zhou E, Liu B, Braginsky, M, Tandon, G. and Huelskamp, S, "On the Development of a Computational Design Methodology for Tailored Fiber Placement Preforms". SAMPE 2020

[17] Koricho, Ermias G., Mahmoodul Haq, and Gary L. Cloud. "Numerical and Experimental Characterization of Hybrid Fastening System in Composite Joints." Joining Technologies for Composites and Dissimilar Materials, Volume 10. Springer, Cham, 2017. 71-80.

[18] Wallin, Markus, Olli Saarela, and Francesco Pento. "Load Response and Failure of Thick RTM Composite Lugs." 23rd Congress of International Council of the Aeronautical Sciences. 2002.

[19] Koricho, Ermias G., et al. "Innovative tailored fiber placement technique for enhanced damage resistance in notched composite laminate." Composite Structures 120 (2015): 378-385.

12. APPENDICES

Appendix 1. Sample TFP Preform Tracker for Clip Bracket

Preform Part #	2020 (Year Started)	12 (Month Started)	14 (Day Started)	_	3 (Run Number)	_	W (Print Head)	Operator	SW	Part Name	Clip Bracket
								Date Finished	12/14/20	Charge Code	M5T031

A. Stitch Programs

1	Clip_Bracket_Divided V4 Kevlar Outlines Joined
2	
3	
4	

B. Thread		C. Tow		D. Backing		E. Needle	
1	Isacord 40 Tex: 27	1	AS4 6K Carbon	1	Fiberglass Plain Weave 2oz PCC	1	Groz-Beckert FG 75/11
2	Serafil 120/2 Tex: 16	2		2		2	Groz-Beckert RG 100/16
3	K-Tech 75 Tex: 40	3		3		3	
4		4		4		4	

F. Stitch Parameters

	Type	*Length*	*Amplitude*	*Line Spacing*	*Notes*
1	Zigzag (TFP)	30inc	18inc	20inc	Carbon
2	Straight Stitch	35inc		70inc	Kevlar 8 stitches/cm2
3	Straight Stitch	18inc		36inc	Kevlar 30 stitches/cm2
4					

Steps

	Programs	*Top Thread*	*Top Thread Weight*	*Bottom Thread*	*Bottom Thread Weight*	*Tow Material*	*Tow Material Weight*	*Backing*	*Machine Head*	*Tension Upper*	*Tension Lower*	*Needle*	*Stitch Parameters*
1.	A:1	B:1		B:2		C:1		D:1	W	1.5N	0.45N	E:1	F:1
Notes:	Carbon [(B/0/0/90/90/0/0), (B/0/0L/45/0L/90/-45), (B/-45/90/0L/45/0/0), (B/0/0/0), (B/0/0/0/0/0)]. Thick thread rotary hook.												
2.	A:1	B:3		B:3		C:		D:1	W	3.0N	0.65N	E: 2	F:2
Notes:	Kevlar 8 stitches/cm2 for ridge sections. Used coated bobbin.												
3.	A:1	B:3		B:3		C:		D:1	W	3.0N	0.65N	E:2	F:3
Notes:	Kevlar 30 stitches/cm2 for body sections. Used coated bobbin. Weight: 18.91g												
4.	A:	B:		B:		C:		D:				E:	F:
Notes:													
5.	A:	B:		B:		C:		D:				E:	F:
Notes:													
6.	A:	B:		B:		C:		D:				E:	F:

University of Dayton Research Institute

Appendix 2. Sample TFP Preform Tracker for Lug Components

Preform Part #	2020 (Year Started)	12 (Month Started)	16 (Day Started)	_	3 (Run Number)	_	W (Print Head)	**Operator**	SW, OB	**Part Name**	LUG C (mirror)
								Date Finished	12/16/20	**Charge Code**	M5T031

A. Stitch Programs

1	Full Lug V6 Joined_C_AS4 (mirror)
2	
3	
4	

B. Thread		**C. Tow**		**D. Backing**		**E. Needle**	
1	Isacord 40 Tex: 27	1	AS4 6K	1	Fiberglass Plain Weave 2oz PCC	1	Groz-Beckert FG 75/11
2	Serafil 120/2 Tex: 16	2		2		2	Groz-Beckert RG 100/16
3	K-Tech 75 Tex: 40	3		3		3	
4		4		4		4	

F. Stitch Parameters

	Type	*Length*	*Amplitude*	*Line Spacing*	*Notes*
1	Zigzag (TFP)	30inc	18inc	20inc	Carbon
2	Straight Stitch	25inc		25inc	Kevlar 16 stitches/cm2
3	Straight Stitch	35inc		35inc	Kevlar 30 stitches/cm2
4					

Steps

	Programs	*Top Thread*	*Weight*	*Bottom Thread*	*Weight*	*Tow Material*	*Weight*	*Backing*	*Machine Head*	*Tension Upper*	*Tension Lower*	*Needle*	*Stitch Parameters*
1.	A:1	B:1		B:2		C:1		D:1	W	1.5N	0.45N	E:1	F:1
Notes:	Carbon [90, 90, 90, 90]. Thick thread rotary hook.												
2.	A:1	B:3		B:3		C:		D:1	W	3.0N	0.65N	E: 2	F:2
Notes:	Kevlar 16 stitches/cm2 top half of lug. Used coated bobbin. No top thread looping.												
3.	A:1	B:3		B:3		C:		D:1	W	3.0N	0.65N	E:2	F:3
Notes:	Kevlar 30 stitches/cm2 bottom half of lug. Used coated bobbin. No top thread looping. Weight: 87.17g												
4.	A:	B:		B:		C:		D:				E:	F:
Notes:													
5.	A:	B:		B:		C:		D:				E:	F:
Notes:													
6.	A:	B:		B:		C:		D:				E:	F:

University of Dayton Research Institute

Appendix 3. Example Image of ZSK Design Software Interface (Lug Component)

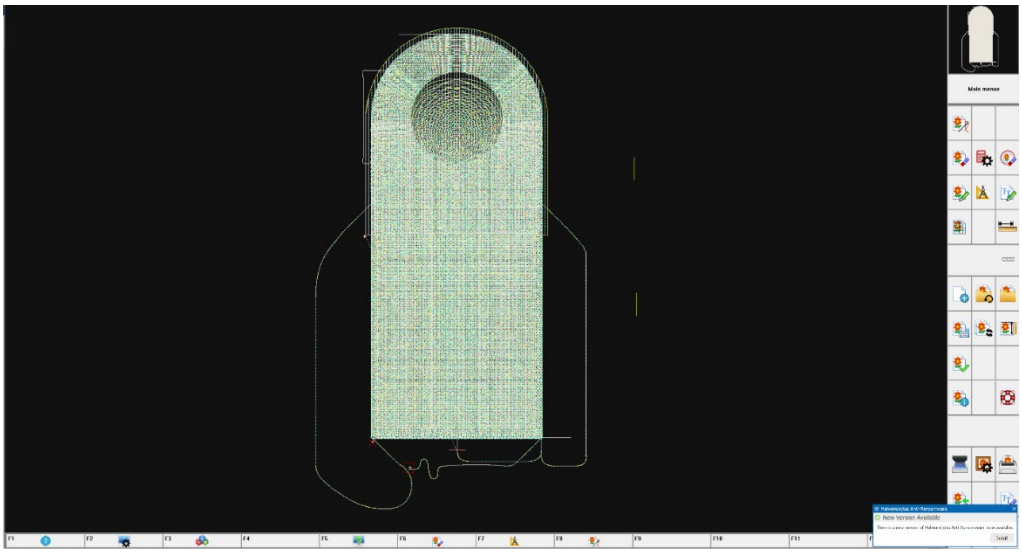

Appendix 4. Close Up of Fiber Path Directions and Stitch Locations

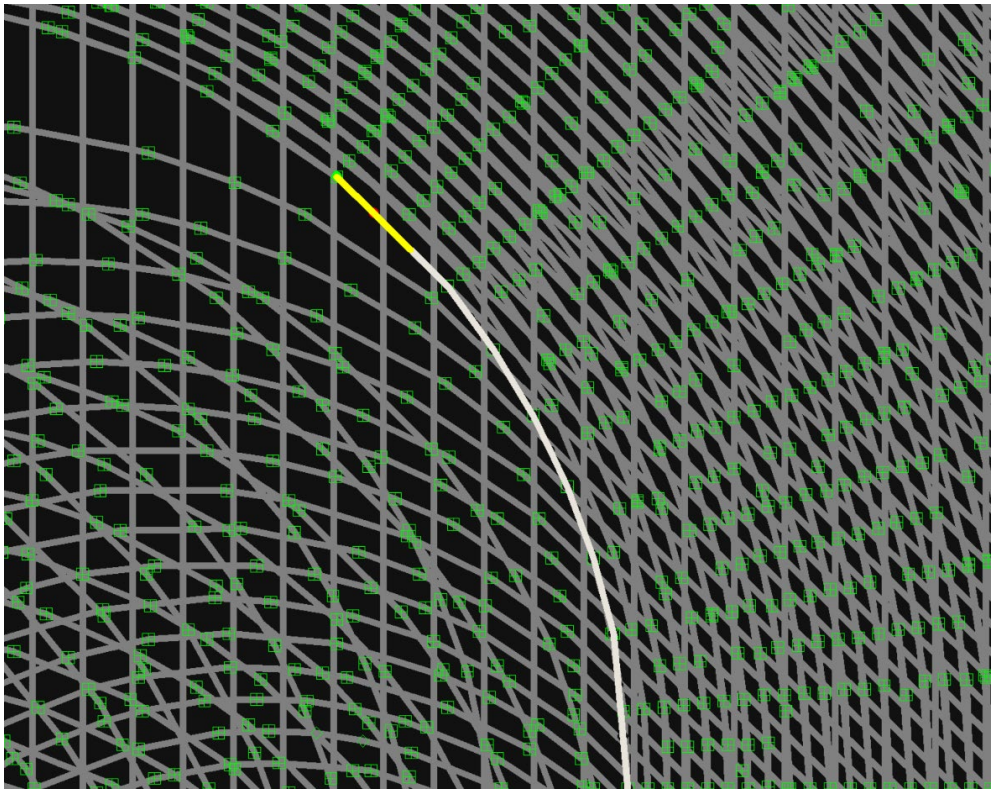

Appendix 5. Example Design Parameters for Stitch/Fiber Locations: Clip Bracket

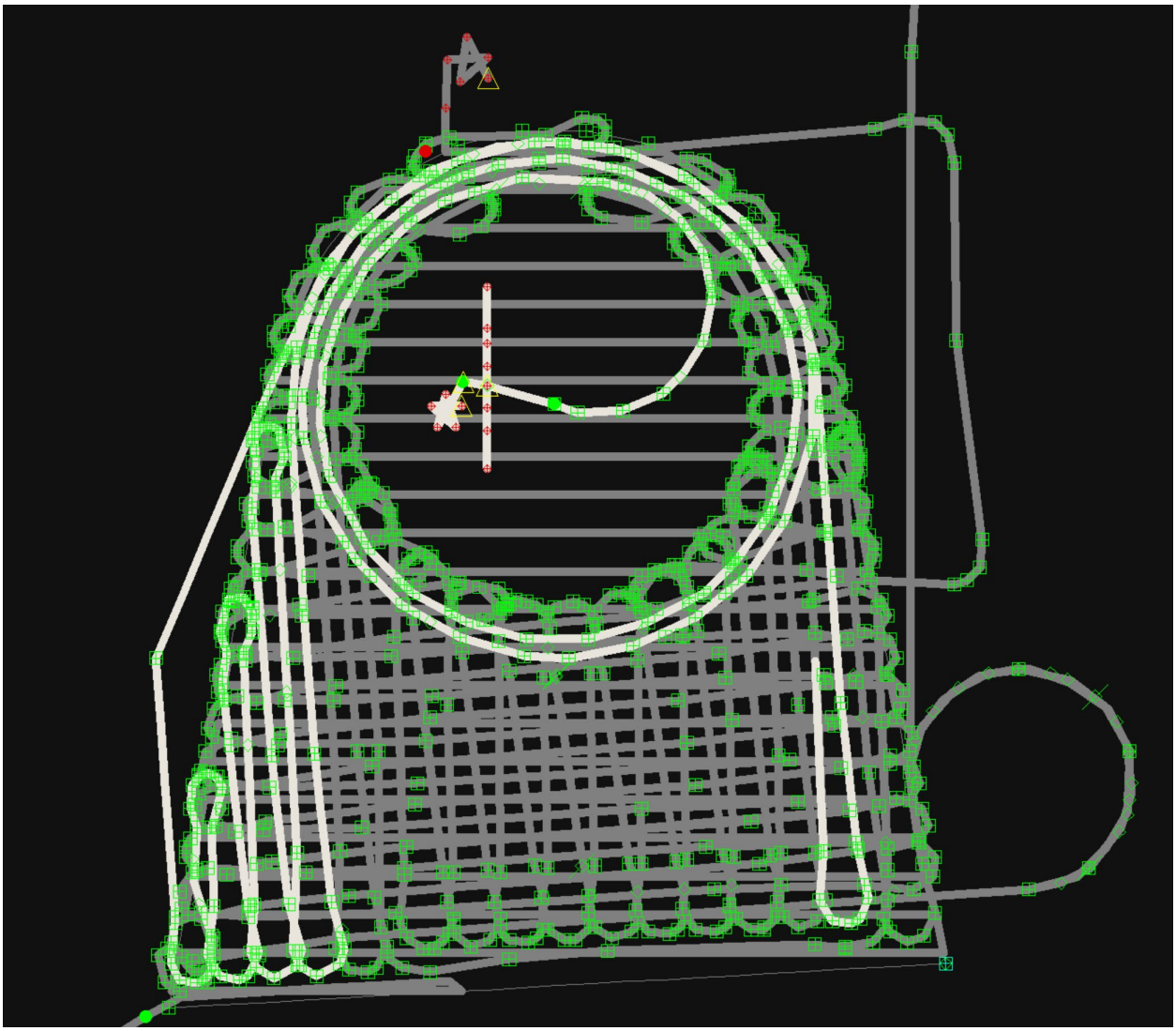

Appendix 6. RTM6 Data Sheet Link for Temperature Impact

https://www.hexcel.com/user_area/content_media/raw/RTM6_DataSheetPDF.pdf